

**Enzymatic synthesis and characterization of grafted
polyesters and their use as steric stabilizers for
cubosomes**

Dissertation

Zur Erlangung des Doktorgrades der Naturwissenschaften
(Dr. rer. nat.)

der

Naturwissenschaftlichen Fakultät II
Chemie, Physik und Mathematik

der Martin-Luther-Universität
Halle-Wittenberg

Vorgelegt von

Herrn Muhammad Humayun Bilal
geb. am 18.01.1983 in Lahore, Pakistan

Gutachter: Prof. Dr. Jörg Kreßler (Martin-Luther-Universität Halle-Wittenberg)
Prof. Dr. Niko Bruns (Adolphe Merkle Institute, Fribourg)

Verteidigungdatum: 11.03.2019

TABLE OF CONTENTS

1	INTRODUCTION.....	1
1.1	ENZYMATIC POLYESTER SYNTHESIS AND GRAFTING.....	1
1.1.1	<i>Lipases</i>	1
1.1.2	<i>Enzymatic synthesis of functional polyesters</i>	4
1.1.3	<i>Grafting of functional polyesters</i>	6
1.2	FUNDAMENTALS OF LIPID SELF-ASSEMBLY.....	8
1.2.1	<i>Lipid polymorphism</i>	10
1.2.1.1	The lamellar phase.....	10
1.2.1.2	The hexagonal phase.....	12
1.2.1.3	The micellar cubic phase.....	12
1.2.1.4	Bicontinuous phases.....	13
1.1.1.1.1	The sponge phase.....	13
1.1.1.1.2	Bicontinuous cubic phases.....	14
1.2.2	<i>Binary phase diagram of GMO-water system</i>	16
1.2.3	<i>The effect of additives on the mesophase behavior of the GMO-water system</i>	18
1.3	STERIC STABILIZERS FOR CUBOSMES.....	20
1.4	AIMS AND OBJECTIVES.....	22
2	FATTY ACID MODIFIED SUGAR BASED POLYESTERS.....	24
2.1	INTRODUCTION.....	24
2.2	EXPERIMENTAL PART.....	26
2.2.1	<i>Materials</i>	26
2.2.2	<i>Syntheses</i>	26
2.2.2.1	Synthesis of poly(xylitol adipate).....	26
2.2.2.2	Synthesis of poly(D-sorbitol adipate).....	26
2.2.2.3	Synthesis of stearyl grafted poly(xylitol adipate) and poly(D-sorbitol adipate).....	27
2.2.3	<i>Preparation of nanoparticles</i>	27
2.2.4	<i>Instrumentation</i>	28
2.2.4.1	NMR spectroscopy.....	28
2.2.4.2	Size exclusion chromatography (SEC).....	28
2.2.4.3	Differential scanning calorimetry (DSC).....	28
2.2.4.4	Dynamic light scattering (DLS).....	28
2.2.4.5	Negative-staining TEM.....	29
2.2.4.6	X-ray diffraction (XRD).....	29
2.3	RESULTS AND DISCUSSION.....	29
2.3.1	<i>Polymerization and grafting</i>	29
2.3.2	<i>Nanoparticles</i>	35
2.3.2.1	Dynamic light scattering.....	35
2.3.2.2	Negative-staining transmission electron microscopy.....	36
2.4	CONCLUSIONS.....	37
3	POLY(GLYCEROL ADIPATE)-G-OLEATE AND THE GMO/WATER SYSTEM.....	38
3.1	INTRODUCTION.....	38
3.2	EXPERIMENTAL SECTION.....	41
3.2.1	<i>Materials</i>	41
3.2.2	<i>Syntheses</i>	41

3.2.2.1	Synthesis of poly(glycerol adipate) (PGA).....	41
3.2.2.2	Syntheses of poly(glycerol adipate)- <i>g</i> -oleate (PGA- <i>g</i> -Ox)	42
3.2.2.3	Synthesis of glycerol monooleate (GMO).....	42
3.2.3	<i>Polymer characterization</i>	43
3.2.4	<i>Sample preparation for X-ray diffraction</i>	43
3.2.5	<i>Preparation of nanoparticles</i>	44
3.2.6	<i>Dynamic light scattering</i>	44
3.2.7	<i>Negative stain transmission electron microscopy</i>	44
3.2.8	<i>Cryogenic transmission electron microscopy</i>	45
3.2.9	<i>X-ray diffraction</i>	45
3.3	RESULTS AND DISCUSSION	46
3.3.1	<i>Syntheses and grafting of poly(glycerol adipate) and glycerol monooleate</i>	46
3.3.2	<i>Characterization of PGA-<i>g</i>-Ox with nanodomains formed by oleate side chains</i>	51
3.3.3	<i>The ternary system GMO/PGA-<i>g</i>-O22/water</i>	53
3.3.4	<i>PGA-<i>g</i>-O22 as a potential stabilizer for GMO based nanoparticles in aqueous dispersions</i>	61
3.4	CONCLUSION	63
4	MULTIGRAFT POLYESTERS AS STABILIZERS FOR CUBOSOMES	65
4.1	INTRODUCTION.....	65
4.2	EXPERIMENTAL PART	67
4.2.1	<i>Materials</i>	67
4.2.2	<i>Syntheses</i>	68
4.2.2.1	Carboxylation of mPEG750 and mPEG1K	68
4.2.2.2	Grafting of poly(glycerol adipate) (PGA) with oleate side chain.....	68
4.2.2.3	PEG grafting of PGA ₂₆ O _x	68
4.2.2.4	Polymer characterization	69
4.2.2.5	Surface Tension Measurements	69
4.2.2.6	XRD measurements	70
4.2.2.7	Dynamic light scattering	70
4.2.3	<i>Preparation of cubosome dispersions</i>	70
4.3	RESULTS AND DISCUSSION.....	71
4.3.1	<i>Polymer synthesis and grafting</i>	71
4.3.2	<i>Graft copolymers as steric stabilizers of cubosomes</i>	78
4.4	CONCLUSION	82
5	SUMMARY	83
6	REFERENCES	86
7	APPENDIX	100
8	ACKNOWLEDGMENT	105
9	CURRICULUM VITAE	106
10	LIST OF PUBLICATIONS	107
11	SELBSTSTÄNDIGKEITSERKLÄRUNG	108

ABBREVIATIONS AND SYMBOLS

ABBREVIATIONS

Asp	Aspartic acid
ATRP	Atom transfer radical polymerization
CAC	Critical aggregation concentration
CAL-B	<i>Candida antarctica</i> Lipase B
CMC	Critical micelle concentration
CMT	Critical micelle temperature
CPP	Critical packing parameter
DCM	Dichloromethane
DDS	Drug delivery system
DMAP	4-Dimethylaminopyridine
DMPE	1,2-Dimyristoyl- <i>sn</i> -glycerol-3-phosphoethanolamine
DMSO	Dimethyl sulfoxide
DOPE	1,2-Dioleoyl- <i>sn</i> -glycerol-3-phosphoethanolamine
DSC	Differential scanning calorimetry
DSPE	1,2-Distearoyl- <i>sn</i> -glycerol-3-phosphoethanolamine
EDC	1-Ethyl-3-(3-dimethylaminopropyl)carbodiimide
eROP	Enzymatic ring opening polymerization
FA	Fatty acid
FI	Fluid isotropic
G1MO	Glycerol-1-monooleate
G2MO	Glycerol-2-monooleate
Gln	Glutamine
Glu	Glutamic acid
GMO	Glycerol monooleate, monoolein
His	Histidine
HLB	Hydrophilic to lipophilic balance
IPMS	Infinite periodic minimal surface
LLC	Lyotropic liquid crystal
MAG	Monoacyl glycerol

MO	Monoolein
NP	Nanoparticle
PBS	Poly(butylene succinate)
P(ODA- <i>b</i> - P(PEGA- OME))	Poly(octadecyl acrylate)- <i>block</i> -poly(ethylene glycol monomethyl ether acrylate)
PC	Diacyl phosphatidyl choline
PCL	Poly(ϵ -caprolactone)
PDI	Polydispersity index
PDSA	Poly(D-sorbitol adipate)
PDSA- <i>g</i> -S _x	Poly(D-sorbitol adipate)- <i>graft</i> -stearate, x stands for mol% grafting of OH groups of polymer backbone with stearate side chain
PEG	Poly(ethylene glycol)
PGMA	Poly(glycerol methacrylate)
PEI	Poly(ethylene imine)
PEO	Poly(ethylene oxide)
PGA	Poly(glycerol adipate)
PGA- <i>g</i> -O _x	Oleate grafted poly(glycerol adipate) where x is the mol% grafting of PGA with oleate side chains
PGA _x O _y PEG _z	Oleate and PEG grafted poly(glycerol adipate), where x is the degree of polymerization of PGA, y and z stand for the number of oleate and PEG side chains, respectively.
PGS	Poly(glycerol sebacate)
PLA	Poly(lactic acid)
PPO	Poly(propylene oxide)
PXA	Poly(xylitol adipate)
PXA- <i>g</i> -S _x	Poly(xylitol adipate)- <i>graft</i> -stearate, x stands for mol% grafting of OH groups of polymer backbone with stearate side chain
RAFT	Reversible addition-fragmentation chain transfer polymerization
RI	Refractive index
ROP	Ring opening polymerization
SAXS	Small angle X-ray scattering
SEC	Size exclusion chromatography

Ser	Serine
TEM	Transmission electron microscopy
Thr	Threonine
WAXS	Wide angle X-ray scattering
XRD	X-ray diffraction
^1H NMR	Proton nuclear magnetic resonance
^{13}C NMR	Carbon-13 nuclear magnetic resonance

SYMBOLS

M_n	Number average molar mass
M_w	Weight average molar mass
r_h	Hydrodynamic radius
ΔG_{agg}	Gibbs free energy of aggregation
ΔH_{agg}	Enthalpy of aggregation
ΔS_{agg}	Entropy of aggregation
v_l	Volume of amphiphilic molecule
l_c	Length of hydrophobic chain of an amphiphile
a_0	Effective area of head group of an amphiphile
χ	Euler-Poincare characteristics
γ	Critical packing parameter
L_2	Isotropic phase
H_2	Reverse hexagonal phase
L_c	Lamellar crystal phase
L_α	Liquid crystalline lamellar phase
L_β^*	Lamellar tilted gel phase
L_β	Lamellar gel phase
$L_{\beta I}$	Lamellar interdigitated gel phase
P_β^*	Lamellar rippled gel phase
S_{lam}	Reciprocal spacing for lamellar phase
ϕ_w	Volume fraction of water
H_1	Normal hexagonal phase
L_3	Sponge phase

ϕ_{lipid}	Volume fraction of lipid
σ	Surface area of the minimal surface per unit volume
r_w	Radius of water channel
N_A	Avogadro's number
$A_{cs}(l)$	Cross-sectional area per lipid molecule
V_{lipid}	Volume of lipid molecule
\tilde{v}_{lipid}	Lipid specific volume
δ	Chemical shift

CHAPTER 1

1 INTRODUCTION

1.1 ENZYMATIC POLYESTER SYNTHESIS AND GRAFTING

Aliphatic polyesters are macromolecules in which the respective monomers are connected by ester bonds. Aliphatic polyesters are biodegradable and biocompatible and thus they are considered as ideal materials for biomedical applications, including surgery and medicine.^{1,2} Poly(lactic acid) (PLA), and poly(butylene succinate) (PBS) are examples of synthetic polyesters which are already in the market for commercial applications.³

There are two methods of polyester synthesis: (a) step-growth polycondensation between diols and diacids / diesters or hydroxyacids / hydroxyesters, and (b) ring-opening polymerization (ROP) of cyclic monomers.⁴ Both methods have advantages as well as disadvantages. For polycondensation, monomers can be derived from renewable resources and are available at low costs, but this method requires conditions of high temperature and vacuum to remove byproducts in order to shift the condensation equilibrium to the forward direction. These high temperatures and vacuum conditions lead to undesired side reaction such as dehydration of diols and β -scission of polyesters to form acid and alkene end groups.⁵ On the contrary, there is no byproduct in ring opening polymerization, and it is carried out at relatively mild reaction conditions. However, this process requires a catalyst which is usually a salt of heavy metals such as tin⁶ and rare earth metals.⁷⁻⁹ The complete removal of these catalysts from the finished product is difficult which makes these products less suitable for pharmaceutical applications. However the enzymatic synthesis of polyesters is an environmentally benign process which helps to produce linear polyesters of monomers with multiple functionalities at ambient reaction conditions without danger of metal contamination of the product.^{10,11}

1.1.1 Lipases

In nature, living organisms such as bacteria e.g. *Pseudomonas cepcia* and *Pseudomonas fluorescens*, and fungi e.g. *Candida cylindracea*, *Aspergillus niger*, *Candida*

rugosa, *Penicillium roqueforti*, *Rhizopus japonicas*, *Rhizomucor meihei*, *Mucor meihei*, *Candida antarctica* and *Yarrowia lipolytica* etc., produce polyesters for their metabolic need.¹² Their synthesis generally involves *in vivo* lipase-catalyzed chain growth polymerization reaction of activated monomers. Lipases are harvested from these living organisms which could be used further for *in vitro* synthesis of polyesters.¹³ Lipases could be derived from animals, (where they hydrolyze ester bond, thus converting triglycerides into glycerol and fatty acids)¹⁴ and could be used for *in vitro* polyester synthesis too. The choice of reaction solvent depends on the lipase origin and the monomer structure.¹⁵ Different types of lipases used for *in vitro* polyester synthesis are comprehensively reviewed by Shoda *et al.*¹⁶ Among all studied lipases for polyester synthesis; *Candida antarctica* lipase B is found to be the best in terms of reactivity, selectivity, and thermal stability, especially when it is immobilized on a support.^{17,18}

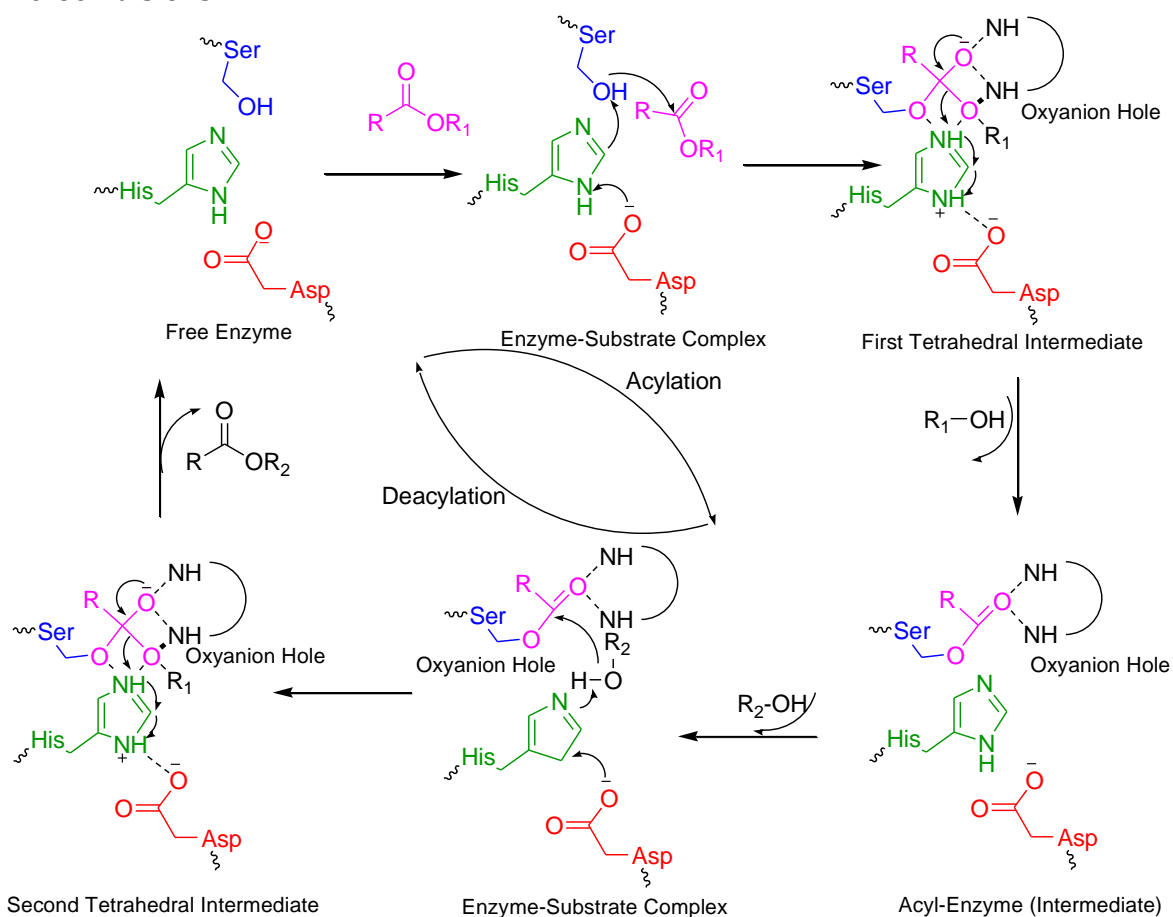
***Candida antarctica* lipase B**

Candida antarctica lipase B (CAL-B) is a globular protein that consists of 317 amino acids having a molar mass of 33 kDa. It possesses an α/β hydrolase fold that consists of a β -sheet core of parallel strands connected on both sides by α -helices, forming an α - β - α sandwich-like shape. Similar to other lipases, CAL-B possesses an active site that is comprised of three amino acids called catalytic triad: a nucleophilic residue (serine), a histidine base and a catalytic acidic residue aspartic acid (Ser105, His224, and Asp187) and it contains two oxyanion holes (Thr40 and Gln106). The active sites of lipases have different shapes, sizes, depth of the pockets, and physiochemical characteristics of their amino acids. The specificity, selectivity and catalytic reactivity of an enzyme depends on its active sites.¹⁹

A general acylation-deacylation mechanism of lipases is shown in Scheme 1.1. In the acylation step, a proton transfer occurs among the Asp105, His224, and Ser187 residue of the catalytic triad. As a consequence, nucleophilicity of Ser187 increases and it nucleophilically attacks the carbonyl group of the substrate, forming the first tetrahedral intermediate with a negative charge on the oxygen of the carbonyl group. The oxyanion hole is formed by at least one hydrogen bond and is responsible for stabilization of charge distribution as well as the status of the tetrahedral intermediate. In the deacylation step, the enzyme is attacked by a nucleophile (R_2 -OH) resulting in a

new carboxylic acid or carboxylic acid ester with regeneration of enzyme. Hydrolysis occurs when $R_2\text{-OH}$ is water, while alcoholysis occurs when $R_2\text{-OH}$ is an alcohol.¹⁹

To increase the activity, selectivity, thermal stability, and tolerance for polar organic solvents and facilitate the recycling and reusing, lipases are normally used in their immobilized form.^{17,18} Support morphology, surface chemistry, and enzyme packing density largely influence the enzyme activity.^{20,21} Lipases can be generally immobilized *via* three different strategies: (1) binding to a solid support (a) by adsorption (by hydrogen bonds or hydrophobic interactions) (b) by ionic binding (e.g. to ion exchange resins), and (c) by covalent binding (e.g. to epoxy groups), (2) cross-linking (e.g. *via* glutaraldehyde), and (3) entrapment (a) in gels (e.g. calcium alginate) (b) in membrane reactors (e.g. hollow fibre reactors), and (c) in reversed micelles of microemulsions.^{20,22}



Scheme 1.1. Acylation-deacylation mechanism of a lipase.¹⁹

The most widely used immobilized enzyme is Novozym 435. In the manufacturing of Novozym 435, gene coded lipase is transferred from a selected strain of *Candida antarctica* to the host organism *Aspergillus oryzae* that produces the

enzyme. The produced enzyme is immobilized onto a macroporous acrylic resin (Product information, Novo Nordisk). The lipase is about 10 wt% of the total weight of immobilized resin.²³ Active site titration of immobilized CAL-B is employed in a non-aqueous solvent. It was found that 50% of Novozym 435's immobilized protein was catalytically active.²⁴

1.1.2 Enzymatic synthesis of functional polyesters

Enzymatic polyester synthesis is the versatile approach to produce polyesters. It is especially useful when there is the need to synthesize functional polyesters.²⁵ Functional polyesters are polyesters possessing pendant functionalities such as mercapto,²⁶ hydroxyl,²⁷⁻²⁹ epoxy,⁴ halides,³⁰ solketal,³¹ azide²⁸ groups, and unsaturated entities³²⁻³⁶ at the polymer main chain. Functional polyesters are classically synthesized by pre-modification of cyclic monomers followed by ring opening polymerization,^{37,38} which involves several protection-deprotection steps carried out by metal-based catalysts, which are toxic and difficult to remove from the product.³⁰ Polycondensation reactions of monomers containing more than two functional groups lead to hyperbranched or cross-linked polymers.³⁹⁻⁴² Since the enzyme is regio-, enantio- and stereoselective,⁴³⁻⁴⁵ this can help to synthesize chiral and optically active compounds.⁴⁵ These features facilitate the production of linear functional polyesters out of monomers bearing multiple functionalities. Many of them are obtained from renewable resources and difficult to polymerize using chemical catalyst. Poly(butylene succinate-*co*-itaconate) is the most recent example of such polymers.⁴⁶ Enzymatic polymerization is carried out at mild reaction condition, so this feature helps to polymerize thermally sensitive monomers.⁴⁷

Many monomers derived from triglycerides are used for enzymatic polyesterification to produce polyesters.⁴⁸⁻⁵² High molar mass biobased polyesters up to 70,000 kDa, from ω -carboxy fatty acid such as 1,18-*cis*-9-octadecenedioic, 1,22-*cis*-9-docosenedioic, and 1,18-*cis*-9,10-epoxy-octadecanedioic acids and diols, were obtained.⁵³ Glycerol, which is a byproduct of biofuel production, was extensively used for the synthesis of functional polyesters under several reaction conditions and in the presence of lipases derived from different origins.⁵⁴⁻⁵⁷ A linear polymer is obtained as the reaction occurs principally at primary hydroxyl groups of glycerol, only 5-10 mol% of secondary hydroxyl groups are reacted at 50°C.⁵⁴ Poly(glycerol sebacate) (PGS), and

poly(glycerol adipate) (PGA) are examples of glycerol-based polyesters.^{34,54,58} They are also synthesized on large scale.^{33,59}

Sometimes terpolymers are synthesized to achieve high molar mass polyesters which are based on two different types of diols^{56,60} or diacids.⁶⁰ Activated diacids and their derivatives such as divinyl esters may also be used to produce polymers with high molar mass. The most common example of diester used for transesterification reactions is divinyl adipate since it is commercially available and provides an irreversible system, as the condensation side product is vinyl alcohol that tautomerizes to acetaldehyde. Acetaldehyde is a gas at room temperature that can easily leave the system, resulting in a high molar mass product.⁶¹

Like glycerol, other multihydroxy alcohols such as erythritol, xylitol, ribitol, D-glucitol, D-mannitol and galactitol obtained by reduction of sugars,⁵² were also subjected to polymerization.⁶² These reduced sugars are difficult to polymerize because they are only soluble in highly polar solvents such as DMF, DMSO, and pyridine. These highly polar solvents reduce the enzyme activity as it can change the enzyme confirmation.^{63,64} Furthermore, these monomers have a high melting point, so bulk polymerization can only give a highly branched polymer.^{56,57,65} However, sugar-based polyesters were synthesized in acetonitrile, using 60-80 wt% CAL-B with respect to total mass of monomers at 60°C.^{61,66}

In all these polymers pendant functionalities came from alcohols. However, the pendant group could also be part of diacids, example of such diacids are malic acid, tartaric acid, fumaric acid, and glutaconic acid. Tartaric acid is highly polar and is difficult to polymerize since it deactivates the enzyme. The apparent inactivity of CAL-B with tartaric acid could arise from the steric demand of α - and β -substituents.⁶⁷ There are several reviews on enzymatic polymerizations that summarize different products obtained through enzymatic reaction.^{3,16}

There are a plethora of factors that can affect enzymatic polymerization including temperature, pressure, water content, enzyme concentration and nature of the solvent. The selection of appropriate organic solvents is crucial as it can alter enzyme selectivity by changing the configuration of monomers.^{68,69} It was found that low polarity solvents, with partition coefficients with water greater than 1.9 such as *n*-hexane, diphenyl ether and toluene are more suitable for enzymatic reactions. In contrast polar solvent strip off water from the active site of an enzyme called bound water necessary for

enzyme activation, hence resulting in low molar mass products due to hydrolytic cleavage of ester links.^{3,46,70,71} The polymer conformation and radius of gyration in a solvent may alter its ability to react.¹³

Enzymatic esterification is a green process that could be carried out in solvent free conditions,⁶⁰ in ionic liquids,⁷² and in super critical carbon dioxide (scCO₂).⁷³⁻⁷⁶ The stoichiometric ratio of DVA/diol is an important factor to generate high molar masses. The molar mass is reduced significantly when the reaction deviates from equimolarity of the functional groups.⁵⁴ Increasing the ratio of enzyme to substrate concentration (E/S) leads to a more rapid attainment of higher molar mass polyesters within a shorter times.⁷¹

Besides polymer synthesis, enzymes could also be used to synthesize monomers from biomass.⁷⁷ Another advantage of enzymatically synthesized polymers is that they can be degraded by the same enzyme that was used previously for their syntheses, hence it helps for polymer biodegradability and recycling.⁷⁸⁻⁸⁰

1.1.3 Grafting of functional polyesters

The presence of functional pendant groups along the polymer backbone is a highly efficient source of tailoring the properties of polyesters including features such as hydrophilicity, biodegradation rates, and bioadhesion.⁸¹

Comb-like polyesters can be synthesized by grafting from, grafting onto and grafting through strategies.⁸² Kalinteri *et al.* obtained amphiphilic comb-like polyesters by direct esterification of fatty acid with pendant hydroxyl groups of the polyester. Later on, they used them to prepare nanoparticle (NP) for drug delivery systems (DDS).⁸³ In another study, Orafai *et al.* have used fatty acid (caprylic and stearic acid) and amino acid (tryptophan) grafted PGA and determined the surface free energy of prepared nanoparticles from these polymers.⁸⁴ Zhang *et al.* have used a one-pot synthesis approach for the preparation of grafted polyesters with unsaturated fatty acids to form polymeric triglyceride analogs.⁸⁵ These grafted polyesters could also be cured to produce biodegradable polymeric networks.^{34,86} Our group has extensively studied poly(glycerol adipate) grafted with saturated and unsaturated fatty acids of various lengths. It was discovered that the degree of substitution is important to attain certain morphologies of nanoparticles obtained in aqueous media. These nanoparticles were

further used as a vehicle for drug delivery systems.^{87,88} Later on, the behavior of these amphiphilic polymers at the air/water interface was studied.⁸⁹

Besides PGA, sugar-based polyesters such as poly(xylitol adipate)(PXA) and poly(D-sorbitol adipate) (PDSA) were also grafted with stearyl chains that produce unique nanoparticles in aqueous media.⁹⁰ Grafted polymers could also be synthesized using other chemistries other than direct esterification. Thus, Naolou *et al.* synthesized comb-like polymers containing blocks of two crystallizable side chains *i.e.* poly(ϵ -caprolactone) and poly(ethylene oxide). They explained comprehensively the crystallization behavior of grafted copolymers.⁹¹ The phase behavior of these amphiphilic polymers at the air/water interface was also investigated.⁹² In another study, polyesters with azide pendant group were synthesized from polycondensation reaction of an azide group-containing diol (synthesized from 3-hydroxymethyl-3-methyloxetane) and grafted with azide-alkyne click reaction using PEO to produce water-soluble polymers.²⁸ Later on, Wu *et al.* synthesized azido functionalized polyesters starting from 2-azido glycerol which after click reaction with PEG, produced a comb-like polymer. This comb-like polymer self-assembles in the form of spherical micelles in aqueous media, and it has a relatively low critical micelle concentration (CMC).⁹³ Yet in another approach, grafted polyesters were obtained using chloro functionalized caprolactone. After polymerization the chloro-functionality was replaced by an azide group which after azide-alkyne click reaction, produced grafted polyesters.⁹⁴⁻⁹⁶ In another approach polyesters with pendant acetylene groups were synthesized by azide-alkyne click reaction with azide functionalized PEG chains or oligopeptides. This produced grafted polymers that could be used for tissue engineering.⁹⁴ Jbeily *et al.* have converted hydroxyl pendant group of polyesters to macro-initiators for atom transfer radical polymerization (ATRP), that after ATRP of poly(glycerol methacrylate) (PGMA) produced a water-soluble copolymer.^{97,98} In another approach a methacrylic backbone was synthesized by ATRP followed by eROP of ϵ -caprolactone to produce a grafted copolymer.⁷⁶ Grafting of functional polyesters can also be used to prepare biodegradable elastomers.⁹⁹ Mecerreyes *et al.* obtained grafted polymers by a combination of ROP and ATRP followed by the formation of polymeric networks using a Micheal type addition.¹⁰⁰

Functional polyesters provide an opportunity to conjugate proteins and drugs with them. In this respect Wersig *et al.* used poly(glycerol adipate) for conjugation of

indomethacin drug.¹⁰¹ In another report Garnett and coworkers have conjugated methotrexate which is an anticancer drug to poly(glycerol adipate) and have done toxicity and degradation studies of the polymer conjugates.¹⁰²

1.2 FUNDAMENTALS OF LIPID SELF-ASSEMBLY

Glycerol monooleate (GMO) is a molecule composed of glycerol acylated with oleic acid (monounsaturated omega-9 fatty acid) mainly at position 1 of glycerol. The chemical structure of GMO is shown in Figure 1.1.

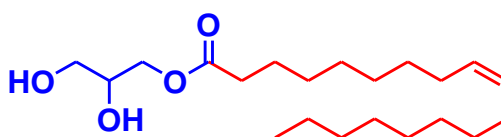


Figure 1.1. Chemical structure of glycerol monooleate (GMO).

The other two hydroxyl groups of glycerol together with the ester bond provide the polar character to this part of the molecule also called the *head* group. They can form hydrogen bonds with water molecules in aqueous medium. In contrast the oleic acid chain is hydrophobic and is usually referred as the *tail*. The resulting glycerol monooleate is an amphiphilic molecule with a hydrophilic-lipophilic balance (HLB) value of 3.8 as determined by Griffin's method.¹⁰³ GMO is also referred to as magic lipid as it shows a rich mesomorphic behavior.¹⁰⁴ Lipids self-assemble into different liquid crystalline structures under varying conditions of temperature (thermotropic phases),^{105,106} pressure (barotropic phases),¹⁰⁷ magnetic fields,¹⁰⁸ water (lyotropic phases),^{105,109} and by the addition of a third component.¹¹⁰⁻¹¹⁵

One of the major driving forces for different self-assemblies of lipids in water is the hydrophobic effect, (which acts to minimize the interface between the hydrocarbon tails of the amphiphile and the aqueous environment) together with others interactions, including van der Waals interactions and head group hydrogen bonding.¹¹⁶ The self-assembling process driven by these forces is spontaneous, i.e. for this process the value of Gibbs free energy of aggregation (Equation 1.1) is negative.^{117,118}

$$\Delta G_{agg} = \Delta H_{agg} - T\Delta S_{agg} \quad 1.1$$

Here ΔS_{agg} is the change in entropy of aggregation and ΔH_{agg} is the change in enthalpy of aggregation. A direct relationship between Gibbs free energy of aggregation and critical aggregation concentration is given by:

$$\Delta G_{agg} = RT \ln(CAC) \quad 1.2$$

where R is universal gas constant and T is the absolute temperature.¹¹⁹ There are several factors which determine or affect the formation of particular structures. The concentration, temperature and shape of an amphiphile play a decisive role. Polymers form micelles when the concentration is equal to or greater than the critical micelle concentration (CMC), and when the temperature is greater than the critical micelle temperature (CMT), also known as the Kraft temperature.¹⁰⁴ Besides micelles, several other self-assemblies are also possible. The fundamental principle behind different self-assemblies of amphiphilic molecules is their shape. The shape of the molecule can be described qualitatively according to the theory by Israelachvili.¹²⁰ This theory is based on the dimensionless packing parameter γ , also called the critical packing parameter or shape factor.^{120,121}

$$\gamma = \frac{v_l}{a_0 l_c} \quad 1.3$$

Where l_c is the length of hydrophobic chain of lipid, a_0 is the effective amphiphile head group area, and v_l is the average volume occupied by an amphiphilic molecule. The hydrocarbon chain length and volume for simple, single chained amphiphiles may be evaluated by the empirical formula.¹²²

$$v_l = (27.4 + 26.9n_c) \text{ \AA}^3 \quad 1.4$$

$$l_c = (1.5 + 1.26n_c) \text{ \AA} \quad 1.5$$

Here, n_c is the number of carbon atoms. The shape factor γ describes the local packing constraint and allows amphiphiles to be categorized by their shape (see Figure 1.2). $\gamma > 1$ gives *type 2* or inverse self-assembly (curvature towards the water regions) e.g. wedge shape molecules like MAG (monoacylated glycerol) and block copolymers having a relatively more hydrophobic character and small head groups. $\gamma < 1$ shows *type 1* or normal self-assembly (curvature towards the chain region). Molecules with the larger head group, $\gamma = 1$ (flat bilayer with nearly zero curvature) e.g. cylindrical shape molecule shows lamellar morphology.¹²³ In case of GMO, the *cis* double bond at the

9,10-position makes the hydrocarbon tail sterically demanding, thus triggering the formation of inverse or *type 2* micelles with $\gamma > 1$.

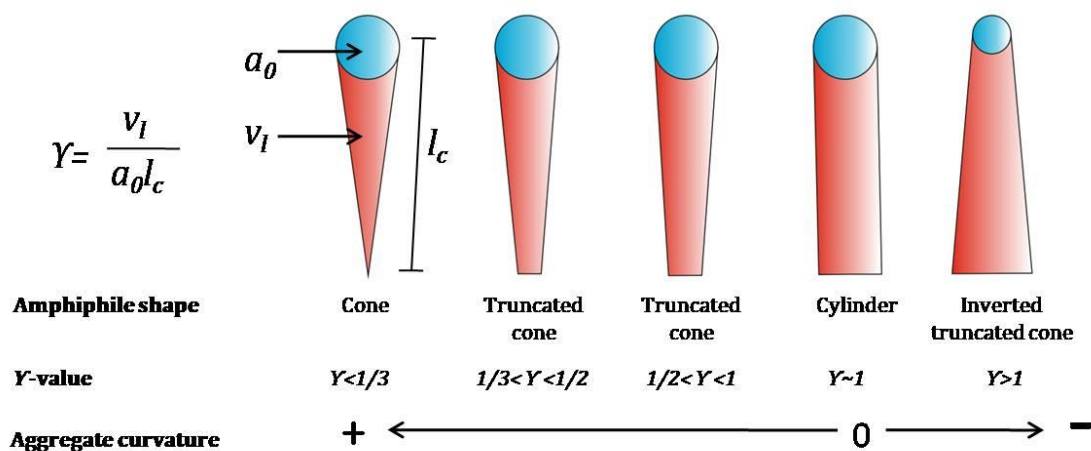


Figure 1.2: The critical packing parameter γ of amphiphiles and the related aggregate curvature (Figure is modified from literature.¹²⁴).

In addition to γ , degree of hydration of amphiphilic molecule is an important factor that leads to different self-assemblies. Most common self-assemblies are lamellar, hexagonal and bicontinuous cubic phases. Additional phases are formed, usually by the incorporation of other components and/or energy. Due to their dimensional arrangement in the nanometer range and solid-liquid mediation, the lipid polymorphs are also called liquid crystalline nanostructures.

1.2.1 Lipid polymorphism

1.2.1.1 The lamellar phase

The lamellar phase consists of a lipid bilayer stacked on each other separated by a water layer. Three main types of lamellar phase have been given in the literature,¹²⁵ crystalline lamellar L_c , fluid lamellar L_α and lamellar gel L_β phases. The lamellar phase is characterized by SAXS peaks which appear in the ratio 1:2:3:4..... Different types of lamellar phases could be distinguished from each other by comparing their characteristic WAXS pattern. In the L_c phase, molecules are ordered into a fixed position. It shows much intense Bragg reflections. The fluid lamellar L_α phase is a true liquid crystalline phase. In this phase, the head groups are completely disordered and the hydrocarbon chains are fluid like. It shows a diffuse scattering in the wide angle region, typically at 4.5 \AA while the lamellar gel L_β phase is formed at high temperatures.

In this phase the hydrocarbon chains are arranged parallel to the layer normal. Some other lamellar phases could also be observed. These are the tilted gel $L_{\beta'}$ phase, the interdigitated gel $L_{\beta I}$ phase, and the rippled gel $P_{\beta'}$ phase.

The tilted gel $L_{\beta'}$ is a tilted version of the L_{β} phase, and different tilt directions with respect to the underlying hexagonal lattice may occur. The tilting occurs when the head group packing requirement is exceeded. Above a certain excess of tilting the packing is stabilized by inter-digitation of the chains (without tilting) allowing head groups to pack in twice the area than that of the normal gel phase. This is called the interdigitated gel phase $L_{\beta I}$. The lamella of $L_{\beta'}$ phase may undergo periodic modulation which results in a rippled phase $P_{\beta'}$; observed at high temperatures just below the fluid lamellar phase L_{α} .¹²⁵⁻¹²⁷ A schematic description of all lamellar phases is shown in Figure 1.3.

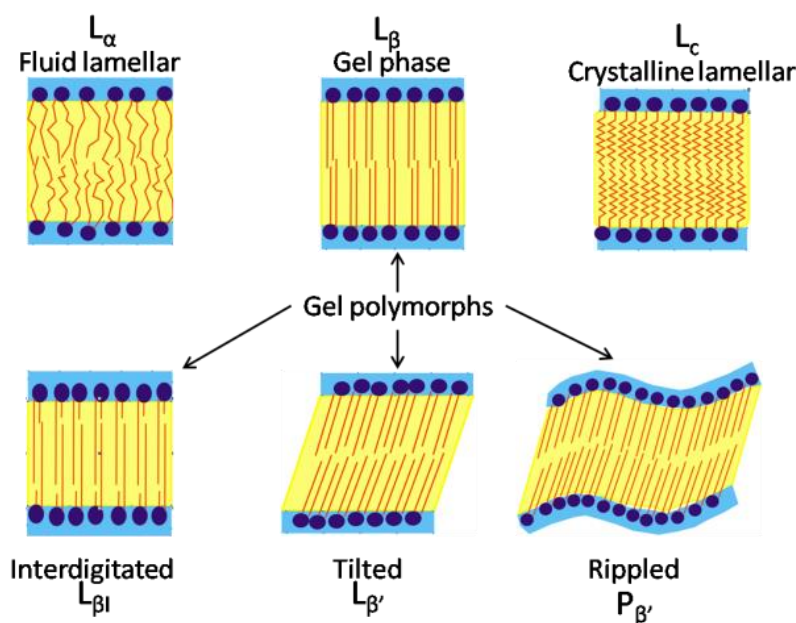


Figure 1.3. Commonly observed crystalline and liquid crystalline lamellar phases observed in lipids. Figure modified from Kulkarni *et al.*¹²³

The lattice parameter for lamellar phases can be calculated from the corresponding reciprocal spacing, $s_{lam} = (n/a_{lam})$, where n is the order of the reflection (1, 2, 3, 4,.....), a_{lam} or d is equal to the lattice parameter of the lamellar phase, i.e. the distance between the repeat unit. In the lamellar phase, the monolayer thickness can be determined using the relation, $d_l = 0.5(a_{lam} - d_w)$ where d_w is the water layer thickness which is $\phi_w d$ (here ϕ_w represents water volume fraction).

1.2.1.2 The hexagonal phase

The hexagonal phase is comprised of a group of micellar cylinders onto a 2-D hexagonal lattice.¹²⁸ The hexagonal phase may be ‘normal’ H_1 or ‘reverse’ H_2 . The normal hexagonal phase has a curvature towards the hydrocarbon chain region of the lipid, in contrast, the reverse hexagonal phase displays a mean curvature towards the aqueous interior. The schematic diagram of the reversed hexagonal H_2 phase is shown in Figure 1.4(a). The hexagonal phase is distinguished by SAXS peaks in the ratio of $1:\sqrt{3}:\sqrt{4} \dots$

For the hexagonal phase, the lattice parameter a_{hex} is calculated from the following relation.

$$a_{hex} = \frac{4\pi\sqrt{h^2 + k^2 + hk}}{\sqrt{3}q} \quad 1.6$$

The diameter of the water cylinder is given by:

$$d_w = \sqrt{\frac{2\sqrt{3}}{\pi}(1 - \phi_l)a_{hex}^2} \quad 1.7$$

Where, ϕ_l is the volume fraction of lipid.

1.2.1.3 The micellar cubic phase

The micellar cubic phase is formed by complex packing of reverse micelles on a cubic lattice that has curvatures larger than the reversed hexagonal phase.¹²⁵ The micellar cubic phase has a $Fd3m$ symmetry. The formation of the micellar cubic phase requires a minimum of two types of amphiphilic molecules, one of which is more strongly polar (e.g. GMO and diacyl phosphatidyl choline (PC)) and the other is weakly polar (e.g. fatty acid (FA) and diacyl glycerol). The incorporation of a weak amphiphilic compound reduces the effective hydrophilicity of the lipid head group region. This dehydration of the head group tends to drive the phase equilibrium towards the inverse phases with increasing interfacial mean curvature. The structure is discontinuous and made up of two populations of reversed micelles. (see Figure 1.4(b)).¹⁰⁴ Per unit cell of the $Fd3m$ cubic phase, there are eight larger inverse micelles, arranged tetrahedrally on a diamond lattice and sixteen small inverse micelles. To explain the existence of two types of micelles, it is assumed that the amphiphile composition is probably inhomogeneous between two types of micelles.^{129,130} This

could be the reason why the $Fd3m$ cubic phase usually does not appear in lipid/water binary systems. GMO does not show this phase in pure water, but with the addition of other components to it, e.g. oleic acid or poly(ethylene imine) (PEI).^{110,131} The $Fd3m$ phase shows a characteristic pattern in the SAXS traces with the peak ratio, $\sqrt{3}, \sqrt{8}, \sqrt{11}, \sqrt{12}, \sqrt{16} \dots$ ¹⁰⁴

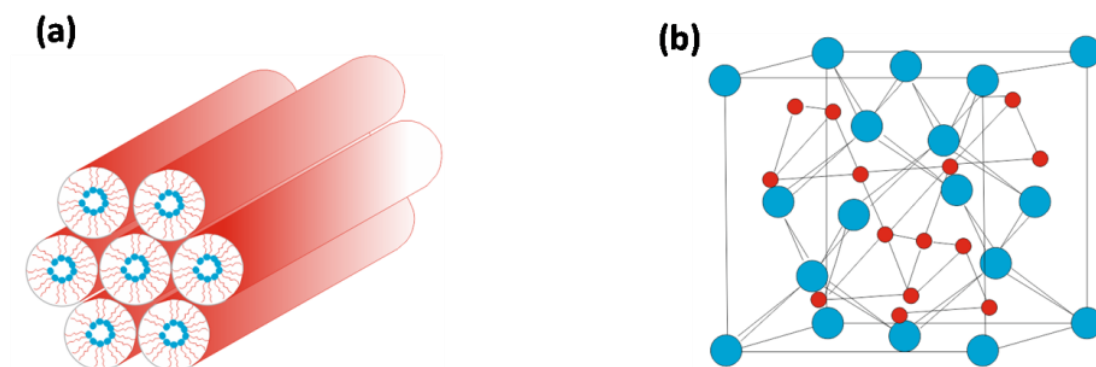


Figure 1.4. Schematic structure of (a) the reverse hexagonal phase (H_2), (b) the cubic phase $Fd3m$. The structure consists of eight larger inverse micelles (polar cores in blue colour) and 16 smaller inverse micelles (polar cores in red colour). The remaining volume is filled by the fluid hydrocarbon chains and water (Figures are modified from literature¹³⁰).

1.2.1.4 Bicontinuous phases

1.1.1.1.1 The sponge phase

The sponge phase L_3 is a bicontinuous phase found in several amphiphiles. This phase has a bicontinuous sponge-like structure with a lipid bilayer separating the polar solvent space into two disconnected volumes, similar to bicontinuous cubic phases. The only difference is that they do not possess long-range order and their structure can be considered as a melted cubic phase.^{132,133} In the phase diagrams, L_3 -phases occupy regions adjacent to lamellar phases and both reversed as well as normal type sponge phases are possible.¹³⁴ It is identified by a broad peak in the SAXS region. The GMO-water system itself does not show this phase unless a third component such as low molar mass PEG¹³⁵ or salt^{136,137} is added.

1.1.1.1.2 Bicontinuous cubic phases

In the last couple of decades, there is an exponential increase in the use of bicontinuous cubic phases in drug delivery system^{138–140} and in membrane protein crystallization.¹⁴¹ Bicontinuous cubic phases have an intermediate curvature between a flat lamellar phase and a cylindrical hexagonal phase. These phases are described on the basis of infinite periodic minimal surfaces (IPMS).¹⁴² IPMS have zero mean curvature H and negative Gaussian curvature K . They consist of parallel curved bilayers, forming a complex network with 3-D cubic symmetry, which separates two continuous but non-intersecting water channels.¹⁴³ Schwarz, for the first time, introduced mathematically, double diamond and primitive surfaces.^{142,144} Later, a closely related structure known as gyroid was introduced by Schoen.¹⁴⁵ The cubic phases are characterized by their crystallographic space groups having $Im3m$ (primitive), $Pn3m$ (double diamond), and $Ia3d$ (gyroid) symmetry identified by corresponding space group numbers 229, 224 and 230.¹²² Schematic diagrams of all bicontinuous cubic phases are shown in Figure 1.5.

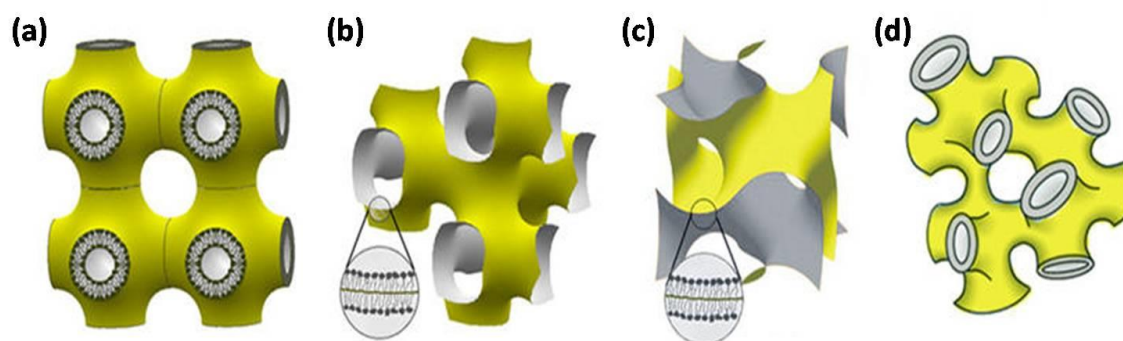


Figure 1.5. Bicontinuous phases formed by lipids. (a) Bicontinuous cubic phase $Im3m$ (Q^P_2 , Q_{229}), (b) bicontinuous cubic phase $Pn3m$ (Q^D_2 , Q_{224}), (c) bicontinuous cubic $Ia3d$ (Q^G_2 , Q_{230}), and (d) sponge phase (Figure is adapted from Koynova *et al.*¹⁴⁶).

The inverse bicontinuous cubic phase of *type 2* consists of a single continuous lipid bilayer wrapped on a minimal surface on either side of which lies a continuous region of water. In the $Im3m$ phase, water channels meet at 90° in 6-way junctions and in the $Pn3m$ phase in 4-way junctions at 109.5° . In the $Ia3d$ phase, water channels meet in 3-way junctions at 120° . Due to the cubic symmetry, they are isotropic, hence appear dark when viewed through a polarized light microscope.^{104,109,122}

The most common way to identify these phases is by their SAXS pattern where the scattering vector q of the Bragg peaks is given by

$$q = \frac{2\pi\sqrt{h^2 + k^2 + l^2}}{a_{cubic}} \quad 1.8$$

where, h , k and l are Miller indices of the Bragg peak, and a_{cubic} is the lattice parameter of the cubic phase. The individual type of the cubic phase is identified by the characteristic ratios as $3m : \sqrt{2}, \sqrt{4}, \sqrt{6}, \sqrt{8}, \sqrt{10}, \sqrt{12}, \sqrt{14}, \sqrt{16}, \sqrt{18}$, $Pn3m : \sqrt{2}, \sqrt{3}, \sqrt{4}, \sqrt{6}, \sqrt{8}, \sqrt{9}, \sqrt{10}, \sqrt{11} \dots$, and $Ia3d : \sqrt{6}, \sqrt{8}, \sqrt{14}, \sqrt{16}, \sqrt{20}, \sqrt{22}, \sqrt{24}, \sqrt{26} \dots$

The monolayer thickness or lipid chain length l_c of the cubic phases is determined by solving the equation 1.9.^{142,147}

$$\Phi_{lipid} = 2\sigma \left(\frac{l_c}{a_{cubic}} \right) + \frac{4}{3}\pi\chi \left(\frac{l_c}{a_{cubic}} \right)^3 \quad 1.9$$

Where l_c is lipid chain length/monolayer thickness, a_{cubic} is the lattice parameter of the corresponding phase, χ is the Euler-Poincare characteristics. The lipid length throughout the unit cell of such cubic phases can be assumed to be constant. The interfacial area integrated over a single monolayer is given by equation 1.10.¹⁴²

$$A_l = \sigma a_{cubic}^2 + 2\pi\chi l_c^2 \quad 1.10$$

σ is a unitless quantity that describes the ratio of the area of the minimal surface in a unit cell to the (unit cell volume)^{2/3}. The space group of the cubic phase determines the type of IPMS associated with the cubic phase and thus, the values of σ and χ are calculated (see Table 1.1).

Table 1.1. The Euler-Poincare characteristic χ and the surface area of the minimal surface per unit volume σ for different types of infinite periodic minimal surface.¹²²

Space group	Space group number*	IPMS Type	χ^{**}	σ^{**}
<i>Pn3m</i>	224	D(Diamond)	-2	1.919
<i>Im3m</i>	229	P(Primitive)	-4	2.345
<i>Ia3d</i>	230	G(Gyroid)	-8	3.091

*Number corresponds to the space group of the cubic lattice.** Type refers to common names used to identify particular IPMS.¹⁴²

The cross-sectional area per lipid molecule at a distance l from the minimal surface is given by¹⁴⁸

$$A_{cs}(l) = \frac{2A(l) \cdot v_{lipid}}{\phi_{lipid} \cdot a_{cubic}^3} \quad 1.11$$

where, v_{lipid} and ϕ_{lipid} are the molecular volume and the volume fraction of the lipid, respectively. By assuming a lipid-specific volume \tilde{v} of $1 \text{ cm}^3 \cdot \text{g}^{-1}$ ($10^{24} \text{ \AA}^3 \cdot \text{g}^{-1}$), v_{lipid} is calculated as

$$v_{lipid} = \frac{M \tilde{v}_{lipid}}{N_A} \quad 1.12$$

Where, M is the molar mass of lipid and N_A is the Avogadro's number. For GMO the value of v_{lipid} is $593 \text{ \AA}^3/\text{molecule}$. The number of lipid molecules in the unit cell of the cubic phase n_{lipid} is given by

$$n_{lipid} = \frac{\phi_{lipid} \cdot a_{cubic}^3}{v_{lipid}} \quad 1.13$$

The radius of the water channel r_w is calculated based on minimal surfaces¹⁴⁷

$$r_w = \left(-\frac{\sigma}{2\pi\chi} \right)^{1/2} a_{cubic} - l_c \quad 1.14$$

Putting values of σ and χ for corresponding cubic phases from Table 1.1, the equation takes the following form, for the Pn3m phase: $r_w = 0.391a_{cubic} - l_c$, for the Ia3d phase $r_w = 0.248a_{cubic} - l_c$, for Im3m phase: $r_w = 0.306a_{cubic} - l_c$.

1.2.2 Binary phase diagram of GMO-water system

To understand the GMO-water polymorphism, the temperature-GMO content in water phase diagram was established by Lutton.¹⁴⁹ He used polarized optical microscopy to identify different phases. He has found lamellar, hexagonal and cubic phases as neat, middle, and viscous isotropic phase, respectively. His phase diagram could not help much as all the cubic phases appear black under polarized optical microscopy, hence one cannot distinguish between different cubic phases. Then, great efforts have been made to explore the equilibrium phase behavior of GMO in water. In this regards, several authors have contributed to identify various phases and explained their structure.¹⁵⁰⁻¹⁵³

Hyde *et al.* presented a complete phase diagram with the help of polarized optical microscopy and X-ray diffraction.¹⁵⁴ The phase behavior was studied for a temperature

range of 20-110°C and for a hydration of 0 to 40 wt%. They identified a different region in the phase diagram labeled with different phases such as fluid lamellar L_α , cubic $la3d$, cubic $Pn3m$, reverse hexagonal H_2 and fluid isotropic L_2 phases quite clearly along with mixed phase regions.¹⁵⁴ Caffery and co-worker have extensively studied the mesophase behavior of several monoacyl glycerols (MAGs) including GMO and determined the structure parameter of the GMO-water system.^{105,155} Briggs *et al.* explained the equilibrium phase behavior for a temperature range from 0 to 104°C and for the hydration level from 0 to 47 wt% in steps of 5°C and average 2 wt% water respectively.¹⁵⁶ The phase region is quite similar as was observed by Hyde *et al.*, however, they ensured that all the observed phases are in equilibrium.

Later, Qui *et al.* described the metastable phase regions (below 20°C) in their phase diagram.¹²¹ Combining the low-temperature region with that of the earlier phase diagram, the new phase diagram was merged which is shown in Figure 1.6. In Figure 1.6 the low-temperature part of the phase diagram is included, showing a crystalline phase $Pn3m$ along with water and ice.

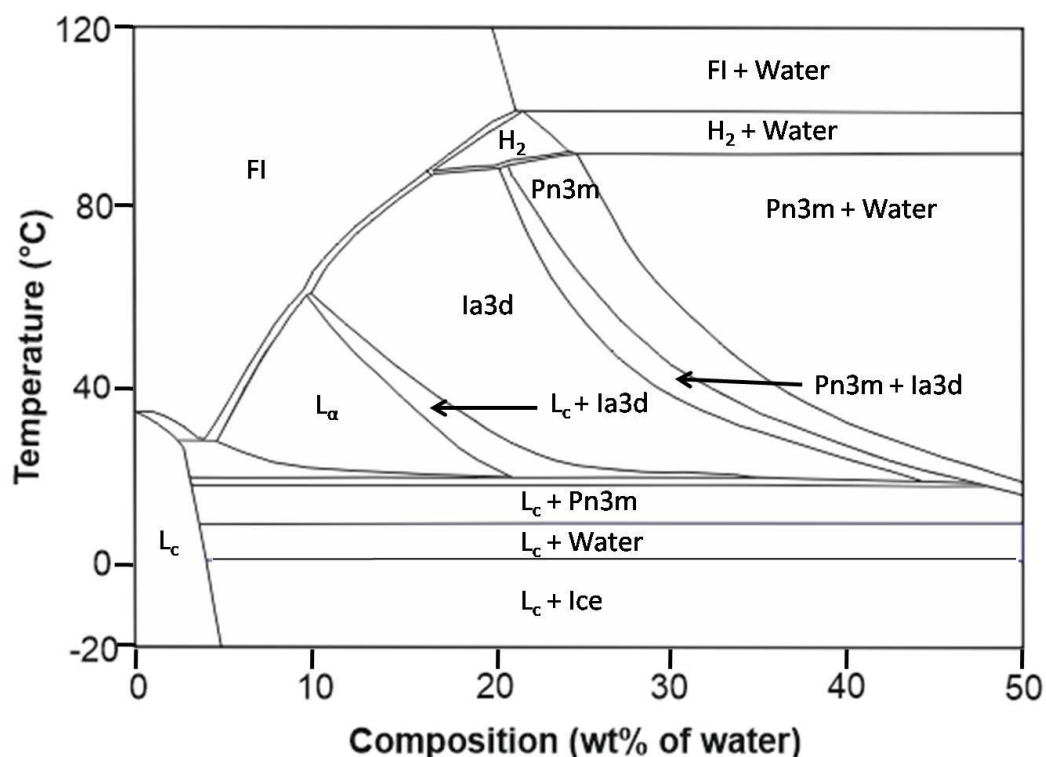


Figure 1.6. Composition phase diagram of the GMO-water system that combines the phase diagram of Briggs *et al.* and that of Qiu and Caffery. (Figure is modified from Qiu *et al.* ¹⁰⁶)

At low temperature and low water content, a lamellar crystalline region L_c exists that contains more than one polymorph. The L_c phase was identified in dry samples

and the polymorphism found in this region was not investigated in detail. At low water content, the L_c phase melts with increasing temperature into a fluid isotropic phase FI , which is also known as inverse micellar phase L_2 .¹⁵⁴

With increasing water content, a phase transition from the crystal lamellar L_c phase into the lamellar liquid crystalline phase L_α takes place. With increasing temperature, the L_α phase melts again into the fluid isotropic FI phase. With further increasing water content, the bicontinuous cubic phases are formed with two different space groups, $Ia3d$, and $Pn3m$. For composition with water contents of 17 wt% or more, with increasing temperature, a phase transition from the bicontinuous cubic phase into an inverse hexagonal phase H_2 and finally into the isotropic FI phase takes place. Above a certain amount of water, phase separation occurs into a structured phase and an excess water phase indicating the maximum water carrying capacity of the individual phase. It is noteworthy that the bicontinuous cubic $Pn3m$ phase can carry more water (~40 wt%) than the H_2 (~25 wt%) or the FI phase (~20 wt%). Excess-water phase separation allows dispersing the respective structured phase into water called a nanostructured emulsion.¹⁵⁷ A more detailed discussion about the dispersion of submicron cubic particles (cubosomes) and their stabilization will be given later in this chapter.

1.2.3 The effect of additives on the mesophase behavior of the GMO-water system

The liquid crystalline phases of the GMO-water system can tolerate a specific amount of a third component. A further addition to the system results in swelling or shrinkage of water channels and ultimately to phase transitions. Misquitta and Caffrey have done a detailed study on the effect of detergent on the mesophase behavior of the GMO-water system. They observed a phase transition from $Pn3m$ to the lamellar L_α phase *via* $Ia3d$ when *n*-alkyl-*b*-D-glucopyranosides were added.¹⁵⁸ Sodium chloride (NaCl) or sodium sulphate (Na_2SO_4) are well-known kosmotropes which show strong hydration behaviour resulting in the dehydration of the GMO head groups. This results in a decrease in occupied surface area of lipid head group and hence the radius of the water channel decreases and so the lattice parameter.^{159,160} On the contrary, a chaotropic electrolyte such as sodium iodide (NaI), sodium thiocyanate (NaSCN), potassium thiocyanate (KSCN), and urea leads to an increase in the hydration of the

monoolein head group resulting in an increase of the radius of the water channel and hence the lattice parameter.^{136,160} Sugars also act as kosmotropes and induce a phase transition from *Ia3d* to *H₂* via *Pn3m*. Some cryoprotectants such as glycerol and DMSO also affect the GMO-water phase behavior. Glycerol (being kosmotropic), when added to hydrated GMO, decreases the lattice parameter of the cubic phase and reduces the cubic phase region. On the other hand, DMSO (being chaotropic) increases the *Pn3m* and *Im3m* coexistence regions and also increases the lattice parameter of cubic phases.^{136,161}

The effect of several biomacromolecules, especially soluble proteins, on the mesophase behavior of the GMO-water system has also been studied. The protein-GMO-water phase diagram was constructed for lysozyme. It shows all three bicontinuous cubic phases.¹⁶²⁻¹⁶⁵

The effect of several amphiphiles having different degrees of unsaturation and hydrocarbon chain lengths on the lipid cubic mesomorphism was also investigated. It was observed that all single chain amphiphiles having $\gamma \geq 1$ results in a phase transition from cubic *Ia3d* to the more negatively curved hexagonal *H₂* phase and ultimately to the *L₂* phase.^{109,122} In some cases, the micellar cubic *Fd3m* phase can be observed between the *H₂* and *L₂* phases.¹⁰⁹

For many molecules, a phase transition from the cubic *Pn3m* to the *L_α* phase occurs via the cubic *Im3m* and cubic *Ia3d* phase. This transition is due to the addition of an amphiphile with $\gamma < 1$ which leads to less negatively curved phases than the cubic phase. Cubosomes are an effective vehicle for drug delivery system. Incorporation of hydrophobic drugs induce a phase transition from cubic *Pn3m* to negatively curved *H₂* and *FI* phases. The hydrophobic character relieves packing frustration of the alkyl chains.¹⁶⁶

Cubic phases are a good source for *in meso* crystallization of membrane proteins. The effect of poly(ethylene glycol) (PEG) of various chain lengths on the cubic phase of the GMO/water system are studied for the purpose of crystallization of proteins.^{141,167} It is reported that a low molar mass PEG such as PEG400 induces a phase transition from cubic *Pn3m* to the *FI* phase of the GMO/water system, while PEG1000 does not induce the phase transition of the cubic *Pn3m* phase of the GMO/water system. However, PEG with higher molar masses (3,500-20,000 g·mol⁻¹) induces a phase

transition of cubic $Pn3m$ to the L_{α} phase as a consequence of osmotic pressure that results in dehydration of the cubic phase.

Kumar *et al.* presented a detailed investigation of the phase behavior of the glycerol monooleate-water-PEI system. According to them, the GMO-water systems containing small fractions (2-4 wt%) of low molecular weight PEI form an ordered reverse micellar cubic phase with $Fd3m$ symmetry. For higher molar mass (25 kDa), the $Fd3m$ phase is formed at 4 wt% PEI, in coexistence with the fluid isotropic FI phase.¹¹⁰

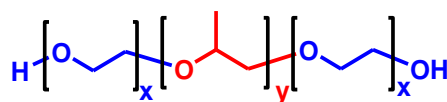
For all solvents and soluble additives, the tendency to interact with the polar-apolar interface was found to be important. The insertion of the soluble additives into the head group region was found to lead to the formation of the less negatively curved L_{α} phase due to a decrease in the γ -value with increasing head group volume ($\gamma > 1$ to ~ 1). This was observed for solvents, strong chaotropic salts, short peptides that interact with the lipid membrane, block copolymers with a relatively large amount of PPO blocks, and a few hydrophilic small molecules.¹⁰⁹ Several additives such as block polymers and PEGylated lipids etc. are used to stabilize submicron particle dispersions of the cubic phase (cubosomes). The details of steric stabilizers used for cubosome dispersions are given in the following section.

1.3 STERIC STABILIZERS FOR CUBOSMES

As discussed before, the bulk cubic phase can be dispersed in water into submicron particles. Submicron particles of bulk cubic phases are called cubosomes. These have gained huge interest for their use as drug delivery vehicle and *in meso* crystallization of membrane proteins.^{138,141,168,169} Cubosome dispersions are obtained by two approaches (a) top-down (dispersing the bulk cubic phase using high energy), and (b) bottom-up (dispersing the lipid in water after dissolving it in an organic solvent).¹⁷⁰ Cubosomes are sterically less stable because of weak van der Waals forces which cannot prevent coalescence. Therefore, a steric stabilizer is always required for the stability of cubosomes. An ideal stabilizer prevents flocculation without disrupting the inner cubic structure. The structure and concentration of stabilizers are two important factors responsible for the stability of a dispersion.¹⁷¹

Most commonly used polymers as steric stabilizers are triblock copolymers consisting a PPO block sandwiched between two PEO blocks. These are known as

Poloxamer™ or Pluronics®. Among pluronics, Pluronic®F127 is the most employed steric stabilizer (see Figure 1.7 for the structure). It consists of a middle block of PPO of 65 monomer units and two blocks of PEO of 100 monomer units to both sides of PPO (PEO₁₀₀-PPO₆₅-PEO₁₀₀) having a molar mass of 12,600 g·mol⁻¹. The PPO block serves as an anchor while the PEO blocks in the water channels or spread outside to provide steric shielding.^{172,173}



Pluronic

F127 ($x = 100$, $y = 65$)

F108 ($x = 132$, $y = 50$)

F68 ($x = 76$, $y = 29$)

P105 ($x = 37$, $y = 56$)

P104 ($x = 27$, $y = 61$)

Figure 1.7. Chemical structure

of some pluronics.

Pluronic® has been employed to several cubosome dispersions, including GMO, glycerol monolinoleate and phytantriol. Among these, GMO was most extensively studied. For a low concentration of Pluronic®F127 (<4 wt% with respect to GMO) cubosomes with *Pn3m* symmetry, and for a higher concentration of Pluronic®F127 (10 wt% with respect to GMO), cubosomes with *Im3m* symmetry are produced.^{131,174} It is important that *Pn3m* symmetry of cubosomes should remain as the change to *Im3m* space group symmetry indicates destabilization of the *Pn3m* cubic symmetry which results in fast drug release.¹⁷⁵

However, the *Pn3m* cubic phase of glycerol monolinoleate¹⁷⁶ or phytantriol¹⁷⁷ retained its symmetry even at high concentration of Pluronic®F127. Besides Pluronic®F127, other pluronics could also be used as steric stabilizers. Chong *et al.* have done a comprehensive investigation on a series of pluronics and conclude that Pluronic®F108 has shown a better stabilization effect for cubosomes than Pluronic®F127.^{178,179} Pluronic®F108 has longer PEG chains compared to Pluronic®F127. It has the structure PEG₁₃₂PPO₅₀PEG₁₃₂ and has a molar mass of 14,600 g·mol⁻¹. After these findings, researchers had frequently used Pluronics®F108 for stabilizing drug loaded cubosomes.^{180,181} Several other low molar mass pluronics such as F68, P104, P105 were also used.^{178,182}

Several lipids, after making them water-soluble by attaching PEG chains are also reported as steric stabilizers for cubosomes, e.g. GMO connected with a short PEG chain (MO-PEG660)¹⁸³ or a long PEG chain containing monoolein (MO-PEG2000).¹⁸⁴ In addition, PEGylated phospholipids were also used as a steric stabilizer. These include PEGylated 1,2-dioleoyl-*sn*-glycerol-3-phosphoethanolamine (DOPE-PEG2000), PEGylated 1,2-distearoyl-*sn*-glycerol-3-phosphoethanolamine (DSPE-PEG2000), and PEGylated 1,2-dimyristoyl-*sn*-glycerol-3-phosphoethanolamine (DMPE-PEG550). They produce cubosomes with *Im3m* symmetry.¹⁸⁵⁻¹⁸⁷ Furthermore, the polysorbate series (Tween® 20, 40, 60, 80) was also studied to investigate their ability of steric stabilization of cubosomes and it was observed that only Tween® 20 and 80, commonly known as polysorbate 20 and polysorbate 80 are better stabilizers compared to other compounds of this series.^{182,188} Chong *et al.* used PEG-stearates (Myrj-series) to stabilize cubosomes from phytantriol in aqueous media. Among all explored PEG-stearates, i.e. PEG-stearates with 10, 20, 25, 40, 45, 50, 55, 100 and 150 PEG units, it was claimed that only those PEG-stearates are able to form aqueous dispersions of cubosomes that have 40 or more PEG repeating units. Those with PEG unit greater than 100 were able to retain the *Pn3m* symmetry.^{179,189}

Grafted polymers were also employed to stabilize cubosome dispersions. Chong *et al.* synthesized grafted copolymers of phytantriol and PEG of various chain lengths. They observed that copolymers with HLB>17 are better stabilizers.¹⁹⁰ In another study, Chong *et al.* synthesized copolymers of poly(octadecyl acrylate)-*block*-poly(polyethylene glycol methyl ether acrylate) (P(ODA)-*b*-P(PEGA-OMe)) by RAFT polymerization. They found that increasing the PEG density in the copolymer leads to better stabilization compared to the linear block copolymer Pluronic®F127. Using this copolymer, they obtained cubosomes with *Im3m* and *Pn3m* symmetries for GMO and phytantriol, respectively.¹¹¹

1.4 AIMS AND OBJECTIVES

As mentioned before in this chapter, enzymatic synthesis of polyesters using CAL-B is a green process, which allows synthesis of polyesters from bio-based building blocks with numerous functionalities. Functional polyesters support the tailoring of polymers with desired properties for conjugation of drugs and proteins. Polymers grafted with hydrophobic side chains (saturated fatty acids of various chain lengths)

result in amphiphilic polymers. The self-assembling behavior of amphiphilic polymers in aqueous media results in diverse morphologies depending on the respective fatty acid and the degree of grafting. The first aim of this work is to produce functional polyesters by enzymatic transesterification reaction of divinyl adipate and multihydroxy alcohols such as sugars (D-sorbitol or xylitol) using CAL-B. These functional polyester backbones are then grafted with stearic acid to obtain amphiphilic comb like polymers. Properties of these polymers in bulk and their aqueous dispersions are analyzed to investigate their self-assembling behavior. The second objective of this work is to synthesize poly(glycerol adipate) and oleate grafted PGAs with various degrees of grafting, and to study the bulk properties of these polymers by ^1H NMR spectroscopy, GPC, DSC, and XRD. Another objective is to study the effect of the mesophase behavior of the GMO-water system after adding graft copolymers. As the unsaturated fatty acids grafted chains in the polymer and in the GMO are identical, they could interact with each other affecting its mesophasic behavior. For this purpose PGA-*g*-O22 is chosen as it has a comparable volume fraction of hydrophobic side chains with that of GMO.

The final aim of this work is to make oleate grafted poly(glycerol adipate) (PGA-*g*-O x) water soluble by grafting a water soluble polymer to the polymer backbone. Poly(ethylene glycol) is a good choice for this purpose as it is a neutral, water-soluble polymer with extraordinary biological properties, which makes it suitable for various applications, including drug delivery, cell encapsulation, and conjugation to biomacromolecules.¹⁹¹ Poly(glycerol adipate) is prepared with different degrees of grafting of oleate chains and low molar mass PEG chains such as PEG750 and PEG1K in order to achieve different degrees of hydrophilicity. The bulk properties of the synthesized graft copolymers are studied using ^1H NMR spectroscopy, GPC, DSC, SAXS, and WAXS. Since amphiphilic graft copolymers have a lower critical aggregation concentration (CAC) than linear block copolymers, the ability of these multigraft copolymers to stabilize the cubosome dispersions are investigated using tensiometry (to find CAC), SAXS (to find the internal structure of cubosomes) and DLS measurements (to find the particle size of structured nanoparticles)

Chapter 2

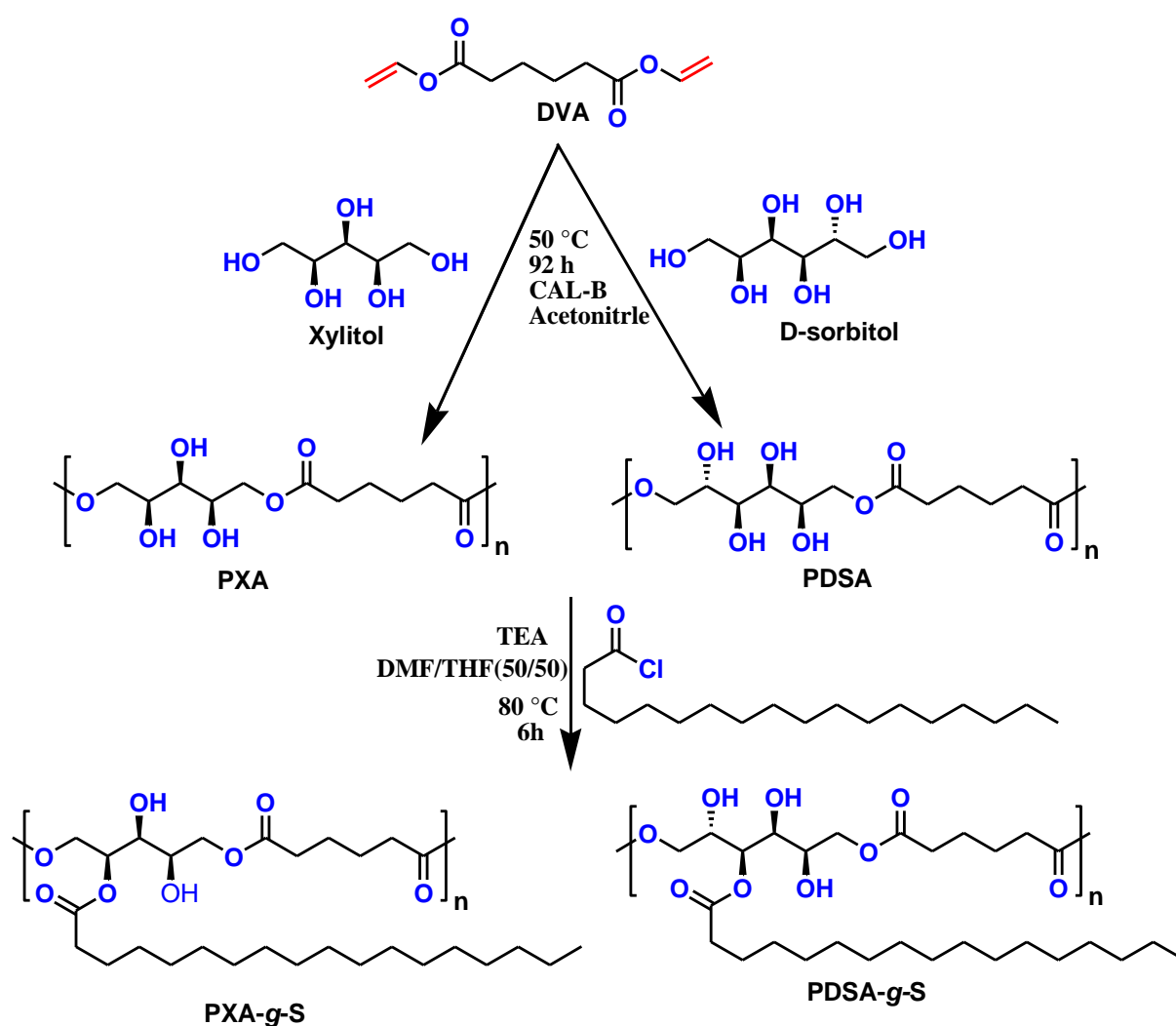
2 FATTY ACID MODIFIED SUGAR BASED POLYESTERS

2.1 INTRODUCTION

Aliphatic functional polyesters are an important class of materials for pharmaceutical and biological applications because of their biocompatibility and biodegradability.¹⁹² The enzymatic synthesis of functional polyesters is an attractive alternative to classical polycondensation or ring opening polymerization, which require an extensive protection and deprotection chemistry for the introduction of functional groups to the polyester backbone.³⁷ The most frequently used enzyme for polycondensation is lipase B from *Candida antarctica* (CAL-B) which is commercially available immobilized on acrylic resins.¹⁹³ Since CAL-B supports the esterification of primary OH-groups rather than secondary OH-groups at reasonably low temperatures, it is frequently employed to prepare linear polyesters from polyols as glycerol or sugars.^{54,61,83,194,195} As second reactants usually divinyl esters,^{83,196} or dimethyl esters^{54,195,197} are employed. A typical polyester with a pendant OH-group in every monomer unit is poly(glycerol adipate) (PGA) obtained by reacting glycerol with divinyl adipate.⁸³ We have extensively studied PGA grafted with several fatty acids. Self-assembled nanoparticles obtained from these amphiphilic polymers have been studied for drug delivery applications.⁸⁷ Different shapes of nanoparticles could be produced in water by the interfacial deposition method depending on the degree of substitution and on the fatty acid used. Important for the structure formation of the nanoparticles is the phase separation between polymer backbone and side chains.^{87,88} Saturated fatty acids with relatively long acyl chains (>C12) tend to crystallize after phase separation whereas unsaturated fatty acids as e.g., oleic acid lead to the formation of two disordered nanophases. The PGA backbone obtained by enzymatic polymerization is hydrophilic but not water soluble and has usually M_n -values below 10,000 g·mol⁻¹. It should be mentioned here that higher molar masses can be achieved at higher polymerization temperatures but then the selectivity between primary and secondary OH-groups is partially lost.⁶⁵ Grafting poly(ethylene oxide) (PEO) chains onto the PGA backbone results in water-soluble polymers.²⁸ When a block copolymer of PEO and poly(ϵ -caprolactone) is grafted

to the polymer backbone, worm-like micelles can be produced.¹⁹⁸ The PGA backbone can also be converted into an ATRP macroinitiator, which leads to a plethora of possible polymer architectures.^{29,98}

Here, we report on the enzymatic syntheses of poly(D-sorbitol adipate) (PDSA) and poly(xylitol adipate) (PXA). Both hydrophilic polyester backbones were modified by grafting with stearic acid chloride which yields amphiphilic polymers (PDSA-*g*-S and PXA-*g*-S). All polymers are characterized by SEC and ¹H NMR spectroscopy. The bulk morphology of the polymers is studied by DSC, WAXS, and SAXS. Furthermore, nanoparticles are prepared from some selected polymers and characterized by DLS and TEM. Scheme 2.1 describes the syntheses of the polymers under investigation.



Scheme 2.1. Synthetic route to stearoyl grafted poly(xylitol adipate) (PXA-*g*-S) and poly(D-sorbitol adipate) (PDSA-*g*-S).

2.2 EXPERIMENTAL PART

2.2.1 Materials

Lipase N435 derived from *Candida antarctica* (CAL-B) immobilized on acrylic resin (Sigma-Aldrich Chemie GmbH, weinheim, Germany) was dried over P₂O₅ for 24 h prior to use. N, N-dimethylformamide (anhydrous, 99.8%), acetonitrile (anhydrous, 99.8%), tetrahydrofuran (anhydrous, 99.9%), xylitol (99%), D-sorbitol (98%), stearyl chloride (90%) and triethylamine were purchased from Sigma-Aldrich. Divinyl adipate (96%) was purchased from TCI GmbH (Eschborn, Germany). All chemicals were used without further purification. All other chemicals used in various stages like, diethyl ether, *n*-hexane, methanol, and dichloromethane were purchased from Carl Roth (Karlsruhe, Germany).

2.2.2 Syntheses

2.2.2.1 Synthesis of poly(xylitol adipate)

Analogous to previously published methods, poly(xylitol adipate) (PXA) can be synthesized in a single step.^{61,66} Xylitol and divinyl adipate were used in a molar stoichiometric ratio of 1:1 in the presence of lipase N435. A weighed amount of xylitol (10 g, 65.8 mmol) and divinyl adipate (13 g, 65.8 mmol) were charged into the reaction flask. Afterward, 40 mL of acetonitrile was added. The solution was stirred for 30 min at 50 °C to equilibrate the temperature. The reaction was started by adding CAL-B (2.3 g, 10 wt% of total mass of monomer). After 92 h the reaction mixture was diluted by addition of an excess of DMF and the enzyme was removed by filtration. The synthesis process is described in Scheme 2.1. The filtrate was collected and the crude product was precipitated twice in diethyl ether. ¹H NMR spectroscopy was used to confirm the purity of the sample. ¹H NMR (400 MHz, DMSO-*d*₆) δ (ppm) 4.86–4.76 (m, 2H), 4.68 (dd, *J* = 18.6, 7.6 Hz, 1H), 4.11–3.92 (m, 4H), 3.73 (s, 2H), 3.38 (s, 1H), 2.29 (s, 4H), 1.52 (s, 4H).

2.2.2.2 Synthesis of poly(D-sorbitol adipate)

Poly(D-sorbitol adipate) (PDSA) was synthesized using the analogous procedure as described for poly(xylitol adipate) but the crude product was dialyzed to remove oligomers using water as dialysis medium and a membrane with a cut-off molar mass of 1000 g·mol⁻¹. ¹H NMR spectroscopy was used to confirm the purity of the samples. ¹H

NMR (400 MHz, DMSO- d_6) δ (ppm) 4.97–4.61 (m, 2H), 4.55–4.30 (m, 2H), 4.28–3.82 (m, 3H), 3.70 (d, $J = 49.1$ Hz, 2H), 3.58–3.33 (m, 2H), 2.37–2.17 (m, 4H), 1.64–1.42 (m, 4H).

2.2.2.3 Synthesis of stearyl grafted poly(xylitol adipate) and poly(D-sorbitol adipate)

Poly(xylitol adipate) and poly(D-sorbitol adipate) with a number average molar mass M_n of 5,000 g·mol⁻¹ and 3,500 g·mol⁻¹, respectively, were used for further modification with stearyl chains using a standard procedure. PXA or PDSA dissolved in DMF/THF (50/50 v/v) were charged into a three neck (100 mL) round bottom flask, equipped with condenser and magnetic stirrer. Triethylamine was added as an acid scavenger. Stearyl chloride was dissolved in THF at room temperature and added dropwise to the reaction mixture. The temperature was raised to 80 °C, and the reaction was stopped after 6 h. The solvent was removed in a rotary evaporator. To remove the salt of trimethylamine and unreacted trimethylamine, the crude product was dissolved in DCM and extracted four times with brine. The organic phase was collected and dried with magnesium sulfate. The crude product was precipitated in *n*-hexane for products with less than 40 mol% grafted chains and in methanol for products with more than 40 mol% grafting, to remove unreacted fatty acid. A slightly brownish solid product was obtained. PXA-*g*-S: ¹H NMR (500 MHz, CDCl₃) δ (ppm): 5.47–4.99 (m, 3H), 4.54–3.7 (m, 4H), 2.35 (d, $J = 42.4$ Hz, 10H), 1.67 (s, 10H), 1.26 (s, 84H), 0.89 (t, $J = 6.9$ Hz, 9H). PDSA-*g*-S: ¹H NMR (400 MHz, CDCl₃) δ (ppm): 5.65–4.76 (m, 4H), 3.5–4.5 (m, 4H), 2.35 (m, 12H), 1.64 (s, 12H), 1.43–1.15 (m, 112H), 0.87 (t, $J = 6.8$ Hz, 12H).

2.2.3 Preparation of nanoparticles

Nanoparticles were prepared using the interfacial deposition method described elsewhere⁸³ with slight modification. In this approach, 150 μ L of 15 mg·mL⁻¹ polymer solution in THF was added slowly to 1.7 mL hot water (above the melting temperature of the polymer) with constant vortexing for 5 min at 45,000 rpm. Turbid dispersions were obtained which were further homogenized using silentCrusher S (Heidolph Instruments GmbH, Schwabach, Germany) for 3 min. 300 μ L cold water was then added for immediate solidification of the particles with vortexing. The organic solvent and small amounts of water were evaporated in a rotary evaporator. A small amount of water was again added to make a 0.1% w/v dispersion.

2.2.4 Instrumentation

2.2.4.1 NMR spectroscopy

^1H NMR spectra of grafted and non-grafted polyester backbones were recorded with a Varian Gemini 400 spectrometer at 400 MHz and 27 °C. Approximately 30 mg of polymer were dissolved in 0.8 mL of CDCl_3 or $\text{DMSO-}d_6$ as solvents, purchased from Armar Chemicals (Döttingen, Switzerland). The NMR spectra were interpreted using MestRec v.4.9.9.6 (Mestrelab Research, Santiago de Compostela, Spain). The assignment of the peaks was made using Chem Office 2004-ChemDraw ULTRA 8, software from Cambridge, UK.

2.2.4.2 Size exclusion chromatography (SEC)

SEC measurements were performed on a Viscotek GPCmax VE 2002 using HHRH Guard-17360 and GMHHR-N-18055 columns and a refractive index detector was used (VE 3580 RI detector, Viscotek, GmbH, Waghäusen, Germany). THF was used as eluent. For all samples, the concentration was $3 \text{ mg}\cdot\text{mL}^{-1}$ and the flow rate was $0.1 \text{ mL}\cdot\text{min}^{-1}$. For PXA and PDSA, the measurements were done with DMF containing 0.01 M LiBr as mobile phase in a thermostated column oven kept at 80 °C. The calibration standards for measurements in THF and DMF were polystyrene and poly(methyl methacrylate), respectively.

2.2.4.3 Differential scanning calorimetry (DSC)

Thermal properties of the polymers were measured using a differential scanning calorimeter (DSC, Mettler Toledo DSC823e module, Mettler-Toledo GmbH, Greifensee Switzerland). All samples were scanned within the temperature range of -50 to 80 °C with a heating rate of 10 °C $\cdot\text{min}^{-1}$. 8 mg to 12 mg of sample material was enclosed in an aluminum pan and placed in the DSC sampler at room temperature. All measurements were performed under constant flow of nitrogen ($10 \text{ mL}\cdot\text{min}^{-1}$).

2.2.4.4 Dynamic light scattering (DLS)

All samples were measured in Plastibrand PMMA disposable cuvettes (Brand GmbH, Wertheim, Germany) with the ALV-NIBS/HPPS spectrometer (ALV-Laser Vertriebsgesellschaft M.B.H., Langen, Germany). As a light source, a He-Ne laser with a power of 3 mW and a wavelength of $\lambda = 632.8 \text{ nm}$ was used. The scattering intensity was

recorded by a photomultiplier at an angle of 173° , and the temporal intensity fluctuations were recorded with a Multiple Tau digital correlator ALV transfer 5000/E (Vertriebsgesellschaft M.B.H., Langen, Germany). The analysis was performed with the ALV Correlator Software 3.0 through the “regularized fit” mode.

2.2.4.5 Negative-staining TEM

Samples for negative-staining TEM were prepared by spreading 3 μL of the dispersion onto a Cu grid coated with a Formvar[®] film (Plano, Wetzlar, Germany). The excess liquid was blotted off after 30 s. Afterward, the grid was placed on a droplet of 1 wt% aqueous uranyl acetate solution and drained off after 1 min. The dried specimens were observed with a Zeiss EM 900 transmission electron microscope (Carl Zeiss Microscopy GmbH, Oberkochen, Germany). Micrographs were taken with a SSCCD SM-1K-120 camera (TRS, Moorenweis, Germany).

2.2.4.6 X-ray diffraction (XRD)

X-ray diffraction patterns were recorded with a 2D detector (Vantec 500, Bruker, AXS, Madison, WI, USA) using Ni-filtered and pinhole collimated Cu $K\alpha$ radiation. The exposure time was 15 min and the sample to detector distance was 9.85 and 27.7 cm for wide and small angle scattering experiments, respectively. The samples were held in glass capillaries (\varnothing 1 mm, Hilgenberg, GmbH, Malsfeld, Germany).

2.3 RESULTS AND DISCUSSION

2.3.1 Polymerization and grafting

The enzymatic syntheses of PXA and PDSA are carried out by a polycondensation (basically a polytransesterification) reaction of xylitol and D-sorbitol, respectively, with divinyl adipate. Since the enzyme reacts preferably with primary hydroxyl groups at reasonably low temperatures, the secondary hydroxyl groups remain unreacted.⁶⁶ As a result, linear PXA and PDSA samples with pendant OH-groups are obtained. PDSA is a water-soluble polymer whereas PXA forms a fine suspension in water. Dynamic light scattering of a $10\text{ g}\cdot\text{L}^{-1}$ suspension of PXA is given in Figure A1 (Appendix).

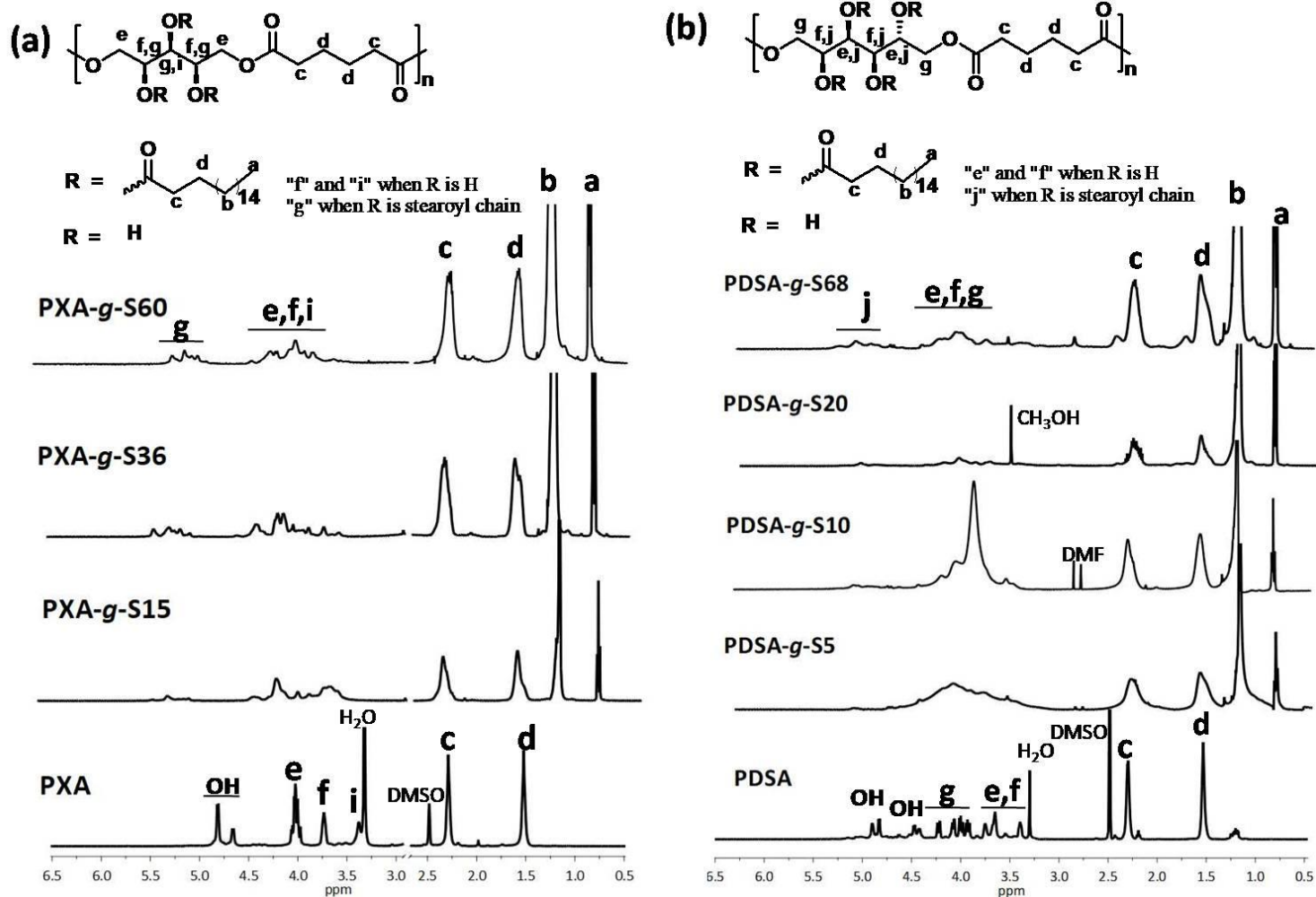


Figure 2.1. ^1H NMR spectra of (a) grafted and non-grafted poly(xylitol adipate), and (b) grafted and non-grafted poly(D-sorbitol adipate) recorded at 27 °C using CDCl_3 and DMSO-d_6 as a solvent for grafted and non-grafted polymers, respectively.

In the second step of the synthesis, the functional polyesters are grafted with stearoyl chains resulting in different degrees of grafting. ^1H NMR spectra of grafted and non-grafted PXA and PDSA are shown in Figure 2.1. The relative increase in the intensity of the peaks belonging to the stearoyl side chains indicates the degree of grafting. The quantitative determination of the degree of grafting is calculated by taking into account the integral values of peaks *a* and *c* using Equation 2.1 for PXA-*g*-S_x and Equation 2.2 for PDSA-*g*-S_x.

$$\text{mol\% degree of grafting} = \frac{0.44 \times a}{c - 0.67a} \times 100 \quad 2.1$$

$$\text{mol\% degree of grafting} = \frac{0.33 \times a}{c - 0.67a} \times 100 \quad 2.2$$

In equations 2.1 and 2.2 *a* stands for the integration area of methyl group protons of stearoyl chains while *c* stands for the integration area of protons of methylene next to the carbonyl group of the polymer backbone and stearoyl side chains. Using Equations 2.1 and 2.2, the mol% of grafted OH groups of polymer backbone calculated for PXA was 15, 36, and 60, whereas, for PDSA, the respective values are 5, 10, 20, and 68.

The grafting is further verified by size exclusion chromatography (see Figure 2.2), where a shift of the peak maximum to lower retention times with increasing degrees of grafting occurs.

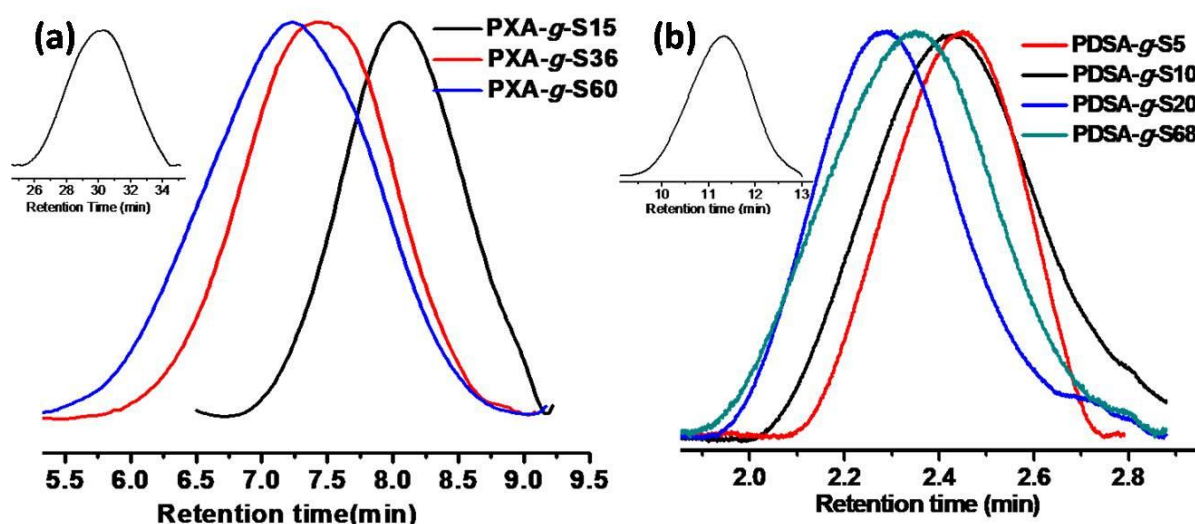


Figure 2.2. Size exclusion chromatography (SEC) traces of (a) stearoyl grafted poly(xylitol adipate) in THF and (b) SEC traces of stearoyl grafted poly(D-sorbitol adipate) in THF. The insets show the SEC traces of the polymer backbones PXA and PDSA, respectively, in DMF.

Due to the insolubility of polymer backbones PXA and PDSA in THF, the measurements are carried out in DMF as eluent while for all other grafted polymers THF is employed. The number average molar masses and the polydispersity index PDI defined as M_w/M_n together with thermal properties of all polymers are given in Table 2.1.

Thermal properties of grafted and non-grafted PXA and PDSA, respectively, are determined by differential scanning calorimetry. PXA and PDSA are amorphous polymers with a glass transition temperature T_g of 5 and 3 °C, respectively. However, all graft copolymers are semicrystalline indicated by the melting endotherms. All details on the phase transitions are summarized in Table 2.1.

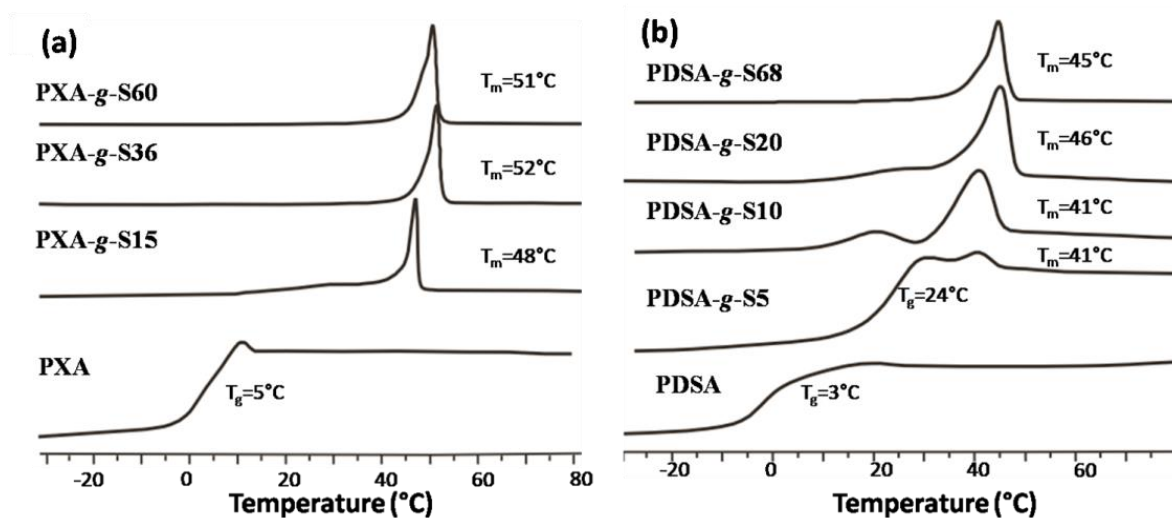


Figure. 2.3. DSC traces of (a) grafted and non-grafted PXA and (b) grafted and non-grafted PDSA. The measurements are carried out with a heating rate of 10 °C·min⁻¹.

The melting temperature T_m is determined from the maximum of the endothermal peak during the heating scan. DSC traces of graft copolymers and polymer backbones are shown in Figure 2.3. As already mentioned, the grafting of saturated fatty acids to this type of polyesters induces crystallinity caused by side-chain crystallization. The melting temperature is about 50 °C in case of PXA-*g*-S_x, whereas for PDSA-*g*-S_x, the melting peak occurs between 41 and 45 °C. For very low degrees of grafting, both a glass transition temperature and a melting endotherm can be observed in the DSC traces.

Table 2.1 The volume fraction of grafted chains, ϕ_{stearoyl} , M_n , PDI , T_m , T_g and ΔH_m of grafted and non grafted polymers.

Polymer	Φ_{Stearoyl}^5	M_n (g·mol ⁻¹)	PDI	T_m (°C) ⁴	T_g (°C) ⁴	ΔH_m (J·g ⁻¹) ⁴
PXA	-	5,000 ¹	2.4 ¹	-	5	-
PXA- <i>g</i> -S15	0.37	7,300 ²	2.3 ³	48	20	60
PXA- <i>g</i> -S36	0.58	10,600 ²	2.6 ³	52	-	100
PXA- <i>g</i> -S60	0.69	14,600 ²	1.8 ³	51	-	85
PDSA	-	3,500 ¹	1.9 ¹	-	3	-
PDSA- <i>g</i> -S5	0.15	4,300 ²	1.4 ³	41	24	1.15
PDSA- <i>g</i> -S10	0.30	4,800 ²	1.9 ³	41	-	36
PDSA- <i>g</i> -S20	0.43	5,800 ²	1.5 ³	46	-	136
PDSA- <i>g</i> -S68	0.71	12,200 ²	1.7 ³	45	-	73

¹Obtained from GPC using DMF as eluent. ²Calculated on the basis of % degree of grafting from the ¹H NMR spectra. ³Obtained from GPC using THF as eluent. ⁴Obtained from DSC at a heating rate of 10 °C·min⁻¹.

⁵Volume fraction of stearyl side chains estimated by Material Studio 4.1

Combined SAXS and WAXS investigations are carried out for polymers in bulk. These comb-like polymers show nanophase separation that arises from the immiscibility of the side chains with the polymer backbone.^{199,200} Ordering of these nanophases strongly depends on the lipophilic volume fraction of the side chains.⁸⁸ For polymers having a relatively low degree of grafting, a low volume fraction of the side chains is obtained, for instance, PXA-*g*-S15 (Figure 2.4(a)) has a volume fraction of the side chains of 0.37.

For this sample, a peak in the small angle regime at $q^* = 0.1136 \text{ \AA}^{-1}$ (the corresponding d -spacing is 55.3 Å) during the heating scan is observed. In the wide angle region, only one single peak is visible ($q_w = 1.5222 \text{ \AA}^{-1}$) superimposed by diffuse scattering. Assuming a hexagonal ordering of the side chains, this peak corresponds to the (110) direction of the hexagonal lattice, having a lattice parameter $a = 4.77 \text{ \AA}$. This can also be assigned as pseudo hexagonal rotator phase R_{II} which is typically appears for alkyl grafted comb like polymers.^{88,201} At the melting temperature of 48°C, the peak in the wide angle region disappears whereas an amorphous halo remains at lower q -values and the peak in the small angle region becomes broader.

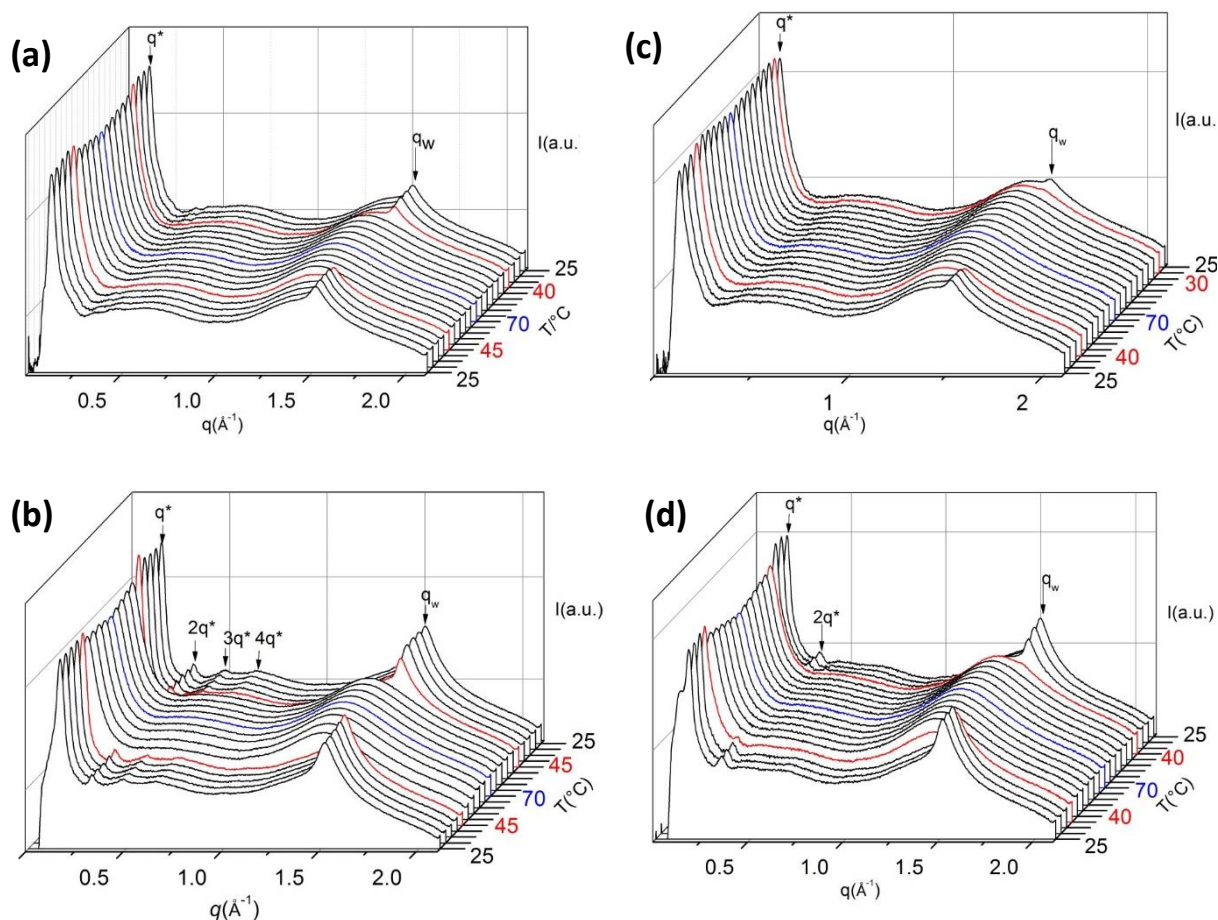


Figure. 2.4. Combined SAXS and WAXS traces during heating and cooling cycles (5 °C step from 25°C to 70 °C and back to 25 °C) of (a) PXA-*g*-S15 (b) PXA-*g*-S36 (c) PDSA-*g*-S10 and (d) PDSA-*g*-S68.

For polymers with relatively high degrees of grafting, a more ordered nanophase separation is observed, e.g. in PXA-*g*-S36 (the volume fraction of hydrophobic side chain is 0.58). Combined SAXS and WAXS heating and cooling scans of PXA-*g*-S36 are shown in Figure 2.4(b). At low temperature, one prominent peak in the small angle region q^* and several higher order peaks as integral multiples of q^* are visible, indicating a lamellar structure caused by nanophase separation of the polymer backbone and the side chains ($d = 38.1 \text{ \AA}$) followed by crystallization of side chains.⁸⁸ In the wide angle region, only one single peak appears q_w . The lattice parameter $a = 4.78 \text{ \AA}$ is nearly identical with that of PXA-*g*-S15. At the melting temperature of 52°C, the first order peak in the small angle region becomes broader and the higher order peaks disappear. This behavior indicates that the lamellar structure is significantly stabilized by the side chain crystallization. After cooling below the crystallization temperature of 45 °C, the higher order peaks appear again.

The sample PDSA-*g*-S10 (Figure 2.4(c)) with a volume fraction of 0.30 of side chains shows a similar scattering pattern as PXA-*g*-S15 with a slightly larger *d*-spacing of 57.1 Å. The sample PDSA-*g*-S68 (Figure 2.4(d)) with higher side chain content (volume fraction of 0.71) shows in the small angle regime again the typical scattering pattern of a lamellar phase with a *d*-spacing of 35.5 Å. The complete data of all SAXS and WAXS measurements are given in Tables A1–A8 in the Appendix. It is interesting to note that the lattice parameters of the hexagonal rotator phase remain the same, independent of the degree of grafting.

2.3.2 Nanoparticles

2.3.2.1 Dynamic light scattering

Dynamic light scattering is employed to determine the size of nanoparticles formed by the graft copolymers. Nanoparticles were prepared by the interfacial deposition method (also called nanoprecipitation method).⁸³ The polymer dispersion in water at a concentration of 1 g·L⁻¹ at 25 °C is used. The average hydrodynamic radius of PXA-*g*-S15 is found to be 69 nm whereas for PDSA-*g*-S10 it is 105 nm. The reason behind the difference in particle sizes of both samples could be the overall hydrophilicity of the polymer chains. Since PDSA-*g*-S10 is more hydrophilic than PXA-*g*-S15, it shows a comparatively higher hydrodynamic radius in water. The particle size distributions of the respective polymer dispersions are shown in Figure 2.5. Since the size and shape of the nanoparticles are important factors for *in vivo* drug release,^{27,202,203} the control of these parameters is important. The size of the nanoparticles can be tailored by choosing appropriate solvents and temperatures for the interfacial deposition method. Any solvent that is miscible with water and that can dissolve the polymer as well will be appropriate for this method.²⁰⁴ A solvent with poor water miscibility results in a decrease in interfacial tension towards the oil in water interface during the preparation process and results in an increase in particle size.²⁰⁵

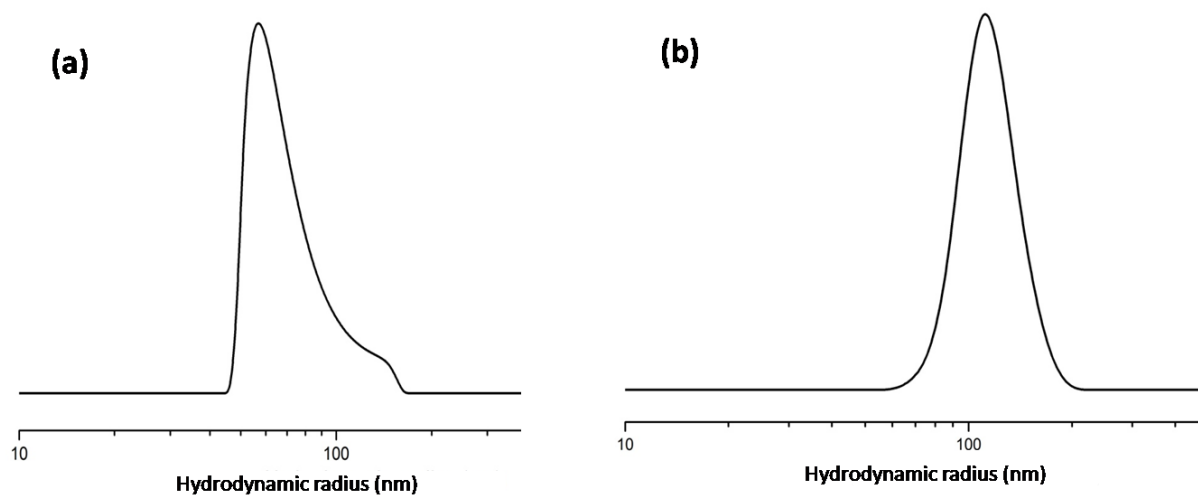


Figure 2.5. (a) Hydrodynamic radius distribution of PXA-*g*-S15 nanoparticles in water with a concentration of $1 \text{ g}\cdot\text{L}^{-1}$ at 25°C and (b) hydrodynamic radius distribution of PDSA-*g*-S10 nanoparticles ($1 \text{ g}\cdot\text{L}^{-1}$ in water at 25°C).

2.3.2.2 Negative-staining transmission electron microscopy

To study the morphology of the nanoparticles, negative-staining TEM on dried nanoparticles was carried out using uranyl acetate as the staining agent. The negative stained TEM images are shown in Figure 2.6.

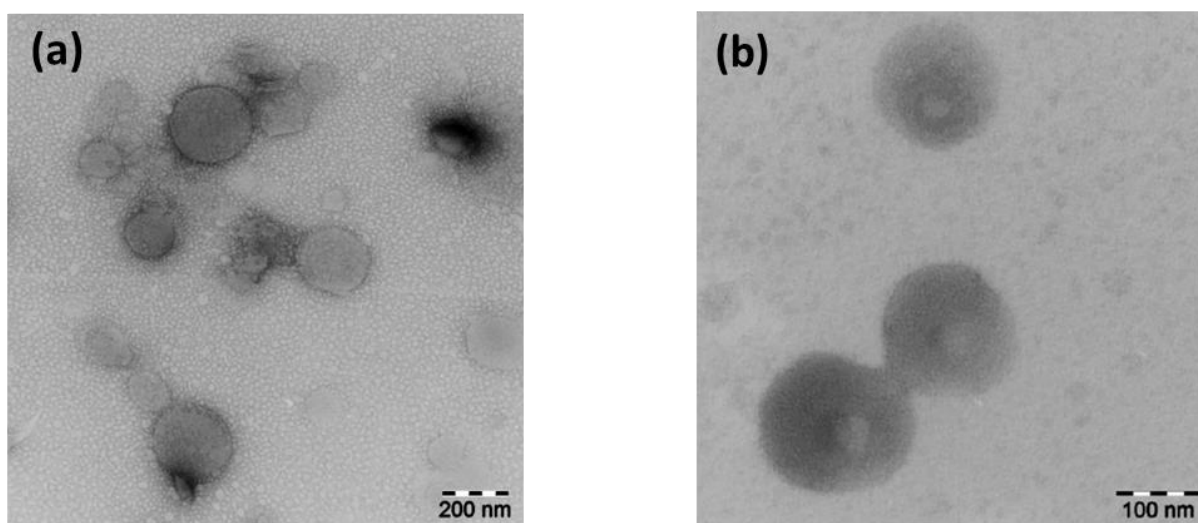


Figure 2.6. Negative-staining electron micrographs of (a) 0.1 wt% dispersion of PXA-*g*-S15 and (b) 0.1 wt% dispersion of PDSA-*g*-S10.

It shows spherical morphologies of the nanoparticles which is a typical behavior of particles formed upon surface energy minimization. It can be seen that PXA-*g*-S15 forms homogeneous nanoparticles (see Figure 2.6(a)) whereas for PDSA-*g*-S10 some kind of

additional aggregation in the nanoparticles is observed (see Figure 2.6(b)). Since the geometry, surface properties and internal structure of nanoparticles strongly influence the drug incorporation,²⁰³ studies are in progress to investigate these characteristics in our graft copolymer systems in more detail.

2.4 CONCLUSIONS

In conclusion, a simple approach for synthesizing sugar based functional polyesters has been used to produce hydrophilic polymers, which were grafted with stearyl chains to obtain amphiphilic graft copolymers. Unlike the initial amorphous polyester backbone, the grafted polyesters are semi-crystalline in nature. These amphiphilic comb-like polymers show a nanophase separation leading to lamellar morphologies which are more pronounced in the case of a relatively high degree of grafting, such as for PXA-*g*-S36 and PDSA-*g*-S68. However, for a small degree of grafting this nanophase separation is less ordered, which results in only one peak in the SAXS traces. A diffraction peak at higher scattering angles (WAXS) in all grafted copolymer samples corresponds to the (110) reflection which indicates the pseudo hexagonal rotator phase that exists until the melt temperature of the polymers is reached. Furthermore, these polymers are able to form well-arranged nanoparticles, prepared by the interfacial deposition method. It would be interesting, in the future, to explore the morphology and properties as e.g. the hydrolytic stability of the nanoparticles formed from these polymers and to develop their applications in drug delivery systems. Due to the biodegradability of these nanoparticles, they might be an alternative to many Pluronic[®] based systems.

CHAPTER 3

3 POLY(GLYCEROL ADIPATE)-*G*-OLEATE AND THE GMO/WATER SYSTEM

3.1 INTRODUCTION

Lipase-catalyzed polyester synthesis was a promising approach for synthesis of biocompatible polymers during the last two decades as it is a green process,^{3,13,65,206–208} and it also offers a simple way to synthesize functional polyesters.^{13,35,54,65,85,208–212} Poly(glycerol adipate) (PGA) is a hydrophilic, biocompatible, and biodegradable polyester with many potential biomedical and pharmaceutical applications.⁸³ The most important advantage of PGA, as compared to other biodegradable polyesters, such as polylactide and poly(ϵ -caprolactone), is the pendant hydroxyl functionality at each structural repeat unit that imparts a hydrophilic character to the polymer and offers an opportunity for convenient post-polymerization reactions. Thus, we and several others synthesized comb-like amphiphilic copolymers based on the PGA backbone,^{27,29,83,90,91,213} including amphiphilic graft copolymers of PGA and fatty acids of various chain lengths, obtained via a simple condensation reaction between pendant hydroxyl groups and fatty acid chlorides. The resulting amphiphilic graft polymers are able to self-assemble in water into self-stabilizing well-defined nanoparticles of diverse shapes with enhanced drug loading efficiency.^{83,214} The length of acyl chains and the degree of substitution play an important role for the structure formation in bulk and in nanoparticles.²⁷ For example, depending upon the degree of substitution, PGA with stearate side chains is found to form spherical nanoparticles with well-defined phase-separated lamellar internal structure at higher degrees of substitution and polygonal nanoparticles with pseudo-hexagonal internal structure at lower degree of acylation.⁸⁸ Long and saturated all-trans acyl-side chains of PGA-*g*-acyl polymers organize into a crystal structure in bulk and nanoparticles which could have an adverse effect on the loading and release properties of these nanoparticles in pharmaceutical and biomedical applications.²¹⁵ Therefore, the design of amphiphilic graft polymers of non-crystallizable long side chains would be more attractive for practical applications. The oleate chain is a C18 chain with a *cis* double bond between C9 and C10 that hinders crystallization strongly. The oleate residue would be an ideal option

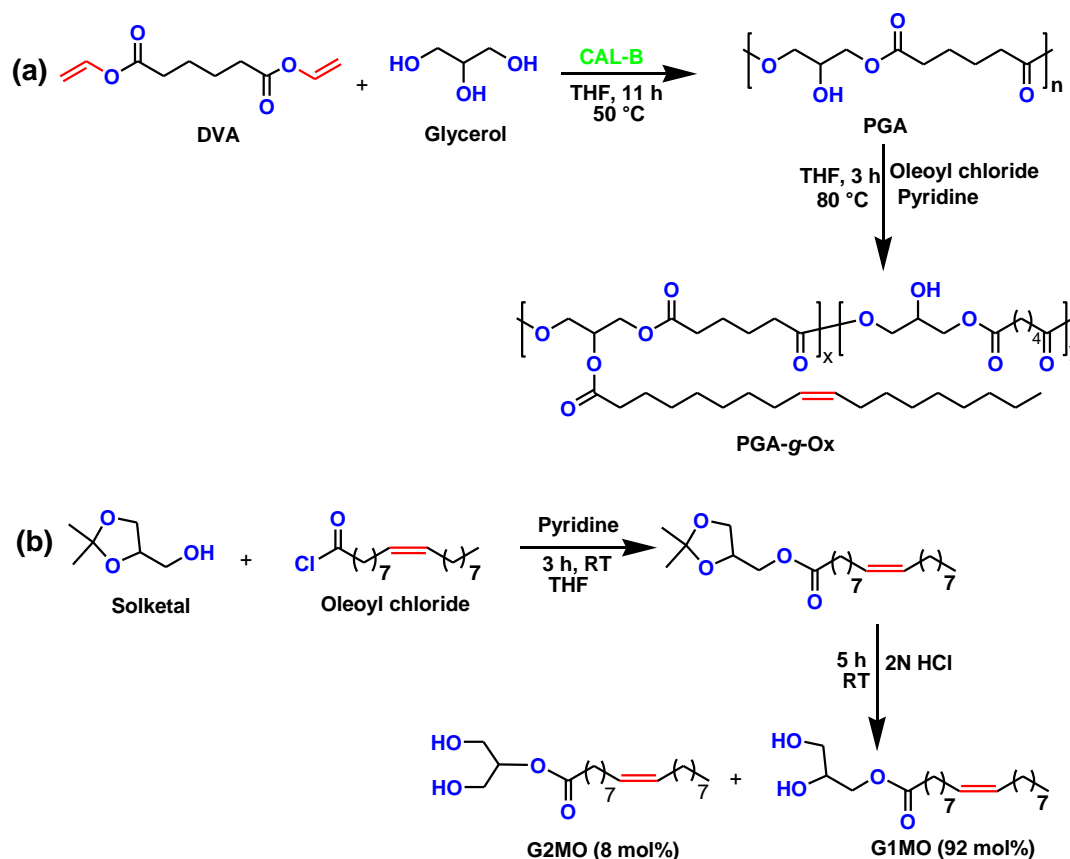
for achieving a completely amorphous amphiphilic PGA based graft copolymer, with potential applications not only in drug delivery systems but also, due to the identical chain structure of the oleate side chains and the hydrophobic oleate tail of glycerol monooleate (GMO) (Scheme 3.1) in tuning the properties of the liquid crystalline phases of GMO and GMO/water, possibly by the integration of the oleate side chains into the lipid bilayers.²¹⁶⁻²¹⁸

Due to the partial oil solubility, GMO is commonly used as a food emulsifier.¹⁰⁴ It self-assembles into a variety of liquid crystalline structures in the presence of different amounts of water and as a function of temperature,^{121,149,155,219} including the important inverse bicontinuous cubic phases with water channels separated by lipid bilayers.²²⁰ The diameter of the water channel in these structures predominantly controls the extent of drug or protein loading and the release behavior.^{221,222} Furthermore, large molecules as proteins could be accommodated only in highly swollen and enlarged water channels of the cubic phases. Therefore, tuning the swelling and enlargement of the water channels is extremely important for enhanced applications of the cubic phases as biocompatible host in numerous applications, such as biosensors and higher loading efficiency for biologically and pharmaceutically active ingredients.^{168,221-223} To achieve this, the introduction of a third component, mostly a low molar mass additive, such as nonionic octyl- β -D-glucopyranoside (β -Glc-OC8),²²¹ the charged surfactant-doped system dioctyl sodium sulfosuccinate,²²¹ neutral sucrose stearate,²²³ charged lipids,²²² cholesterol,²²² and nucleic acids,²²⁴ to name a few, to the GMO/water system has been explored.

For certain applications, such as nasal and intravenous drug delivery,²²⁵ the bulk liquid crystalline phases could be fragmented and stabilized in aqueous dispersions into submicron size particles with cubic geometry maintaining the well-defined internal cubic structure, generally named as cubosomes. The commercially available Pluronic® F127, an amphiphilic triblock copolymer of poly(ethylene glycol) and poly(propylene oxide), has been found to offer the most effective and long-term steric stability to the cubosomes.^{131,225-229} However, several other amphiphilic species, including PEG-lipid copolymers,^{114,230} polyethoxylated stearates (Myrj series),²³¹ modified cellulose,²³² and polysorbate 80²³¹ have also been investigated.

The main objective of the current study is to employ amphiphilic oleate grafted PGA, PGA-*g*-oleate for systematic investigation of its influence on the GMO/water mesophase behavior and its potential application as a nanoparticle stabilizer in aqueous dispersions.

Thus, the enzyme-catalyzed synthesis of linear PGA was carried out using divinyl adipate and glycerol, which was subsequently transformed into PGA-*g*-oleate (PGA-*g*-Ox) by reacting with oleoyl chloride. Samples with various degrees of grafting were synthesized and characterized by differential scanning calorimetry (DSC), and small angle X-ray scattering (SAXS) for nanophase separation. The samples are named PGA-*g*-Ox, where x represents the degree of grafting (mol% of the pendant OH groups esterified). Systematic studies were carried out at room temperature on the GMO/PGA-*g*-O22/water ternary systems and a ternary phase diagram was constructed. It was observed that the addition of polymer to the GMO/water system induces swelling of the cubic phase and enlargement of water channels. Preliminary investigations on the potential application of PGA-*g*-O22 as a steric stabilizer of structured nanoparticles in aqueous dispersions were carried out using different transmission electron microscopy (TEM) techniques.



Scheme 3.1: (a) Enzymatic synthesis of poly(glycerol adipate) (PGA) and post-polymerization modification with oleoyl chloride and (b) synthesis of glycerol monooleate (GMO).

3.2 EXPERIMENTAL SECTION

3.2.1 Materials

Glycerol ($\geq 99.5\%$), anhydrous tetrahydrofuran (THF, water content 0.02%), oleoyl chloride ($\geq 89\%$), and Novozym 435 (derived from *Candida antarctica* type B (CAL-B) immobilized on an acrylic macroporous resin) ($5000 \text{ U}\cdot\text{g}^{-1}$, water content 1-2%) were purchased from Sigma Aldrich. Novozym 435 was dried under vacuum at $4 \text{ }^\circ\text{C}$ and over P_2O_5 for 24 h before use. Divinyladipate (DVA, 96%) was purchased from TCI-Europe and was used as received. Acetone, *n*-hexane, ethyl acetate, methanol, dichloromethane (DCM), and pyridine were purchased from Carl Roth. Solketal (97%) was purchased from Alfa Aesar and used as received.

3.2.2 Syntheses

3.2.2.1 Synthesis of poly(glycerol adipate) (PGA)

The PGA backbone was synthesized by enzymatic solution polymerization according to the procedure described previously.^{27,233} Briefly, glycerol (22.6 g, 245 mmol) and an equimolar amount of divinyl adipate (50.7 g, 245 mmol) were charged into a 250 ml three neck round bottom flask equipped with an overhead mechanical stirrer and a reflux condenser containing CaCl_2 drying tube at its outlet. Subsequently, 45 ml of THF was added to the reaction flask. The mixture was stirred for 30 min at $50 \text{ }^\circ\text{C}$, and then CAL-B (1.42 g Novozym 435, 2 wt% with respect to the monomers) was added to start the polymerization. The reaction mixture was cloudy at the start due to the insolubility of glycerol in THF. However, as the reaction proceeded the turbidity disappeared upon the formation of oligomers. After 11 h the reaction mixture was diluted by the addition of a small amount of THF and the enzyme beads were filtered off. THF was removed by rotary evaporator to recover the final product (49 g) as a slightly yellow and viscous polymer that was used without further purification. The molar mass of PGA was measured using GPC as $M_n = 4,800 \text{ g}\cdot\text{mol}^{-1}$, with a polydispersity index (PDI) of 2.0. The ^1H NMR and inverse-gated ^{13}C NMR spectra are shown in Figure A2 in the Appendix and Figure 3.2(a), respectively. The assignment of the peaks was made following the literature.^{57,197,234}

3.2.2.2 Syntheses of poly(glycerol adipate)-*g*-oleate (PGA-*g*-Ox)

The acylation of the PGA backbone was achieved with various degrees of grafting by the reaction between pendant hydroxyl groups of the PGA backbone and oleoyl chloride in analogy to the grafting procedure with different fatty acids.^{27,83,233} A typical procedure for 15 mol% intended degree of grafting was in such a way that PGA (4.0 g, 19.8 mmol) was dissolved in 50 ml THF in a 100 ml three neck round bottom flask equipped with a condenser and magnetic stirrer. After the addition of pyridine (3.9 g, 49 mmol) the reaction flask was transferred to an ice bath. After cooling it for approximately 30 min, the oleoyl chloride (0.88 g, 2.97 mmol) diluted with 5 ml THF was added drop-wise at 0°C. The reaction was allowed to proceed at room temperature for approximately 20 min and then under reflux for 3 h. The reaction mixture was filtered to remove the pyridinium salt. The solvent was evaporated by rotary evaporator, and the crude product was dissolved in dichloromethane (DCM) and extracted three times with brine. The organic phase was separated and dried over sodium sulfate. To ensure the complete removal of the unreacted fatty acid, the filtrate was concentrated by rotary evaporator and precipitated three times in ice-cold *n*-hexane. The purification of graft polymers with a degree of grafting greater than 40 mol% was carried out via column chromatography using the eluent (1) acetone : *n*-hexane = 5 : 95 v/v and (2) acetone. The characteristic ¹H NMR and inverse-gated ¹³C NMR spectra are shown in Figure A3 and Figure A4(b), respectively, in the Appendix. The assignment of the peaks was done according to the literature.^{57,58,234}

3.2.2.3 Synthesis of glycerol monooleate (GMO)

Glycerol monooleate was synthesized from solketal, and oleoyl chloride following the procedure reported elsewhere.²³⁵ Briefly, solketal (5 g, 37.8 mmol), anhydrous THF (80 ml), and pyridine (6 ml) were added into a 100 ml three neck round bottom flask, equipped with a septum, and magnetic stirrer bar. The reaction flask was placed in an ice bath. Oleoyl chloride (13.6 g, 45.3 mmol) was added drop-wise to the reaction mixture. The reaction was allowed to run for 3 h at room temperature. The pyridinium salt was removed by filtration and the solvent was removed by rotary evaporator. The crude product was dissolved in DCM and extracted three times with water. In the next step, cleaving of the solketal was carried out in 2.0 N HCl in methanol for 5 h. The acid was neutralized with 1.0 N NaOH. The reaction mixture was concentrated in a rotary evaporator, and the crude product was dissolved in DCM and washed three times with

brine. The organic phase was concentrated by evaporating most of the solvent, and the final product was recovered after column chromatography using (1) *n*-hexane : ethyl acetate 70/30 v/v and (2) *n*-hexane : ethyl acetate 50/50 v/v as the eluent. The purified GMO was a mixture of G1MO (glycerol-1-monooleate) 92 mol% and G2MO (glycerol-2-monooleate) 8 mol% (Scheme 3.1) due to acyl migration in acidic media during the cleaving step.²³⁶ The purity of the product was confirmed by ¹H NMR spectroscopy as shown in Figure A5 in the Appendix.

3.2.3 Polymer characterization

¹H NMR spectra and inverse gated (quantitative ¹³C NMR) spectra were recorded on a Varian Gemini NMR spectrometer at 400 MHz and 126 MHz respectively at 27 °C in CDCl₃. For ¹H NMR spectroscopy the concentration of polymer was ~4 % w/v in CDCl₃. For ¹³C NMR spectroscopy the concentration of polymer was ~30 % w/v in CDCl₃.

The number average molar mass (M_n), the weight average molar mass (M_w), and the polydispersity index (M_w/M_n) were measured using Viscotek GPC_{max} VE 2001 with a column set CLM3008 (guard column) and 1GMHHR (analytical column) equipped with VE 3580RI refractive index detector using polystyrene standards and THF as the eluent with a flow rate of 1 ml·min⁻¹ at 22°C (column temperature). The thermal behavior of the polymers was investigated by NETZSCH DSC 204F1 Phoenix. The samples were heated at 10 °C·min⁻¹ to 110°C, held for 10 min, followed by cooling to -80°C with 10 °C·min⁻¹, held at -80°C for 10 min and then heated in the second heating run with 10 °C·min⁻¹ to 60°C. The glass transition temperature T_g was defined as the inflection point of the second heating run.

3.2.4 Sample preparation for X-ray diffraction

Samples for X-ray diffraction studies were prepared by taking the desired amount of GMO and PGA-*g*-O22 in an Eppendorf tube and melt mixed at 50 °C with repeated cycles of spatulations and vortexing, followed by the addition of the desired amount of water and subsequent cycles of spatulations and vortexing for homogenous mixing. Each sample was stored at room temperature for 24 h before measurement. All compositions are given in wt%.

3.2.5 Preparation of nanoparticles

PGA-*g*-O22 and GMO/PGA-*g*-O22 hybrid nanoparticles were prepared by the interfacial deposition method.^{27,83,233} In detail, a solution of 10 mg of GMO/PGA-*g*-O22-90/10 v/v in 100 μ L acetone was added slowly to 1.5 ml water (40 °C) in an Eppendorf tube with constant vortexing for 2 min. The dispersion was further homogenized using a Heidolph SilentCrusher S for 5 min. The organic solvent and a small amount of water were removed by rotary evaporator at room temperature to have the final concentration of the dispersion of 1 % w/v.

3.2.6 Dynamic light scattering

The particle size in aqueous dispersion was determined by an apparatus for simultaneous static and dynamic light scattering experiments (ALV-Laser Vertriebsgesellschaft mbH, Langen, Germany) with a He-Ne laser (632.8 nm, 20 mW). The thermostated sample cell was placed on a precision goniometer ($\pm 0.01^\circ$) that enabled the photomultiplier detector to move from 20° to 150° scattering angle. The intensity time-correlation functions $g^2(\tau)$ were recorded with an ALV-5000E multiple tau digital correlator. The minimal sampling time of this correlator was 12.5 ns. The cylindrical sample cells were made of Suprasil quartz glass by Hellman (Muellheim, Germany) and had a diameter of 10 mm. The pair correlation function f was analyzed to obtain the effective diffusion coefficients D_{eff} of the dispersion. The hydrodynamic radius R_h of the equivalent hydrodynamic hard sphere was calculated *via* the Stokes-Einstein equation

$$R_h = \frac{k_B T}{6\pi\eta D_{eff}} \quad (3.1)$$

Where k_B is the Boltzmann constant and η is the viscosity of the solvent at temperature T.

3.2.7 Negative stain transmission electron microscopy

The negatively stained samples were prepared by spreading 5 μ L of the nanoparticle dispersion onto a Cu grid coated with a Formvar-film (PLANO, Wetzlar, Germany). After 1 min excess liquid was blotted off with filter paper and 5 μ L of 1 wt% aqueous uranyl acetate solution was placed onto the grid and drained off after 1 min. The dried specimens were examined with an EM 900 transmission electron microscope (Carl Zeiss Microscopy GmbH, Oberkochen, Germany). Micrographs were taken with a SSCCD SM-1k-120 camera (TRS, Moorenweis, Germany).

3.2.8 Cryogenic transmission electron microscopy

Vitrified specimens for cryo-TEM were prepared by a blotting procedure, performed in a chamber with controlled temperature and humidity using a LEICA grid plunger. A drop of the sample solution ($1 \text{ mg}\cdot\text{ml}^{-1}$) was placed onto an EM grid coated with a holey carbon film (C-flat, Protochips Inc., Raleigh, NC). Excess solution was then removed with filter paper, leaving a thin film of the solution spanning the holes of the carbon film on the EM grid. Vitrification of the thin film was achieved by rapid plunging of the grid into liquid ethane held just above its freezing point. The vitrified specimen was kept below 108 K during storage, transfer to the microscope, and investigation. Specimens were examined with a LIBRA 120 PLUS instrument (Carl Zeiss Microscopy GmbH, Oberkochen, Germany), operating at 120 kV. The microscope is equipped with a Gatan 626 cryotransfer system. Images were taken with a BM-2k-120 Dual-Speed on axis SSCCD-camera (TRS, Moorenweis, Germany).

3.2.9 X-ray diffraction

X-ray diffraction patterns were recorded with a 2D detector (Vantec 500, Bruker) using Ni-filtered and pin hole collimated Cu K_{α} radiation. The exposure time was 15 min, and the sample to detector distance was 9.85 and 27.7 cm for wide and small angle scattering experiments, respectively. The samples were held in glass capillaries (\varnothing 1 mm, Hilgenberg, Germany). For calculating the lattice parameters of the selected cubic phases, the X-ray diffraction patterns were recorded with an Anton-Paar compact Kratky camera using Ni-filtered and slit collimated Cu K_{α} X-rays. The data were background corrected and desmeared.²³⁷ The lattice parameter a of the cubic phase was calculated by^{104,238}

$$d_{hkl} = \frac{2\pi}{q_{max}} = \frac{a}{\sqrt{h^2+k^2+l^2}} \quad (3.2)$$

Where d_{hkl} is the distance between planes, q_{max} is the scattering vector at the peak maximum, and h , k , and l are the Miller indices of the scattering plane. The individual cubic phase is distinguished by the characteristic peak position ratios; for $Pn3m = \sqrt{2}, \sqrt{3}, \sqrt{4}, \sqrt{6}, \sqrt{8}$ etc. (indexed as $(hkl) = (110), (111), (200), (211), (220)$) and for $Ia3d = \sqrt{6}, \sqrt{8}, \sqrt{14}, \sqrt{16}, \sqrt{20}$ etc. (indexed as $(hkl) = (211), (220), (321), (400), (420)$). The lamellar phases show peak ratios of 1, 2, 3, 4 etc. Representative SAXS traces and their indices are given in Figure A7 in the Appendix.

3.3 RESULTS AND DISCUSSION

3.3.1 Syntheses and grafting of poly(glycerol adipate) and glycerol monooleate

The enzyme-catalyzed synthesis of poly(glycerol adipate) (PGA) was carried out using glycerol and divinyl adipate in THF at 50°C in the presence of *Candida antarctica* Lipase B (CAL-B) (Scheme 3.1). Although PGA can also be produced by adipic acid or its alkyl esters instead of its vinyl esters, but to achieve high molar masses it is necessary to remove side products to shift the condensation equilibrium to the forward direction. The advantage of using divinyl adipate is that it is an irreversible procedure for lipase-catalyzed acylation, as the leaving group is vinyl alcohol that tautomerizes to acetaldehyde which is a gas, and it easily leaves the system resulting in high molar mass polymers, compared to polymers obtained from adipic acid or its alkyl ester, where the side product is water, methanol or ethanol^{197,209,239} for which one must apply low pressure and high temperature. These conditions usually favour branching.⁶⁵ In this work, under the applied reaction condition, the regioselectivity of the enzyme was well under control as can be seen in ¹³C NMR spectrum (see Figure 3.2(a)).

From the spectrum the molar ratio of the various modes of the substituted glycerol unit was estimated from the integrated areas of the methine peak A-D: 1-substituted (T_G) : 1,2-disubstituted ($L_{1,2}$) : 1,3-disubstituted ($L_{1,3}$) : trisubstituted (D) = 4 : 4 : 90 : 2. On the basis of these data, the mol% regioselectivity at primary OH groups is calculated to 98 mol% using equation 3.3.⁵⁷

$$\% \text{ regioselectivity of primary OH groups} = \frac{T_G + (L_{1,2}) + 2(L_{1,3}) + 2(D)}{T_G + 2(L_{1,2}) + 2(L_{1,3}) + 3(D)} \times 100 \quad 3.3$$

The mol% degree of branching of polymers are determined by Frechet equation (Equation 3.4)²⁴⁰ or by Frey equation (Equation 3.5)²⁴¹

$$\text{mol}\% \text{ degree of branching} = \frac{T_G + T_A + D}{T_G + T_A + L_{1,2} + L_{1,3} + D} \times 100 \quad 3.4$$

$$\% \text{ degree of branching} = \frac{2D}{L_{1,2} + L_{1,3} + 2D} \times 100 \quad 3.5$$

here, T_A is terminal adipic acid unit. Since the quantitative determination of T_A could not be done precisely. As a consequence the mol% degree of branching defined by Frey

(Equation 3.5) is preferred for our calculation. The mol% degree of branching is calculated to 4 mol%.

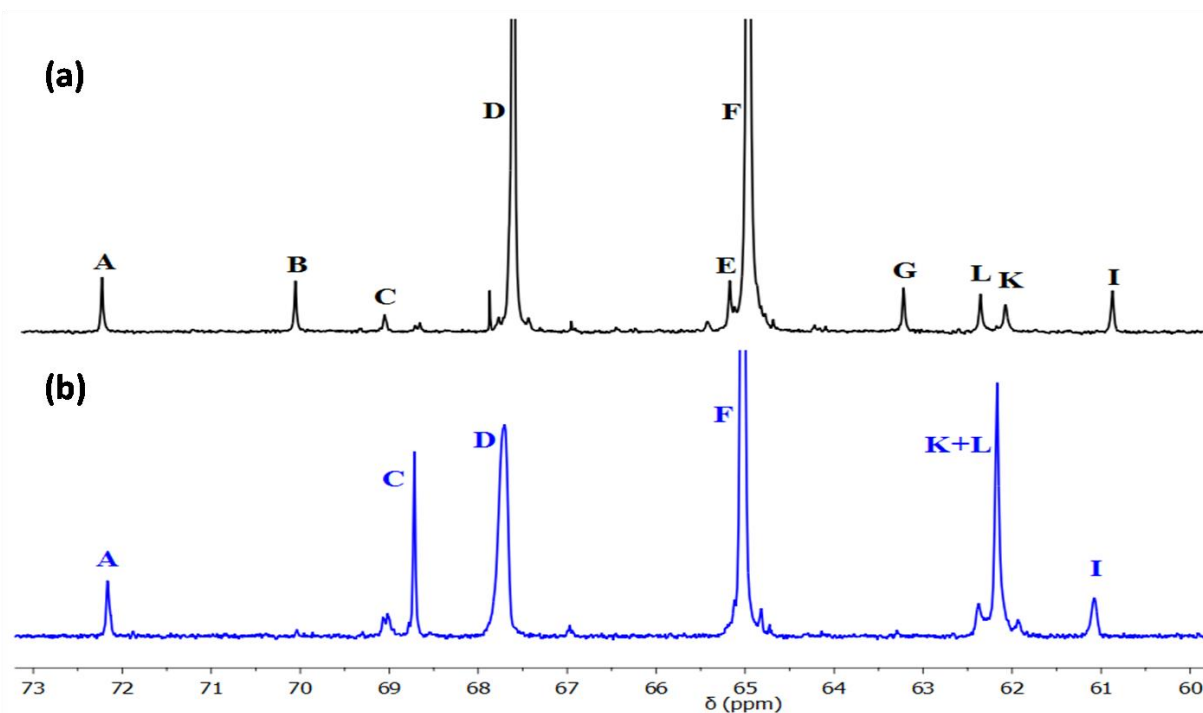
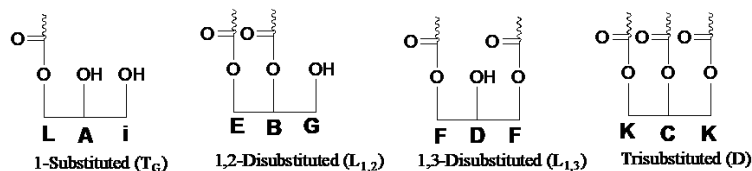


Figure 3.2. Expanded, inverse-gated ^{13}C NMR spectra of (a) PGA and (b) PGA-*g*-O22 recorded at 27°C in CDCl_3 .

Enzymatic transesterification is very sensitive to moisture, thus, certain moisture conditions can lead to depolymerization.²⁰⁸ The source of moisture is the enzyme itself,^{61,70,242} so careful optimization is needed to obtain the best results in terms of molar mass, the rate of reaction, and the polydispersity index. In the present work, the enzymatic polymerization was optimized at two different temperatures (30°C and 50°C). The corresponding change in molar mass and PDI with respect to time is shown in Figure 3.3.

In Figure 3.3a the reaction was carried out at 50°C using 2 wt% CAL-B with respect to the monomers in THF. This system gives the highest number average molar mass (4800 $\text{g}\cdot\text{mol}^{-1}$) and the polydispersity index of $M_w/M_n = 2.0$ within 11 h. Beyond 11 h the molar

mass continuously decreases with increasing *PDI*. These findings indicate the presence of deacylation steps explained by Kobayashi.²⁰⁸ The reason of this deacylation is the presence of trace amounts of water in the system.^{61,243} The source of water is the enzyme itself, although the enzyme was dried over P₂O₅ for 24 h and anhydrous THF was used for the reaction. The complete removal of water is not possible as there always remains a small amount of water within the active site of enzyme called "surface bound water".²³⁹ This surface bound water is important for the enzyme activity as proteins are rigid in organic solvents.²⁴⁴ It also increases the dielectric constant of the active site and makes it suitable to attack. A polar solvent such as THF, unbound the bounded water during the course of reaction that consequently leads to deacylation after some time.²⁴² However, reaction optimization studies at 30°C shown in Figure 3.3b reveal a slow reaction because of the low mobility of the oligomers as the highest molar mass was obtained after 25 h.

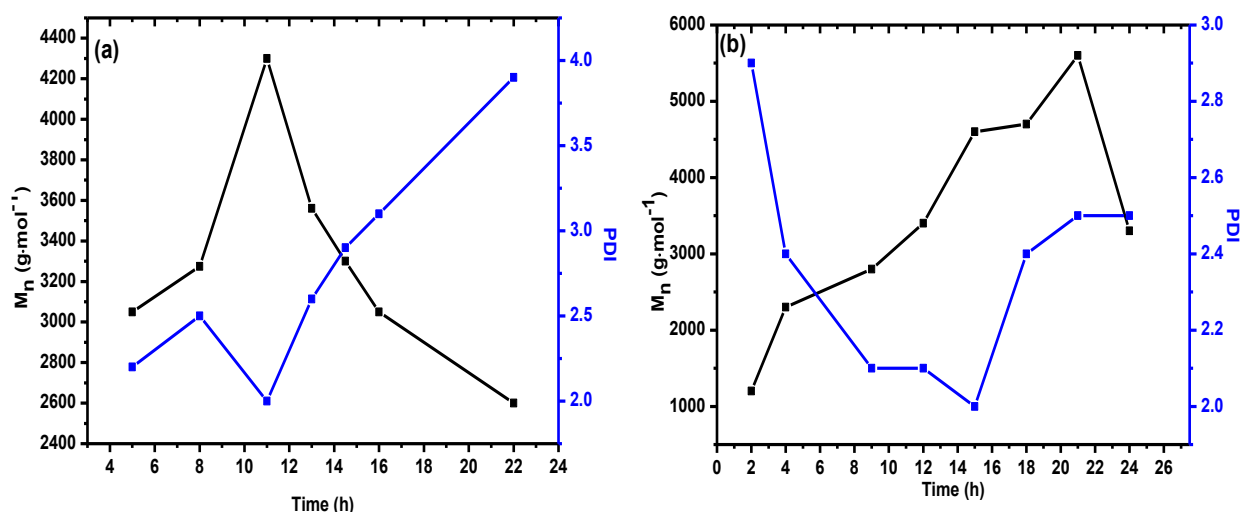


Figure 3.3. Optimizing the reaction conditions using 2 wt % CAL-B with respect to total mass of monomers at (a) 50°C (b) 30°C.

For the current work, PGA of molar mass of $M_n = 4,800 \text{ g}\cdot\text{mol}^{-1}$ and the polydispersity index of $M_w/M_n = 2.0$ obtained at 50 °C and 11 h of reaction time was considered for further grafting. It is worth mentioning here that no polymeric materials were formed in the absence of enzyme, indicating that the polymerization took place through enzyme catalysis, which is consistent with previous findings.^{57,245}

In the next step of synthesis, the oleate side chains were grafted onto the PGA backbone by an esterification reaction between the pendant OH groups of the PGA and oleoyl chloride in THF at 80°C in the presence of pyridine.⁸⁸ The successful synthesis is

verified by ^1H NMR spectroscopy as shown in Figure 3.4, where, in addition to the signals of the PGA backbone, signals due to the oleate side chains are observed.

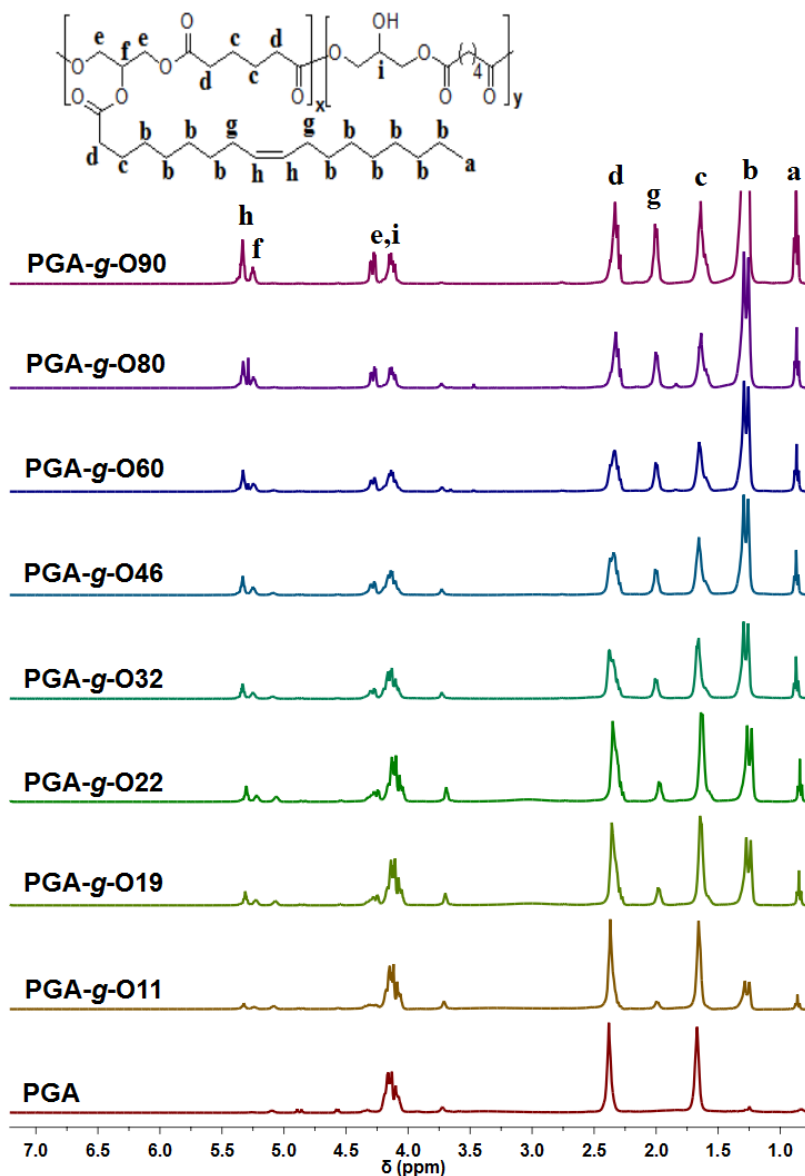


Figure 3.4: ^1H NMR spectra of PGA and the respective PGA-*g*-O_x, measured at 27 °C in CDCl_3 .

The degree of grafting is calculated from the respective ^1H NMR spectrum using the following formula

$$\text{mol}\% \text{ degree of grafting} = \frac{a \times 1.33}{d - 0.67a} \times 100 \quad (3.6)$$

where a represents the integral area of the methyl proton peak of oleate side chains and d is the combined area of the methylene protons of PGA backbone and the oleate side chain next to carbonyl groups.

In addition, the quantitative ^{13}C NMR spectrum (see Figure 3.2(b)) helped to quantify the different types of the substituted glycerol unit as mentioned before. For PGA-*g*-O22 the ratio of integrated areas of the methine peak A-D; 1-substituted : 1,2-disubstituted : 1,3-disubstituted:trisubstituted = 7 : 0 : 70 : 23. On the basis of these data, the trisubstituted glycerol unit is calculated as 23% that fits with the degree of oleate grafting obtained using the ^1H NMR spectrum.

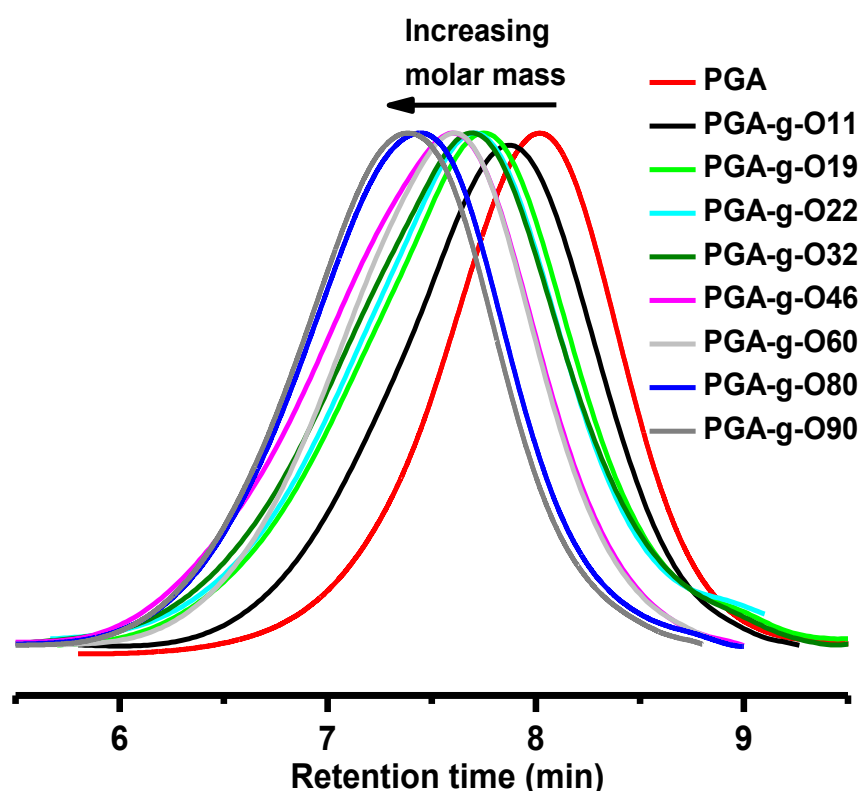


Figure 3.5: GPC traces of the synthesized PGA and the respective PGA-*g*-O_x, measured in THF at 22 °C. The calibration was performed with polystyrene standards.

The polyester modification could also lead to the cleavage of the polymer backbone, but in this study, no significant cleavage was observed as a successive shift of the GPC traces (see Figure 3.5) to higher molar masses, with increasing degree of grafting is observed. Table 3.1 summarizes all data of the polymers under consideration.

Glycerol monooleate (GMO) was synthesized following the previously reported procedure.²³⁵ The final product was a mixture of G1MO (glycerol-1-monooleate, 92 mol%) and G2MO (glycerol-2-monooleate, 8 mol%) (calculated from the ^1H NMR spectrum shown in Figure A4 in the Appendix).

Table 3.1: Characteristic data of the synthesized PGA and PGA-*g*-Ox.

Sample	M_n (g/mol) ^a	M_w/M_n ^b	T_g (°C) ^c	Φ_{oleate} (vol. %) ^d	d (Å) ^e
PGA	4,800	2.0	-24	0	-
PGA- <i>g</i> -O11	5,600	2.1	-30	16	66.0
PGA- <i>g</i> -O19	6,100	2.4	-33	24	51.5
PGA- <i>g</i> -O22	6,400	2.0	-35	27	48.2
PGA- <i>g</i> -O32	6,900	2.6	-38	33	44.9
PGA- <i>g</i> -O46	7,700	2.6	-42	40	38.5
PGA- <i>g</i> -O60	8,500	2.1	-47	46	35.3
PGA- <i>g</i> -O80	9,800	2.3	-53	53	32
PGA- <i>g</i> -O90	10,600	1.9	-57	56	30.9

^aAll molar masses except for PGA are calculated on the basis of mol% degree of grafting calculated from the respective ¹H NMR spectra. Molar mass of PGA is obtained from GPC using THF as eluent against polystyrene standards (degree of polymerization is 24).

^bThe polydispersity index M_w/M_n is obtained from the GPC data (Figure 3.5).

^cObtained from the DSC thermograms shown in Figure 3.7.

^dVolume fraction of oleate side chain is calculated by Materials Studio software 4.1.

^eThe characteristic length d was calculated from the respective *peak II* maximum in Figure 3.6.

3.3.2 Characterization of PGA-*g*-Ox with nanodomains formed by oleate side chains

The flexibility and dynamics of the grafted chains control the crystallization of the side chains in graft copolymers with flexible backbone.^{246–248} For example, in our previous studies, the PGA backbone was modified with all-trans stearate side chains that could crystallize and hence induced phase separation of the saturated alkyl side chains.^{88,90} In the system under investigation, however, the presence of cis-double bonds makes the oleate side chains incapable of packing into a crystalline structure. Therefore, completely amorphous graft copolymers were anticipated. Thus, the X-ray scattering profiles (Figure 3.6) of PGA and PGA-*g*-Ox exhibit only a typical broad amorphous halo in the wide angle regime (*peak I*) with a maximum at approximately $2\theta = 20^\circ$ and no Bragg reflections indicating the absence of crystals. The broad halo appears due to the average distance between neighbouring atoms in the amorphous state. In the small angle regime, *peak II* shifts to higher q -values with increasing grafting density which is an evidence of

nanophase separation of the oleate side chains into nanodomains. According to Bragg's law, and the definition of the scattering vector q , *peak II* reflects a characteristic length of $d = 2\pi/q_{max}$ in the range of 66 Å for PGA-*g*-O11 to 30.9 Å for PGA-*g*-O90. The decreasing length d with increasing degree of grafting can be attributed to the higher volume fraction of the nanodomains with increasing degree of grafting.

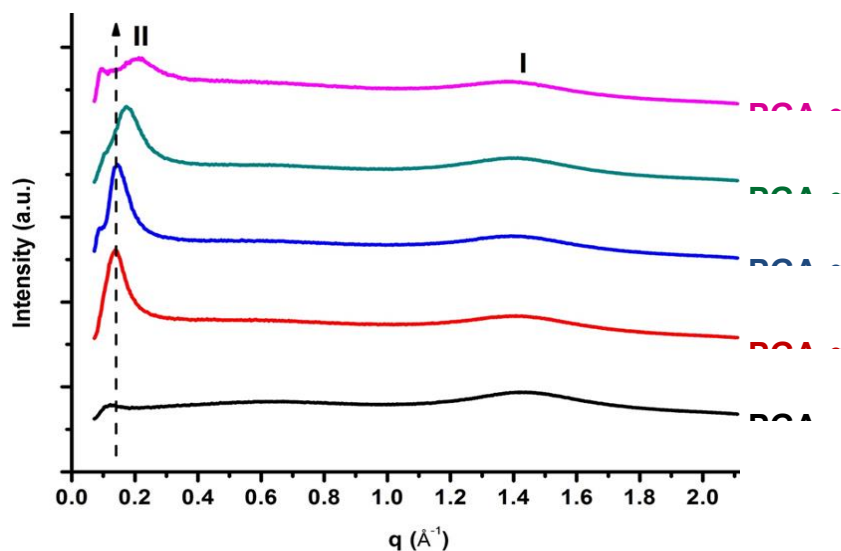


Figure 3.6: Combined SAXS and WAXS profiles of PGA and PGA-*g*-Ox. *Peak I* in the WAXS region of the trace indicates the amorphous halo and *peak II* in the SAXS region is caused by nanophase separation between the polymer backbone and grafted side chains.

The absence of higher order reflections, however, suggests the formation of less ordered structures and hence the bulk phase morphology could not be identified from SAXS data.^{83,91,233} Further evidence of the amorphous nature of the synthesized graft polymers comes from differential scanning calorimetry (DSC) measurements (Figure 3.7) that exhibit only a glass transition temperature of the PGA backbone in unmodified PGA and all PGA-*g*-Ox samples.

A glass transition temperature of $T_g \sim -24$ °C is recorded for the unmodified PGA, which is consistent with the literature⁹² and it decreases progressively for PGA-*g*-Ox from -32 °C to -60 °C when x is varied from 11 to 90. Thus, the grafted oleate side chains induce an internal plasticization by reducing the steric hindrance to the segmental mobility of the PGA.

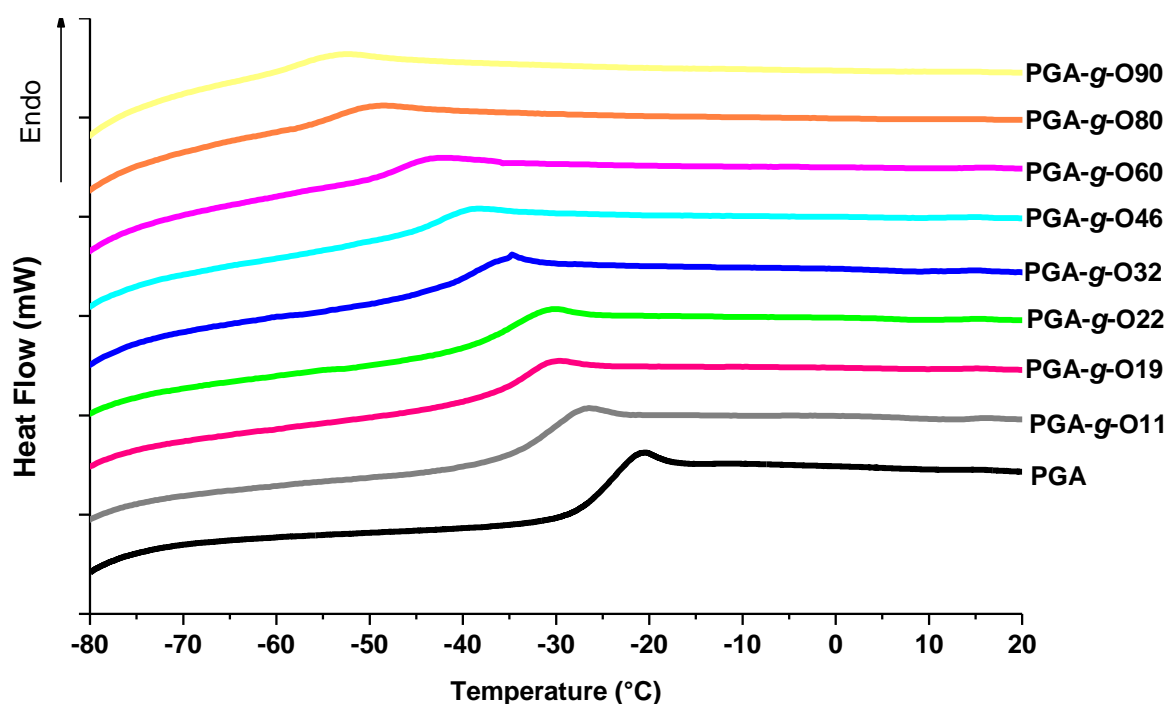


Figure 3.7: Differential scanning calorimetry traces of the PGA and the PGA-*g*-O_x recorded with a heating rate of 10 °C·min⁻¹.

3.3.3 The ternary system GMO/PGA-*g*-O22/water

To identify various liquid crystalline phases, SAXS is employed and a detailed ternary phase diagram of GMO/PGA-*g*-O_x/water at 25 °C is constructed for one of the synthesized PGA-*g*-O_x, namely PGA-*g*-O22. This graft copolymer is selected since it has a similar volume ratio of oleate chains to polar polymer backbone (27 vol. %) as the volume ratio of the oleate chain to the glycerol polar head group in GMO (30 vol. %). The GMO/PGA-*g*-O22/water ternary phase diagram is depicted in Figure 3.8. If an excess of water is observed during preparation, this is indicated by brackets in the phase diagram.

Firstly, the focus is given to the behavior of the binary systems along the three axes (GMO-axis (GMO/water), PGA-*g*-O22-axis (GMO/PGA-*g*-O22), and water-axis (PGA-*g*-O22/water)) in the constructed ternary phase diagram. The GMO/water binary system has been studied in literature mainly in the range of large GMO contents.

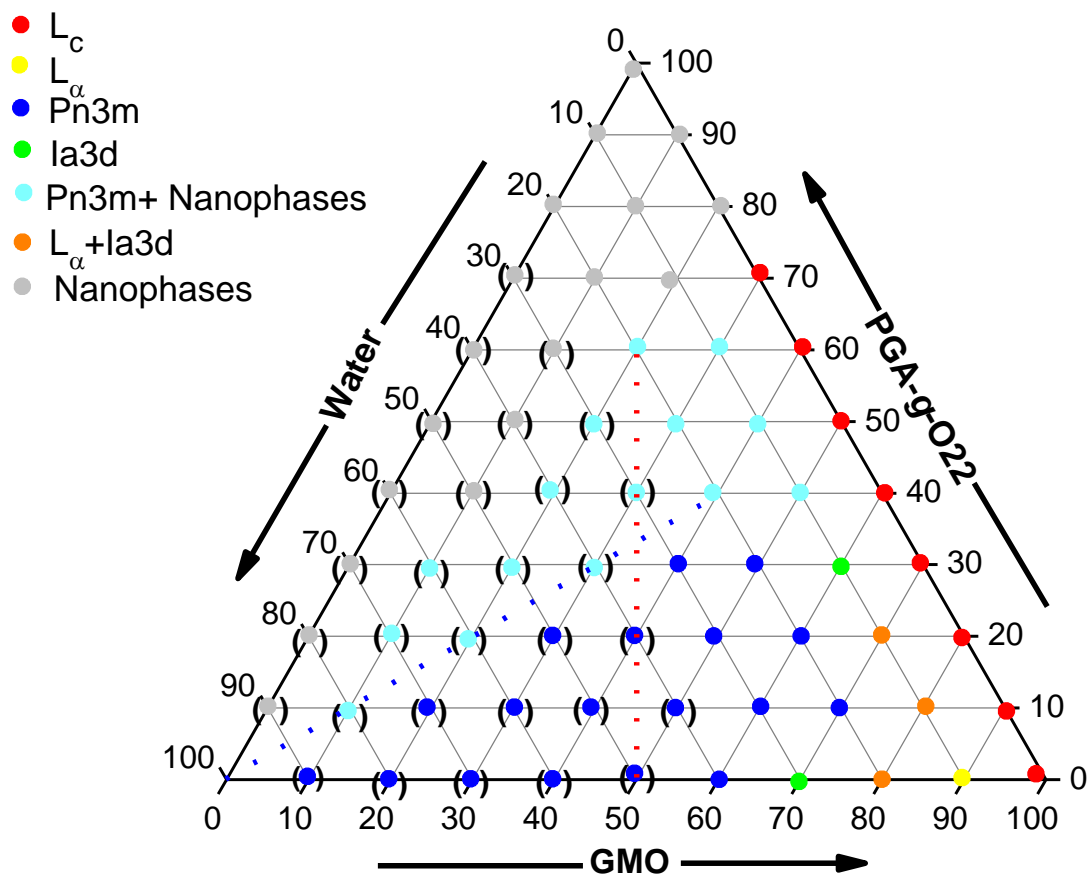


Figure 3.8. Ternary phase diagram of the GMO/PGA-*g*-O22/water system at 25°C. The compositions in wt% indicates the feed ratios of the blends, while the brackets indicate those compositions where an excess of water is observed. The red dotted line indicates the direction of constant GMO/water ratio with varying PGA-*g*-O22 concentration whereas the blue dotted line represents a constant GMO/PGA-*g*-O22 ratio with varying water concentration.

Figure 3.9(a) shows that GMO forms in bulk a lamellar crystal L_c phase with Bragg reflections observed by wide angle X-ray scattering (WAXS, see inset of Figure 3.9a). Upon increasing amounts of water, a liquid crystalline lamellar L_α phase can be observed where the GMO molecules are arranged in bilayers separated by water channels and without Bragg reflections in the WAXS range. This is followed by a mixture of L_α and the cubic $Ia3d$ phase. The system GMO/water-70/30 exhibits exclusively the $Ia3d$ phase and GMO/water-60/40 forms another cubic phase with $Pn3m$ symmetry. At high water concentrations, the double diamond cubic phase of $Pn3m$ symmetry remains existent with an excess of water of hydration which is in agreement with literature data.^{219,249,250} The SAXS pattern of all discussed liquid crystalline phases are shown in Figure 3.9.

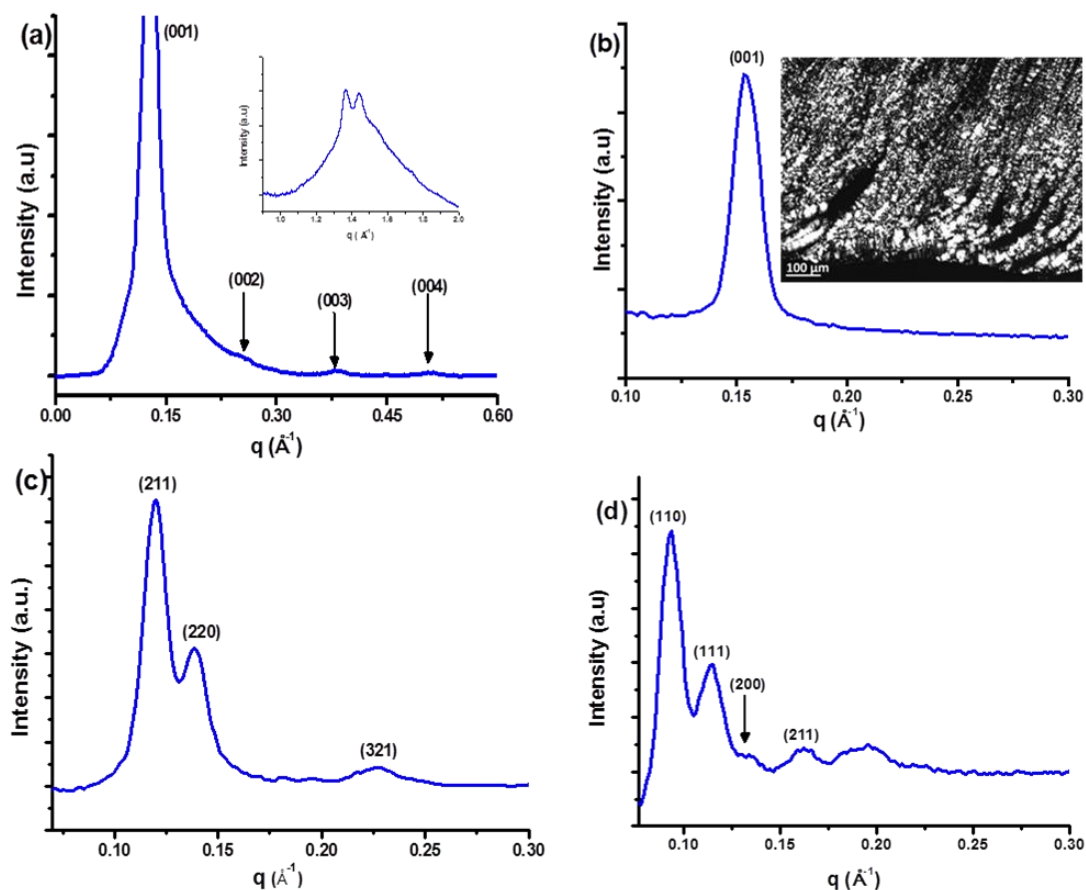


Figure 3.9. SAXS pattern at 25°C of (a) GMO/PGA-*g*-O22- 80/20, (lamellar crystalline phase), the inset shows the scattering behavior in the WAXS regime, (b) GMO/water - 90/10, (liquid crystalline lamellar, L_{α} phase), the inset shows its optical micrograph, (c) GMO/PGA-*g*-O22/water -60/30/10 (gyroid cubic phase with $Ia3d$ symmetry), (d) GMO/PGA-*g*-O22/water - 60/10/30 (double diamond cubic phase of $Pn3m$ symmetry). All the compositions are in wt%.

The PGA-*g*-O22 axis represents the binary blend system GMO/PGA-*g*-O22. Starting again with neat GMO it can be observed that with increasing amount of PGA-*g*-O22 the lamellar crystal L_c phase remains present up to the system GMO/PGA-*g*-O22-30/70 (see Figure 3.11b). The relative peak positions in the SAXS range of 1:2:3:4 etc. (for indexing see Figure 3.9) can be observed, and the typical Bragg reflections in the WAXS trace indicate again the formation of a crystalline phase (see Figure 3.10).

When the polymer content reaches 80 wt% in the system GMO/PGA-*g*-O22 -20/80 the SAXS pattern is dominated of that by neat PGA-*g*-O22 (cf. Figure 3.11b). The SAXS peak as a result of the nanophase separation of PGA-*g*-O22 is not influenced by the presence of up to 20 wt% GMO. Thus, it can be concluded that the structure formation of neither GMO nor PGA-*g*-O22 is influenced by the presence of the other compound significantly.

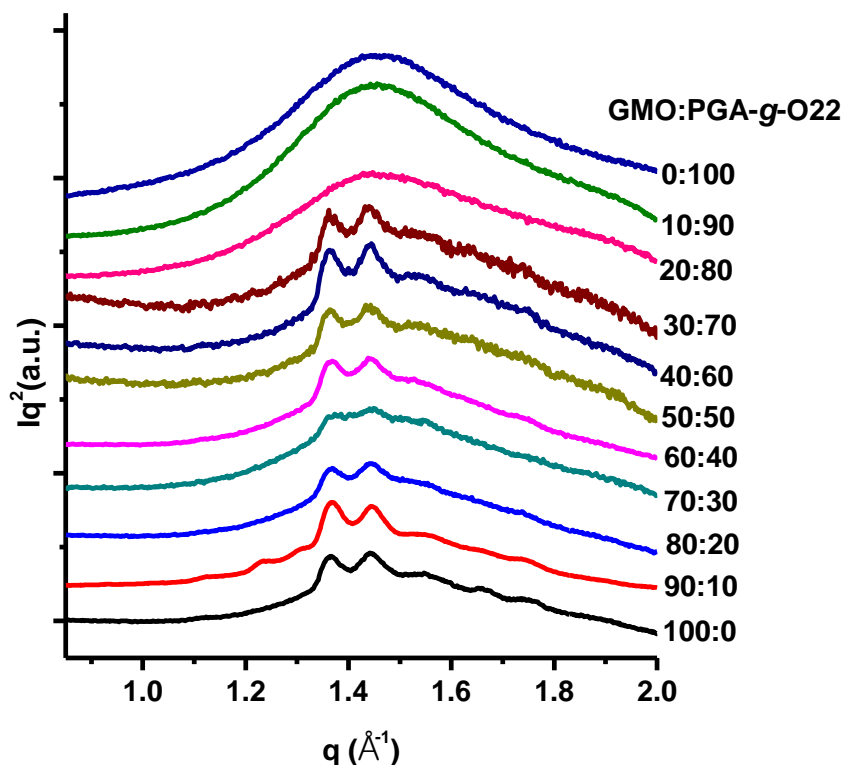


Figure 3.10. WAXS patterns of GMO/PGA-*g*-O22 binary system.

The disappearance of the scattering peaks of the L_c phase of GMO, beyond GMO/PGA-*g*-O22-30/70 could be either due to the complete disintegration of the GMO microstructure due to higher polymer content or the insignificant contribution of GMO to the scattering due to its small content in the mixture.

The third binary system along the water-axis represents the binary system PGA-*g*-O22/water. As can be seen in Figure 3.11(c), the peak in the SAXS trace of PGA-*g*-O22 attributed to the nanophase separation of the oleate side chains into nanodomains within a matrix of the polar polymer backbone shifts to larger q -values when the water content in the blends is increased up to 20 wt% and remains constant upon further increase of the water content. This agrees with the observation that PGA-*g*-O22 swells in water but is not soluble in water. As given in Table 3.1, for dry PGA-*g*-O22, the average distance between the nanodomains is $d = 48.2 \text{ \AA}$ calculated from the SAXS peak. With an increase of the water content to 20 wt%, the distance between the nanodomains increases slightly to approximately $d = 52.3 \text{ \AA}$ caused by the swelling of the polar matrix. Higher amounts of water do not result in a further increase of the distance, but an excess of water can be detected.

The presence of excess water, indicated by the brackets in Figure 3.8, can be detected in the full ternary phase diagram for all samples with at least 30 wt% of water, unless the amount of GMO exceeds the amount of water (i.e., left of the red dotted line in Figure 3.8). Swollen polymer, marked as ‘nanophases’ in Figure 3.8, is present in all samples with a polymer content greater than GMO (i.e., above the blue dotted line in Figure 3.8), only in case of water free samples, the behavior is different as described above.

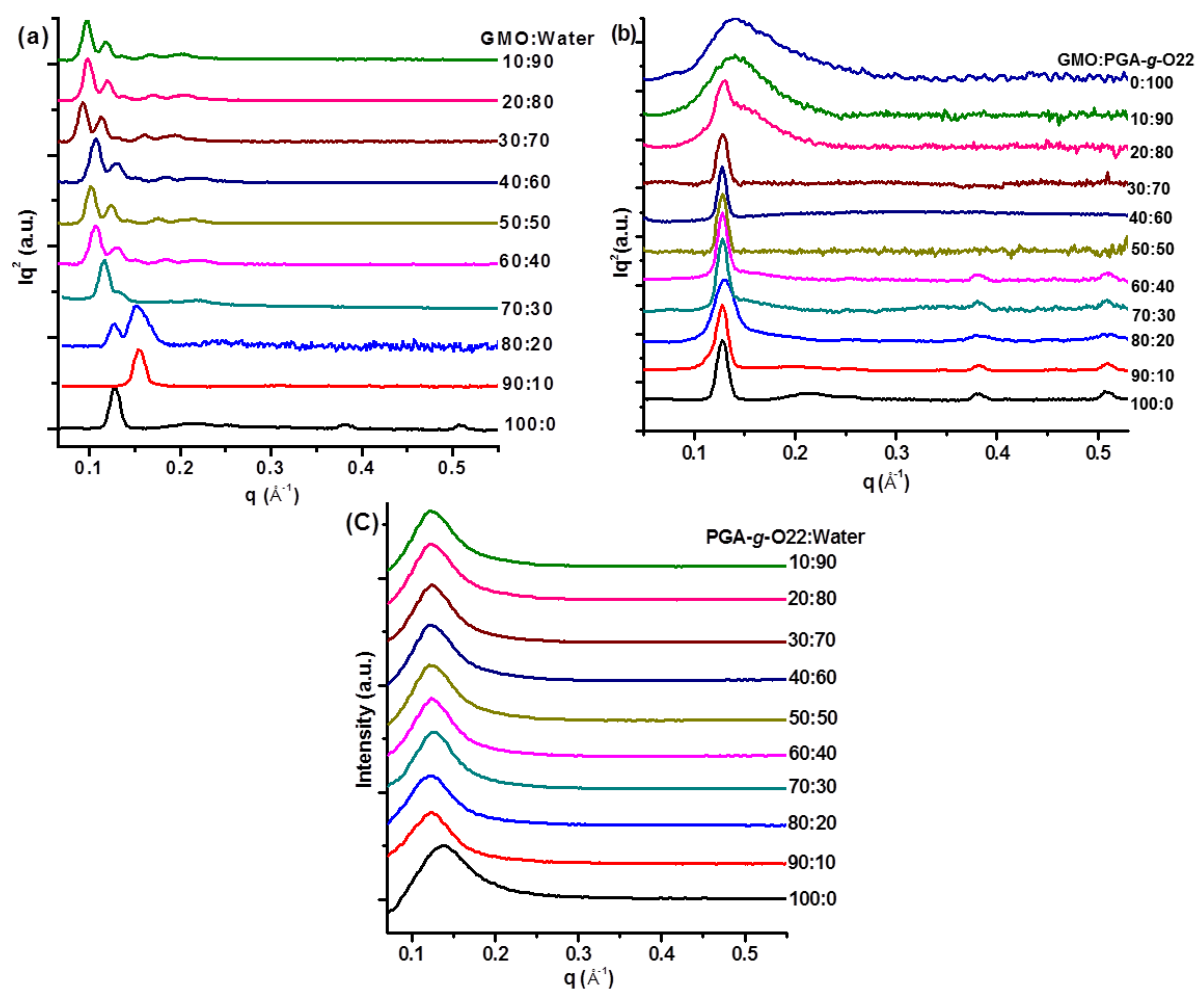


Figure 3.11: SAXS patterns of binary systems at 25 °C of (a) GMO/water, (b) GMO/PGA-g-O22, and (c) PGA-g-O22/water. The corresponding compositions are given in wt%.

For samples with a higher GMO than polymer content, the same mesophase structures as in the neat GMO-water system (i.e., $Pn3m$, and $Ia3d$) can be observed, without an indication of a separate polymer phase. It can be assumed, that PGA-g-O22 is included to a certain extent in the GMO/water system. For example, the $Ia3d$ morphology at GMO/water - 70/30 can also be found in the mixture of GMO/PGA-g-O22/water-60/30/10. In this case, almost all free water should be incorporated into the polymer, i.e. the swollen polymer substitutes the water in the gyroid cubic phase. However, with only

a partial substitution of water by the swollen polymer, the double diamond cubic phase with $Pn3m$ symmetry is formed. This structure can be identified by the SAXS peak ratios of $\sqrt{2}, \sqrt{3}, \sqrt{4}, \sqrt{6}, \sqrt{8}$, according to the $Pn3m$ symmetry for GMO/PGA-*g*-O22/water - 60/10/30. This morphology is also the most stable one when water or polymer exists in excess.

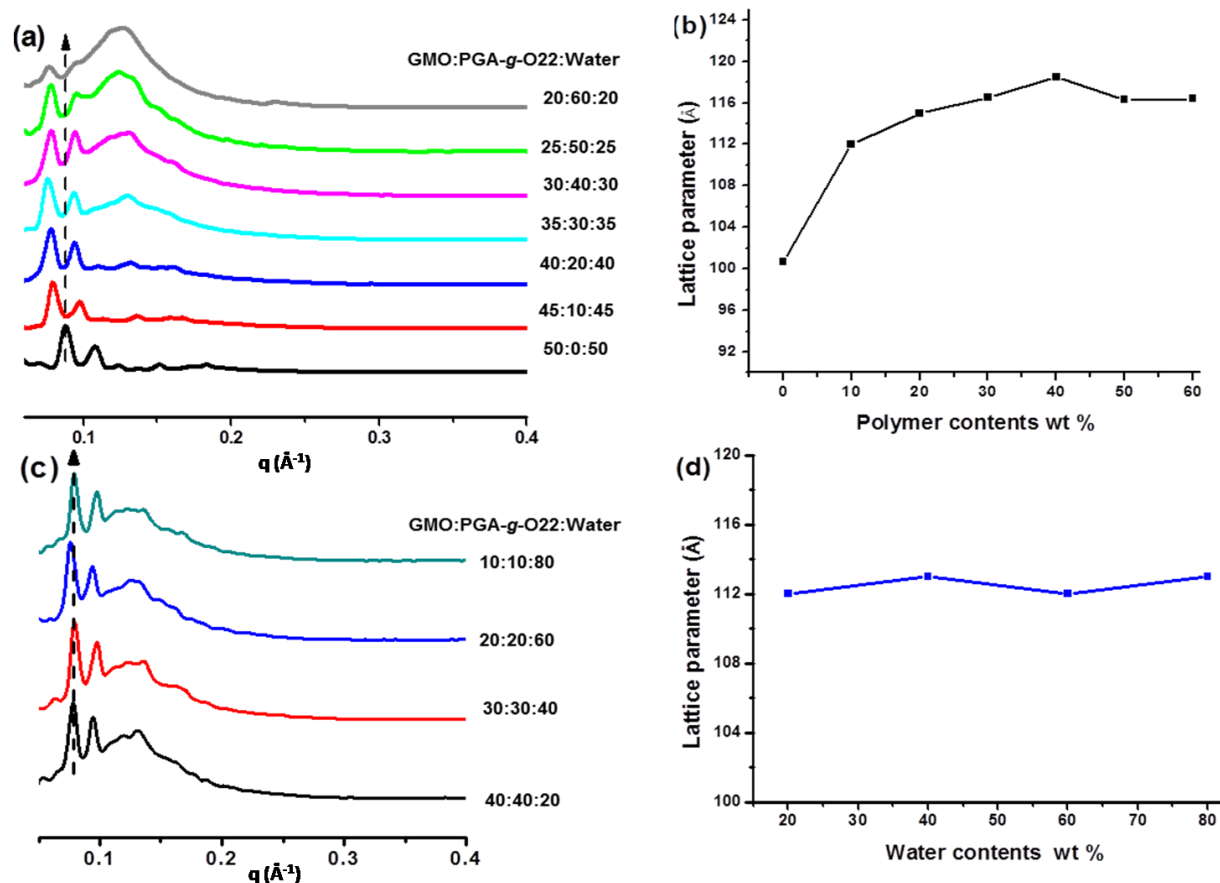


Figure 3.12: (a) SAXS profiles and (b) the respective lattice parameter of the $Pn3m$ cubic phase of GMO/PGA-*g*-O22/water ternary systems with a constant GMO/water ratio while increasing the polymer content from 0 to 60 wt%. (c) SAXS profiles and (d) the respective lattice parameter with increasing water content from 20 to 80 wt% while keeping the GMO/PGA-*g*-O22 ratio constant at 1: 1.

As discussed above, GMO forms a liquid crystalline lamellar L_α phase in the GMO/water binary system. Starting in this phase at GMO/PGA-*g*-O22/water - 90/0/10, and keeping the total amount of water constant, the addition of polymer reduces by absorption the amount of available water, until at GMO/PGA-*g*-O22/water-60/30/10 almost all water is in the swollen polymer ($Ia3d$ morphology). Between both points, a mixture of both phases, L_α and $Ia3d$, can be observed. Further addition of polymer leads to an excess of a swollen polymer phase, and the $Pn3m$ morphology is formed. This

transition is equivalent to that of the binary GMO/water system from low to high amounts of water. To obtain more information on the polymer incorporation into the cubic phases, various compositions, with a constant GMO/water ratio of 1:1 and increasing polymer content, and with the constant GMO/polymer ratio of 1:1 and increasing water content are investigated by SAXS.

Figure 3.12 (a) depicts the SAXS profiles of seven GMO/PGA-*g*-O22/water systems, all with the same GMO/water ratio of 1:1 but with increasing polymer content from 0 to 60 wt%. The relative peak positions are $\sqrt{2}, \sqrt{3}, \sqrt{4}, \sqrt{6}, \sqrt{8}$ according to the $Pn3m$ space group of the cubic phase. The first peak maximum shifts towards lower q -values with increasing polymer content (shown by an arrow in Figure 3.12(a) which is a clear reflection of the cubic phase swelling due to the polymer insertion into the lipid bilayer. The corresponding lattice parameter, calculated according to Equation 3.2, is plotted as a function of polymer content in Figure 3.12(b). It increases significantly from approximately $a = 101 \text{ \AA}$ in the absence of polymer to approximately $a = 116 \text{ \AA}$ in the presence of 30 wt% PGA-*g*-O22. At higher polymer contents, the lattice parameter remains almost constant and the polymer background scattering, however, becomes more dominant.

The water channels diameter of the cubic phase can be calculated from the geometry of the structure.^{147,250} For GMO-water system with the $Pn3m$ cubic phase the diameter of the water channel is given by equation 3.7.

$$d_w = 0.782a - 34.3 \text{ \AA} \quad (3.7)$$

At room temperature, the water channel diameter for the $Pn3m$ cubic phases increased from 44.7 \AA in the absence of PGA-*g*-O22 to approximately 56.4 \AA with 30 wt% PGA-*g*-O22. Due to the identical chain structure of the oleate side chains of the PGA-*g*-O22 and the hydrophobic oleate tail of the GMO, it is assumed that the hydrophobic oleate side chains of the PGA-*g*-O22 penetrate the lipid bilayer while the PGA backbone, equipped with hydrophilic hydroxyl group and polar ester bonds, stays at the interface. The data show further that, the $Pn3m$ cubic phase is stable and stays largely intact with increasing polymer content. In contrast, while keeping the ratio of GMO/PGA-*g*-O22 constant 1 : 1 while increasing the water amount from 20 to 80 wt% (Figure 3.12(c)), the lattice parameter of the $Pn3m$ phase exhibits almost negligible changes as depicted in Figure 3.12(d), an indication of the fully swollen cubic phase state. By comparing the data of

Figure 3.12 (b) and 3.12 (d), it can be concluded that it is mainly the PGA-*g*-O22 content in the composition that controls the cubic phase swelling and the water channel enlargement.

The observation of the water channel enlargement and cubic phase swelling (cf. Figure 3.13), due to the addition of PGA-*g*-O22 to the GMO/water system, is very significant keeping in mind that mostly low molar mass additives, such as non-ionic octyl- β -D-glucopyranoside (β -Glc-OC8)²²¹ and charged surfactant-doped systems dioctyl sodium sulfosuccinate (AOT)²²¹ neutral sucrose stearate,²²³ charged lipids,²²² cholesterol,²²² and nucleic acids,²²⁴ to name a few, have been observed to generate the cubic phase swelling and water channel enlargement. Furthermore, the addition of Pluronic® F127 to the GMO/water system has been found to transform the cubic phase symmetry from the double diamond $Pn3m$ to the primitive $Im3m$ that reflects the destabilization and disruption of the internal liquid crystalline structure.^{27,29,213} The current study, however, signifies that amphiphilic grafted polymers, of a suitable design, could be a potential alternative and be exploited for tuning the behavior and properties of the lipid bicontinuous cubic phases for improved stability and applications.

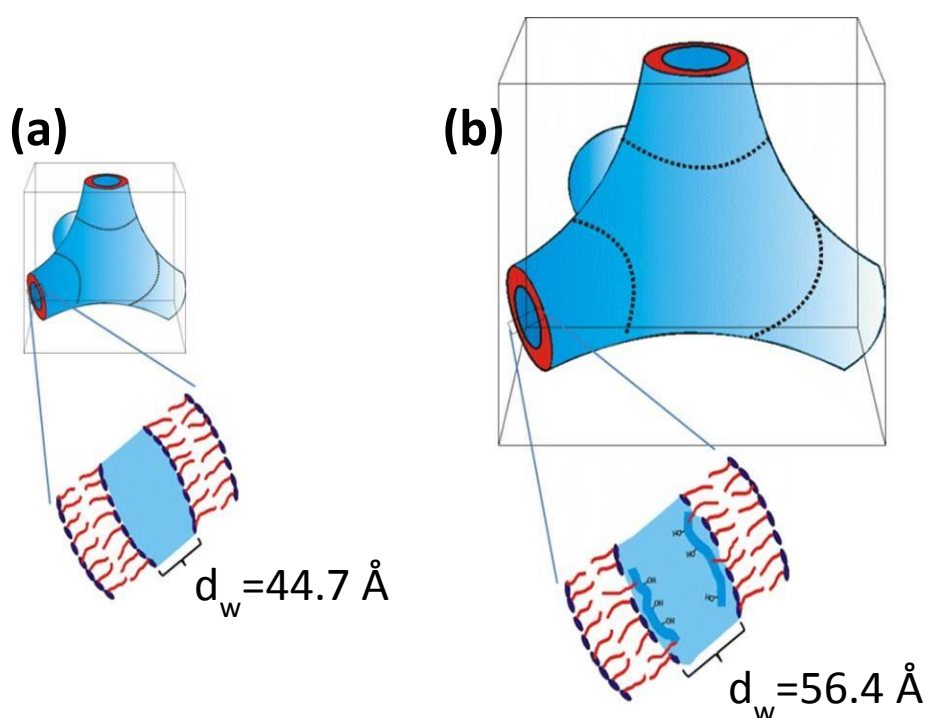


Figure 3.13: Schematic illustration of swelling of the $Pn3m$ cubic phase. (a) Standard cubic phase from GMO/water - 50/50. (b) The swollen $Pn3m$ cubic phase of the ternary system containing GMO/PGA-*g*-O22/water - 30/40/30.

Additionally, PGA-*g*-Ox is biocompatible, biodegradable, and most important, in comparison to the traditional lower molar mass additives, the possibility of fine-tuning the behavior of PGA-*g*-Ox by structural adjustment with varying the hydrophobic/hydrophilic balance, molar mass, and the degree of grafting could open up a new avenue in material design for controlling the lipid liquid crystalline phase behavior and properties for enhanced biomedical and pharmaceutical applications.

3.3.4 PGA-*g*-O22 as a potential stabilizer for GMO based nanoparticles in aqueous dispersions

As discussed above, the system GMO/water is frequently used to prepare cubosomes or other structured nanoparticles which usually require stabilization by Pluronic® type block copolymers.²⁴⁹ The preceding results on the integration of PGA-*g*-O22 into the cubic phases formed by the GMO/water system led us to explore their potential application as a steric stabilizer of nanoparticles in aqueous dispersions. Employing the so-called interfacial deposition method, where the acetone solution of PGA-*g*-O22 and GMO, with calculated composition, is added slowly to water with regular vortexing for homogenization and evaporation of the acetone. The particle size in the resulting aqueous dispersion, determined by dynamic light scattering, is found to be $R_h = 70$ nm, 65 nm and 63 nm for PGA-*g*-O22, GMO/PGA-*g*-O22- 90/10 and 80/20, respectively (see Figure 3.14).

The formation of nanoparticles with an internal structure is visualized by cryo-TEM. The cryo-TEM images of the 1 wt% aqueous dispersions of GMO/PGA-*g*-O22-90/10 (Figure 3.15(a)) and 80/20 (Figure 3.15(b)) reveal the formation of nanoparticles in the range of approximately 100 nm with well-defined internal structure. This is a strong indication that the synthesized amphiphilic graft copolymers could potentially be employed for the steric stabilization of internally structured nanoparticles in aqueous dispersion. The formation of nanoparticles is also verified by negative-stain TEM of a 0.2 wt% aqueous dispersion of GMO/PGA-*g*-O22 - 90/10 as depicted in Figure 3.15(c). This image is in agreement with other negative-stain TEM images of cubosomes.²⁵¹ In contrast to cryo-TEM, negative-stain TEM is not able to show the internal structure of these nanoparticles since it is lost during the drying process of sample preparation.

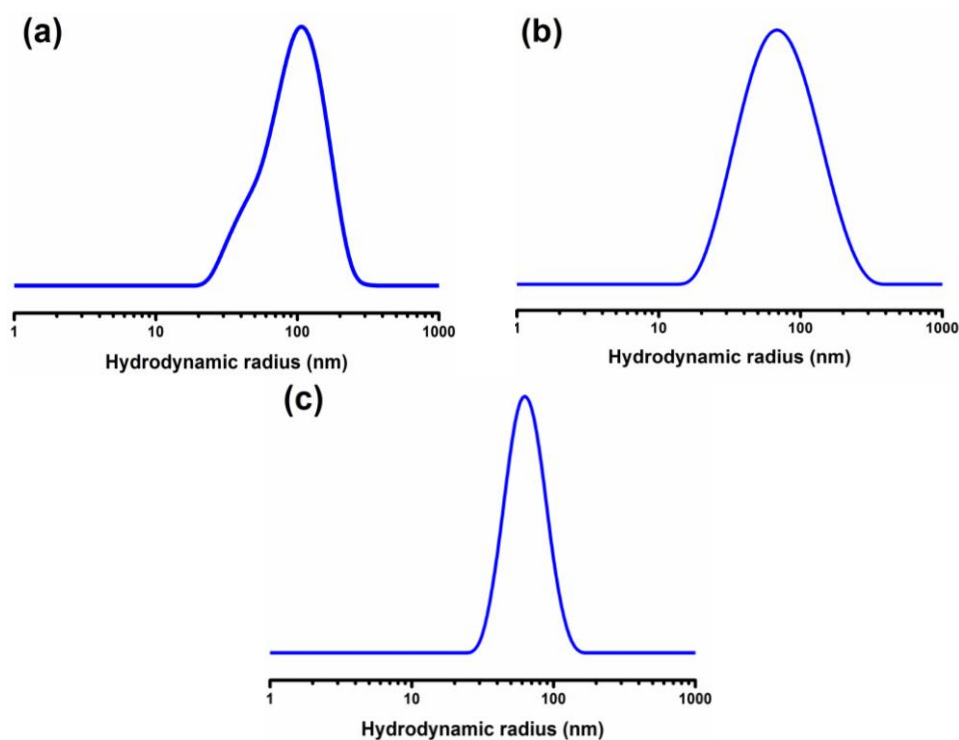


Figure 3.14. Hydrodynamic radius distribution of (a) PGA-*g*-O22 (b) GMO/PGA-*g*-O22 - 90/10 (c) GMO/PGA-*g*-O22 - 80/20 in water at a concentration of 5 g·L⁻¹, scattering angle of 90°, and at a temperature of 20°C.

The amphiphilic PGA-*g*-O22 copolymer could not be dispersed directly in water. However, the interfacial deposition method created a stable aqueous dispersion with self-assembled spherical nanoparticles as shown in the negative-stain TEM image (Figure 3.15(d)) of a 0.2 wt% aqueous dispersion of PGA-*g*-O22. In our previous studies on PGA grafted with stearate side chains (PGA-*g*-Sx), the formation of self-assembled nanoparticles, with well-defined structure due to phase separation that is driven predominantly by the crystallization of the saturated flexible stearate side chains, was observed.⁸⁸

Due to the presence of the *cis* double bond, as discussed above, the oleate side chains cannot pack into a well-defined crystalline lattice and hence, PGA-*g*-Ox and the resulting nanoparticles are amorphous in nature. However, the amorphous nature of the PGA-*g*-Ox nanoparticles could be more useful and beneficial for pharmaceutical or other active ingredient delivery applications, as the crystallinity of the matrix has been found to have a significant influence on the drug loading and release rates.²⁵² Generally, the amorphous matrix shows a higher capability of incorporating additives as compared with the crystalline matrix that often leads to expulsion of drugs.²⁵³

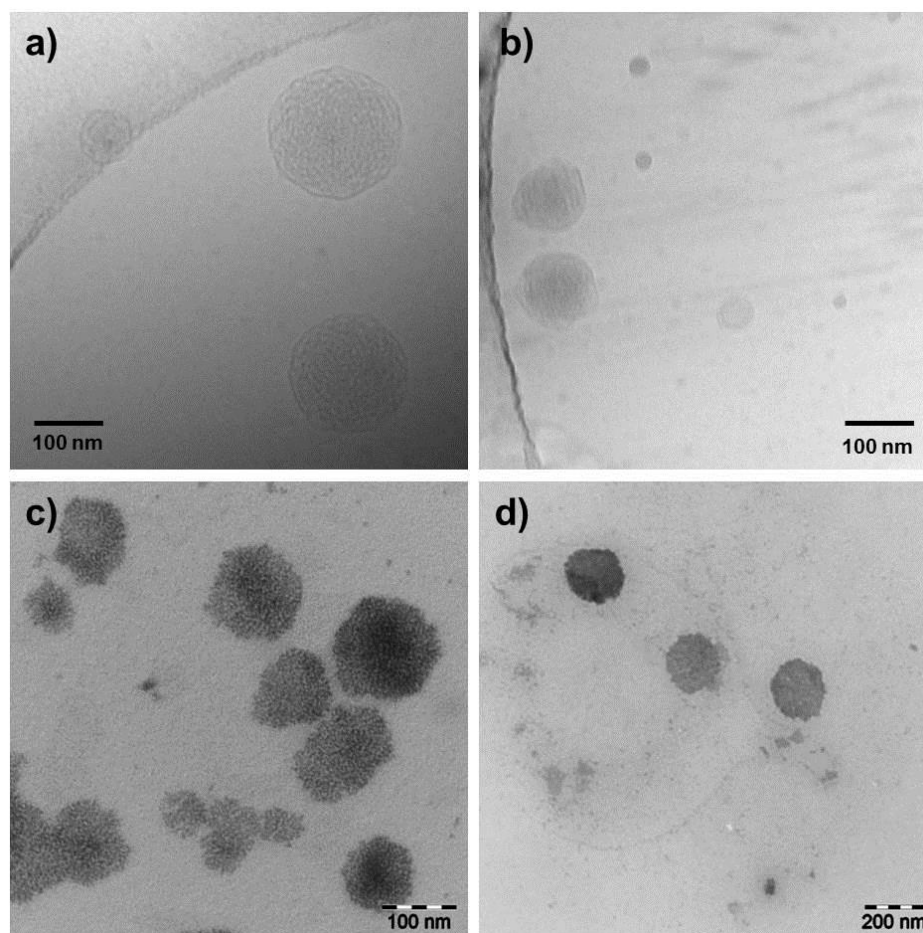


Figure 3.15: Cryo-TEM images of 1 wt% aqueous dispersions of (a) GMO/PGA-*g*-O22 -90/10 and (b) GMO/PGA-*g*-O22 -80/20. TEM images of uranyl acetate stained 0.2 wt% dispersions of (c) GMO/PGA-*g*-O22 - 90/10, and of (d) PGA-*g*-O22.

3.4 CONCLUSION

Amphiphilic graft copolymers with poly(glycerol adipate) (PGA) backbone and oleate side chains have been synthesized with various degrees of grafting, ranging from 11 to 90 mol%. The resulting PGA-*g*-O_x grafted polymers are amorphous in nature with phase separation of the oleate side chains into nanodomains. To evaluate the influence of the PGA-*g*-O_x on the mesophase behavior of the system glycerol monooleate (GMO)/water, a detailed ternary phase diagram of GMO/PGA-*g*-O22/water is constructed with the help of small angle X-ray scattering (SAXS) investigations. The addition of PGA-*g*-O22 to the GMO/water system, while maintaining a constant GMO/water ratio of 1: 1, induces swelling and enlargement of water channels in the inverse bicontinuous cubic phase. This is attributed to the integration of oleate side chains of the polymer into the lipid bilayers. Preliminary investigations reveal that the synthesized amphiphilic graft

polymers could potentially be used for the stabilization of the dispersed structured nanoparticles. In future, we shall study if different degrees of grafting of PGA-*g*-Ox could produce more robust cubic phase swelling of the system GMO/water with even more enlarged water channels.

Chapter 4

4 MULTIGRAFT POLYESTERS AS STABILIZERS FOR CUBOSOMES

4.1 INTRODUCTION

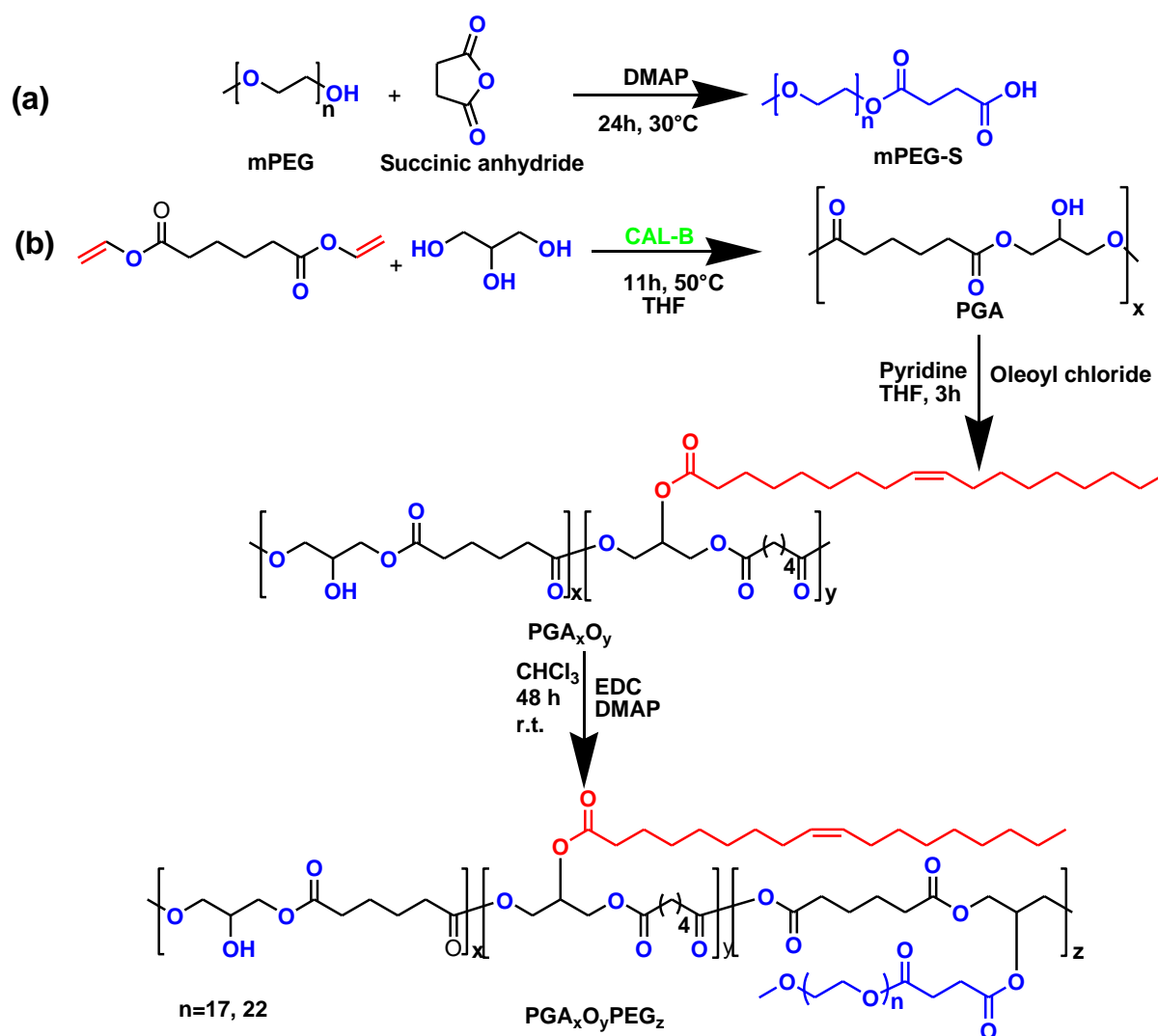
As mentioned before, bicontinuous cubic lyotropic liquid crystalline phases are of significant interest because of the high interface to volume ratio, which makes them promising candidates for drug delivery system. In addition, they are used for *in-meso* crystallization of proteins for structure determination. Growing numbers of molecules are being synthesized that form inverse bicontinuous cubic phases,^{254,255} however, lipids such as glycerol monooleate (GMO) and phytantriol are extensively used and studied.^{107,140,171,228,230,256–259} When water is added to these lipids, a viscous gel-like cubic phase is formed. The high viscosity of cubic phases limits their application as they are difficult to handle. The easy solution to this problem is to break this bulk cubic phase into submicron particles called cubosomes.

Cubosomes are typically prepared by dispersing cubic phases of lipids or by dispersing homogeneous solutions of lipids in solvents like ethanol in water. Former methods need more energy (such as sonication).^{182,249,260} However, both methods require the presence of steric stabilizer to avoid flocculation caused by van der Waals interactions. There are several molecules that can serve as steric stabilizers such as the PEG-stearate series (Myrj-series),^{166,261} PEGylated phospholipids,^{186,262,263} PEGylated monooleate,^{183,184} sorbitan monooleate (e.g., Tween 20, 40, 60 80),^{188,264} bile salts,²⁶⁵ amphiphilic proteins (albumin, β -casein),^{182,266} and Pluronics[®]. However, Pluronic[®]F127 a triblock copolymer of PEG and PPO (PEG₁₀₀PPO₆₅PEG₁₀₀) is being extensively used to stabilize cubosome dispersions because of its performance.^{178,190,226,267–270} Chong *et al.* investigated a series of pluronics and discovered that Pluronic[®]F108 having longer PEG chains is even a better stabilizer than Pluronic[®]F127.¹⁷⁸ Besides linear block copolymers, graft copolymers can be used as steric stabilizers. The graft copolymers have low crystallinity, melting temperature, and CMC, so that they could better serve as steric stabilizers. There is not much work reported on the use of graft copolymers as steric stabilizers. Chong *et al.* have used the brush-like copolymer poly(octadecyl acrylate)-*block*-poly(polyethylene glycol methyl ether acrylate) (P(ODA-*b*-P(PEGA-OME))

synthesized by reversible addition-fragmentation chain transfer (RAFT) polymerization, as a steric stabilizer of phytantriol and glycerol monooleate cubosomes. They found that phytantriol cubosomes stabilized with (P(ODA-*b*-P(PEGA-OME)) copolymers have a double diamond $Pn3m$ cubic symmetry while cubosomes from GMO have primitive $Im3m$ cubic symmetry.¹¹¹ There is always the need to introduce and investigate new materials to improve steric stabilization of lyotropic liquid crystalline dispersions.

Previously, enzymatically synthesized poly(glycerol adipate) was grafted with varying degree of oleate side chains, and their bulk properties were studied. In addition, a selected graft copolymer PGA-*g*-O22 was further studied to investigate its effect on the mesophase behavior of the GMO-water system. From the ternary phase diagram of the PGA-*g*-O22/GMO/water system, it was found that PGA-*g*-O22 stabilizes the cubic $Pn3m$ phase. For a high concentration of polymer the lattice parameter increased with increasing polymer concentration but the cubic symmetry retains.²⁷¹ These findings motivate us to further assess these graft polyesters for their ability towards steric stabilization of lyotropic liquid crystalline cubic dispersion (cubosomes). But these polymers are not water soluble to be used as a steric stabilizer directly. Therefore, a modification is required to make the polymer water soluble. The water solubility is typically achieved by adding a polymer with such properties as hydrophilicity, neutrality, the absence of hydrogen bond donors, the presence of hydrogen bond acceptors and it should have low toxicity and immunogenicity.^{272,273} Poly(ethylene glycol) has all these features. Furthermore, the introduction of PEG chains to a polymer improves the pharmacokinetics and pharmacodynamics of drug delivery system (DDS).¹⁷¹

Poly(glycerol adipate)s with varying degrees of grafting of oleate and PEG side chains were synthesized to achieve a range of polymers with different hydrophilic to hydrophobic volume fractions. The properties of all synthesized graft copolymers were studied by ¹H NMR spectroscopy and gel permeation chromatography. The thermal properties are studied by differential scanning calorimetry. Furthermore, the ability of polymers as steric stabilizers of cubosomes was studied by visual assessment. The internal morphology was investigated by SAXS. The particle size of cubosomes was determined by dynamic light scattering (DLS). Scheme 4.1 describes the syntheses of the polymers under investigation



Scheme 4.1: Synthetic route to (a) carboxylation of poly(ethylene glycol monomethyl ether), and (b) PEG and oleate grafted poly(glycerol adipate)($\text{PGA}_x\text{O}_y\text{PEG}_z$)

4.2 EXPERIMENTAL PART

4.2.1 Materials

Glycerol, anhydrous THF, pyridine, *Candida antarctica* lipase B immobilized on acrylic resin commercially known as Novozym 435 (used after drying over P_2O_5 for 24 h before use), succinic anhydride, oleoyl chloride and mPEG750 were purchased from Sigma Aldrich. N-(3-dimethylaminopropyl)-N-ethylcarbodiimide hydrochloride (EDC), chloroform, n-hexane, diethyl ether and methanol were purchased from Carl Roth. Divinyl adipate and mPEG1K was purchased from TCI-Europe. The glycerol monooleate used for this work was previously synthesized (see section 3.2.2.3) and is a mixture of G1M0 (92

mol%) and G2MO (8 mol%). The PGA used for this work was synthesized as described by Kallinteri *et al.*⁸³ It has M_n of 5,300 g·mol⁻¹ and *PDI* of 1.9.

4.2.2 Syntheses

4.2.2.1 Carboxylation of mPEG750 and mPEG1K

Carboxylation of poly(ethylene glycol) monomethyl ether (mPEG) was carried out as described by Lu *et al.*²⁷⁴ with a small modification. In a typical experiment mPEG1K (10 g, 10 mmol) was added to a 250 mL three neck round bottom flask equipped with magnetic stirrer, heating plate and reflux condenser containing a CaCl₂ drying tube at its opening. 200 mL chloroform was added. After this, DMAP (0.122 g, 1 mmol) and succinic anhydride (2 g, 20 mmol) were added. The reaction was allowed to run for 24 h at 30°C. After this time, the reaction mixture was transferred into a separating funnel and the crude product was washed three times with brine solution. The organic phase was collected and dried by MgSO₄. The crude product was recrystallized using ethyl acetate to have pure succinyl mPEG1K (mPEG1K-S). The purity was confirmed by ¹H NMR spectroscopy. (cf. Figure 4.1)

4.2.2.2 Grafting of poly(glycerol adipate) (PGA) with oleate side chain

PGA used for the grafting with oleate has $M_n = 5,300$ g·mol⁻¹ and *PDI* = 1.9. PGA was grafted with oleate side chains according to the procedure described in section 3.2.2.2. Three types of oleate grafted PGAs were synthesized, i.e. PGA₂₆O₄, PGA₂₆O₇, and PGA₂₆O₁₃. The purity of the sample was confirmed by ¹H NMR spectroscopy. A representative spectrum of all three products PGA_xO_y is shown in Figure 4.1.

4.2.2.3 PEG grafting of PGA₂₆O_x

Oleate grafted polymers are further grafted with PEG chains *via* esterification. In a typical experiment PGA₂₆O₄ (1g, 4.08 mmol) was placed in a three neck 100 mL round bottom flask equipped with a septum and magnetic stirrer. The flask was placed in an ice bath. 60 mL chloroform was then charged into the reaction flask. A weighed amount of mPEG1K-S (0.9 g, 0.8 mmol), EDC (2.3 g, 12.2 mmol) and DMAP (0.15 g, 1.22 mmol) were then added. The ice bath was removed after 1 h and the reaction was allowed to run for 48 h at room temperature. After this time the reaction mixture was transferred into a separating funnel and washed 3 times with brine. The organic phase was dried with MgSO₄, filtered and the solvent was evaporated

on a rotary evaporator. The crude product was further purified to remove un-reacted mPEG1K-S by dialysis in water using regenerated cellulose membrane having a cut off molar mass of 10 kDa for 7 to 10 days. After drying the solvent, the slightly yellowish solid product was obtained. The purity of the sample was confirmed by ^1H NMR spectroscopy. ^1H NMR (400 MHz, CDCl_3): δ 5.37 – 5.28 (m, 2H), 5.24 (s, 1H), 4.36 – 4.24 (m, 5H), 4.21 (dd, $J = 9.8, 4.9$ Hz, 2H), 4.18 – 4.02 (m, 5H), 3.84 – 3.42 (m, 88H), 3.36 (s, 3H), 2.7-2.6 (m, 4H), 2.41-2.25 (m, 6H), 2.02-1.93 (m, 4H), 1.72 – 1.54 (m, 6H), 1.36 – 1.09 (m, 20H), 0.86 (t, $J = 6.8$ Hz, 3H).

4.2.2.4 Polymer characterization

^1H NMR spectra were recorded on a Varian Gemini NMR spectrometer at 400 MHz and 25°C in CDCl_3 . The number average molar mass M_n , weight average molar mass M_w , and polydispersity index M_w/M_n for polymer backbone and oleate grafted PGA were measured using ViscotekGPCmax VE 2001 with a column set CLM3008 (guard column) and 1GMHHR (analytical column) equipped with VE 3580RI refractive index detector using polystyrene standards and THF as the eluent with a flow rate of 0.1 mL·min $^{-1}$ at 22 °C (column temperature). For mPEG grafted polymers, the measurements were done with DMF with 0.01 M LiBr as mobile phase in a thermostated column oven kept at 80 °C. The calibration standards for the measurements were poly(methyl methacrylate) samples.

Differential scanning calorimetry (DSC) measurements were performed under nitrogen flow using a Mettler Toledo DSC 822e module. About 8-12 mg of the sample was filled in aluminum pans. For all measurements, the sample was first heated to $T = 125$ °C in order to remove the previous thermal history, and after holding this temperature for 5 min, they were cooled to $T = -50$ °C with the rate of 10 °C·min $^{-1}$. The samples were heated again to 80°C at 10 °C·min $^{-1}$ to record their melting endotherm.

4.2.2.5 Surface Tension Measurements

The surface tension γ of aqueous solutions of the polymers was measured as a function of polymer concentrations at 25°. Plotting γ versus polymer concentration (log C) yields the critical aggregation concentration (CAC) indicated by the intersection of the extrapolation of the two linear regimes where the curve shows an abrupt change in the slope (see Figure 4.5).

4.2.2.6 XRD measurements

For XRD measurements, the cubic gel phase or cubosome dispersions were loaded into a capillary of 1.5 mm diameter. The capillary was sealed with epoxy resin on both sides. X-ray scattering experiments were performed in transmission mode using a SAXSLAB laboratory setup (Retro-F) equipped with an AXO microfocus X-ray source with an AXO multilayer X-ray optic (ASTIX) as a monochromator for Cu K α radiation ($\lambda=0.154$ nm). A DECTRIS PILATUS3 R 300K detector was used to record the two-dimensional scattering patterns. For cubic gel phase or cubosome dispersions the samples were loaded into a capillary of diameter 1.5 mm while for the bulk polymer, the sample holder is a 2 mm thick aluminum disc. The measurements were performed at room temperature for a q -range 0.25 - 7 nm $^{-1}$ for the cubic gel phase or cubosome dispersions. For the measurements of bulk polymer a q -range of 0.25 - 7 nm $^{-1}$ and 1 - 29 nm $^{-1}$ to cover the small and wide angle scattering range respectively.

4.2.2.7 Dynamic light scattering

DLS measurements were performed using an ALV/DLS-5000 instrument (ALV GmbH, Langen, Germany). As a light source, a 20 mW He-Ne gas laser (632.8 nm, 20 mW) was used (Uniphase Laser, Palo Alto, California). The DLS instrument was equipped with a goniometer for automatic measurements between scattering angles θ of 30 and 90°. The correlation functions were analyzed by the CONTIN method, which gives information on the distribution of decay rates Γ . Apparent diffusion coefficients were obtained from $D_{app} = \Gamma/q^2$ (where $q = (4\pi n/\lambda) \sin(\theta/2)$, λ is the wavelength of the light, n is the refractive index, and θ is the scattering angle). Finally, apparent hydrodynamic radii were calculated *via* the Stokes-Einstein equation.

$$R_h = \frac{k_B T}{6\pi\eta D_{app}} \quad (4.1)$$

Where, k_B is the Boltzmann constant and η is the viscosity of the solvent at temperature T.

4.2.3 Preparation of cubosome dispersions

Cubosome dispersions were prepared, using a top-down approach. A weighed amount of GMO was taken in an Eppendorf tube. During heating the sample to 50°C GMO was melted. A calculated amount of 2 wt% of stabilizer solution was added to achieve 1,

3, 5, and 10 wt% of GMO and mixed with strong spatulation to obtain the cubic gel phase also known in literature as the bulk cubic phase.^{249,275-277} The samples were further diluted with distilled water and homogenized using silentCrusher S for 15 min with a break of 1 min at a speed of 45,000 rpm after every 1.5 min mixing to provide 10 wt% (of combined mass of GMO and stabilizer) dispersions.

4.3 RESULTS AND DISCUSSION

4.3.1 Polymer synthesis and grafting

Poly(glycerol adipate) was successfully synthesized using CAL-B catalyzed polycondensation reaction. The reaction was carried out at 50°C. Since enzymes are regioselective to a great extent, as only 4% branching was observed²⁷¹ under this reaction condition, so a linear poly(glycerol adipate) is obtained. As discussed before, a steric stabilizer must have a hydrophobic part that could anchor to the lipid bilayer.¹⁷¹

For this work, oleic acid is selected as a hydrophobic chain, which is also part of GMO. The grafting of PGA with oleate chains was carried out by simple esterification of activated acid and pendant -OH groups of the polymer backbone using pyridine as an acid scavenger. Oleate grafted poly(glycerol adipate) was further grafted with mPEG chains. For this purpose mPEG was reacted with succinic anhydride catalyzed by DMAP. The succinyl mPEG was grafted to the polymer backbone by simple esterification reaction using EDC as a coupling agent in the presence of DMAP. Graft copolymers with different degrees of oleate side chains and mPEG chains were synthesized. The variation in grafting yields polymers with different hydrophilic to lipophilic balance, which is an important factor in order to understand the stabilization ability of graft copolymers. The graft copolymers are represented by $\text{PGA}_x\text{O}_y\text{PEG}_z$, where x is the degree of polymerization of PGA, y stands for the number of oleate side chains connected to the polymer backbone, whereas z stands for number of grafted PEG chains.

The syntheses of the graft copolymers were confirmed by ¹H NMR spectroscopy. A representative spectrum of carboxylated mPEG, PGA_x , PGA_xO_y , and $\text{PGA}_x\text{O}_y\text{PEG}_z$ are shown in Figure 4.1.

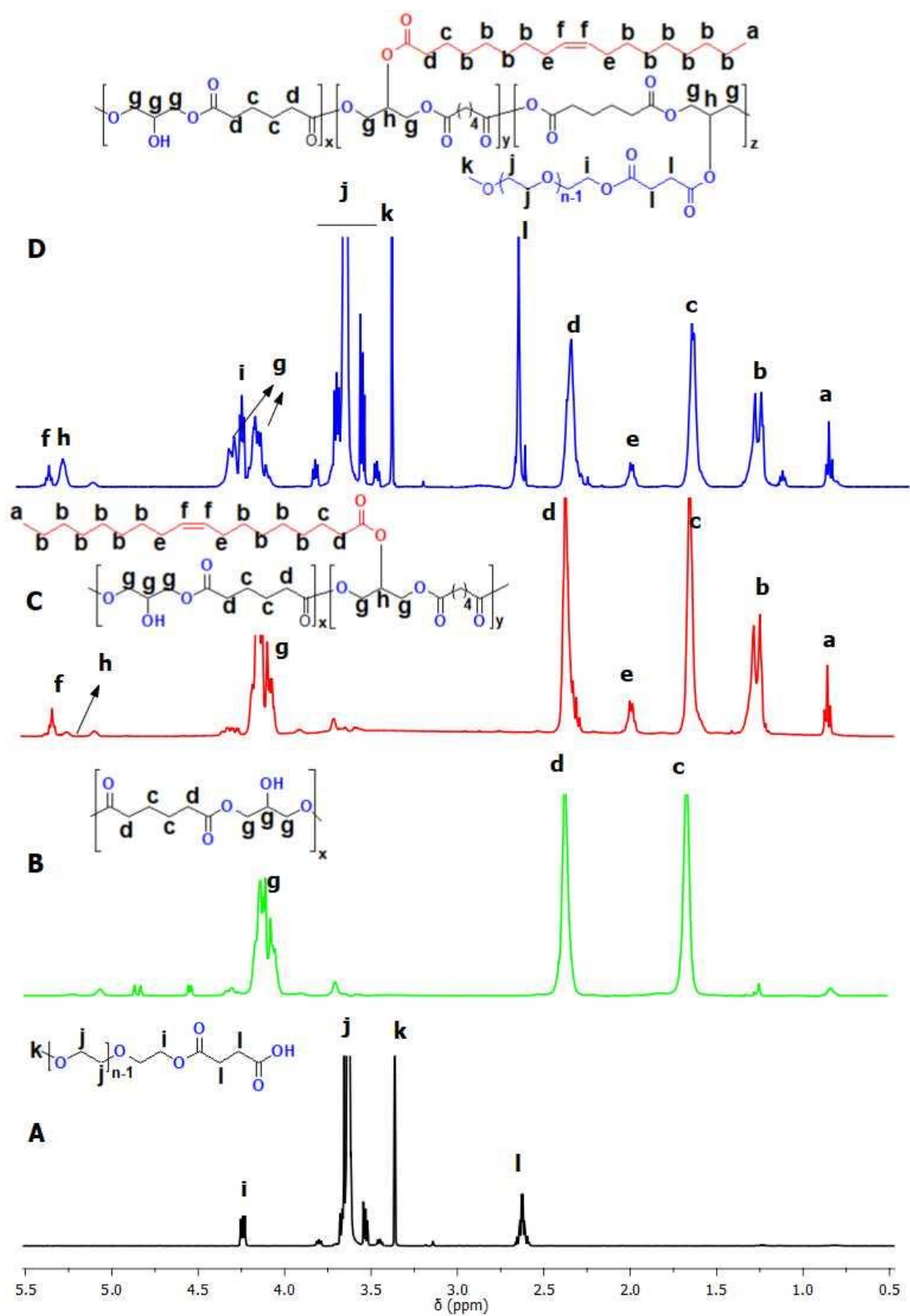


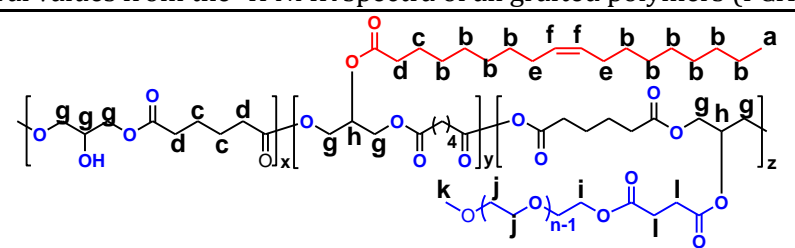
Figure 4.1: ^1H NMR spectrum of (A) mPEG1K-S, (B) PGA₂₆, (C) PGA₂₆O₄, (D) PGA₂₆O₄PEG1K₁₇ recorded at 27 °C using CDCl_3 as a solvent.

All the peaks are very well assigned, indicating the purity of the products. The integral values of all the grafted polymers are given in Table 4.1. The degree of grafting of oleate side chains and mPEG side chains is calculated by equations 4.2 and 4.3, respectively, using integral values of the ^1H NMR spectrum of a particular product.

$$\text{mol\% oleate chain grafting} = \frac{1.33 \times a}{d - 0.67a} \times 100 \quad (4.2)$$

$$\text{mol\% mPEG grafting} = \frac{k}{g+h} \times \frac{5}{3} \times 100 \quad (4.3)$$

Table 4.1: Integral values from the ^1H NMR spectra of all grafted polymers ($\text{PGA}_x\text{O}_y\text{PEG}_z$).



Polymers	a	b	c	d	e	f	g	h	i	j	k	l
$\text{PGA}_{26}\text{O}_4\text{PEG}_{750}^{16}$	3	20	30.1	30.9	3.76	1.58	28	5.1	9.9	335	12.9	20
$\text{PGA}_{26}\text{O}_4\text{PEG}_{1\text{K}}^{17}$	3	20.4	27.5	27	3.6	1.79	25.4	4.3	8.3	380	11.6	15.3
$\text{PGA}_{26}\text{O}_6\text{PEG}_{750}^{16}$	3	20.6	17.9	17.8	4.4	1.54	16	3.6	4.9	178	6.94	11
$\text{PGA}_{26}\text{O}_4\text{PEG}_{1\text{K}}^{17}$	3	19.4	17.7	17	3.7	1.65	15.2	3	5.1	240	7.28	10
$\text{PGA}_{26}\text{O}_{13}\text{PEG}_{750}^{16}$	3	20	11.6	11.6	3.2	1.31	9.2	1.7	1.2	35	1.56	2.4
$\text{PGA}_{26}\text{O}_{13}\text{PEG}_{1\text{K}}^8$	3	20.4	11.3	12	3.6	1.65	8.5	2	1.1	59.3	1.94	2.7

All the synthesized polymers are further characterized by gel permeation chromatography. Because DMF is not a good solvent for oleate grafted polymers, the GPC measurements of PGA and oleate grafted PGAs were carried out in THF.

The GPC traces of PGA and oleate grafted PGA are shown in Figure 4.2. In the figure 4.2 a successive shifting of the peak to the higher molar mass confirms the grafting reaction. GPC traces of all graft copolymer samples $\text{PGA}_x\text{O}_y\text{PEG}_z$ are shown in Figure 4.3. From the analysis of these chromatograms, it is noticed that the PDI of some of the oleate grafted polymers increased after grafting with mPEG chains instead of decreasing. This could be a sign of hydrolytic cleavage of the ester bond. Since the removal of unreacted mPEG-S chains was difficult, the products were dialyzed with water for 7 to 10 days. The exposure of the product to water for such a long time might lead to cleavage of ester links.

However, this hydrolytic cleavage is not very big as all the products have symmetric and unimodal molar mass distributions.

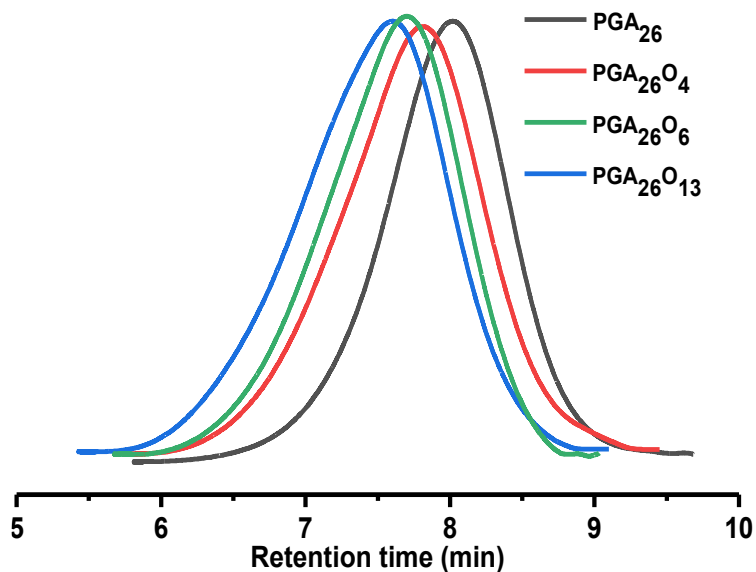


Figure 4.2: GPC traces of PGA and oleate grafted PGA, measured in THF, against polystyrene standards at temperature 22°C.

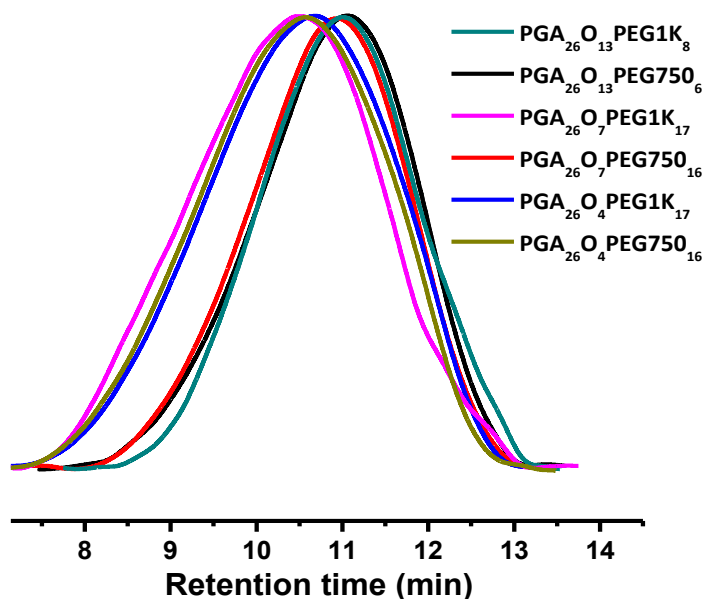


Figure 4.3: GPC traces of all grafted polymers $\text{PGA}_x\text{O}_y\text{PEG}_z$ measured in DMF with 0.01 M LiBr as eluent at 25°C.

The thermal properties of all the polymers were determined by differential scanning calorimetry. It was observed that the polymer backbone (PGA) and all oleate grafted polymers are amorphous since a melting peak from these polymers is not observed.

However, a glass transition temperature was observed that decreases with increasing degree of grafting which is consistent with previous findings (see Table 4.2.).²⁷¹ The DSC traces of PGA and PGA_xO_y are shown in Figure 4.4.

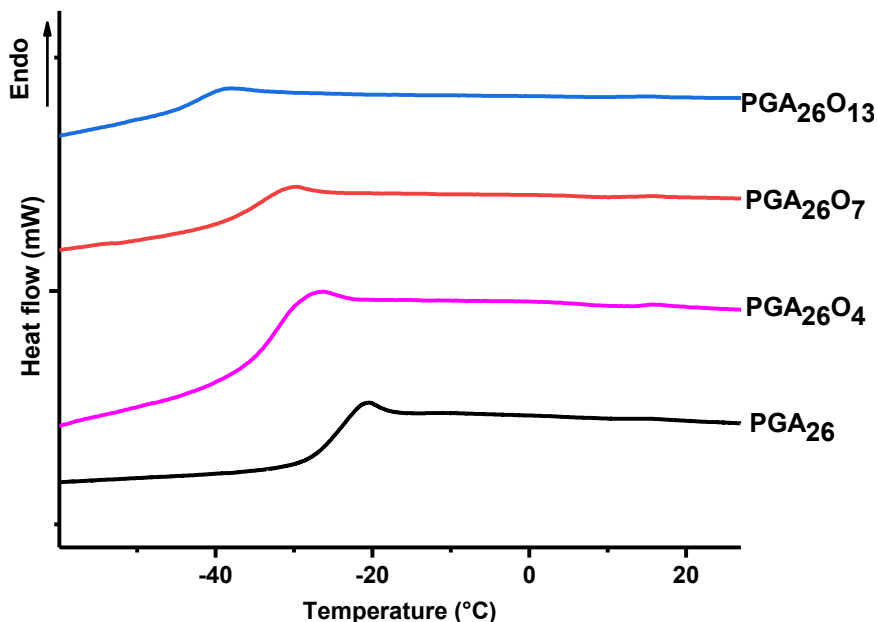


Figure 4.4: DSC traces of PGA and oleate grafted PGA recorded at a heating rate of 10°C·min⁻¹.

The oleate grafted PGAs are then further grafted with mPEG750 and mPEG1K side chains. The DSC traces of mPEG grafted PGA_xO_y are shown in Figure 4.5. It is observed that after grafting with PEG side chains, all the polymers become semi-crystalline.

The phenomenon of cold crystallization was also observed in some samples where the volume fraction of PEG is relatively small.²⁷⁸ The cold crystallization temperature of the products PGA₂₆O₄PEG750₁₆, PGA₂₆O₇PEG750₁₆, PGA₂₆O₁₃PEG750₆, and PGA₂₆O₁₃PEG1K₈ is -35.6, -35.9, -9.4 and -30.8 °C, respectively. The reason of this cold crystallization is that in these sample during the cooling step the chains do not have enough time to organize themselves as the mobility is hindered by neighboring chains. So during the heating scan, they organize themselves and achieve an ordered state.^{278,279} The melting temperatures T_m , glass transition temperatures T_g , crystallinity, number average molar masses M_n and polydispersity index PDI of all graft copolymers are given in Table 4.2.

The crystallinity of the graft copolymers was calculated by the following relation,

$$X = \frac{\Delta H_m}{\Delta H_m^0 \cdot w_{PEG}} \quad (4.4)$$

Here, w_{PEG} is the mass fraction of PEG chains in the graft copolymer, ΔH_m is the melting enthalpy of the corresponding PEG chains in the polymer, ΔH_m^0 is the melting enthalpy of 100% crystalline PEG. The value of ΔH_m^0 is $197 \text{ J}\cdot\text{g}^{-1}$.²⁸⁰

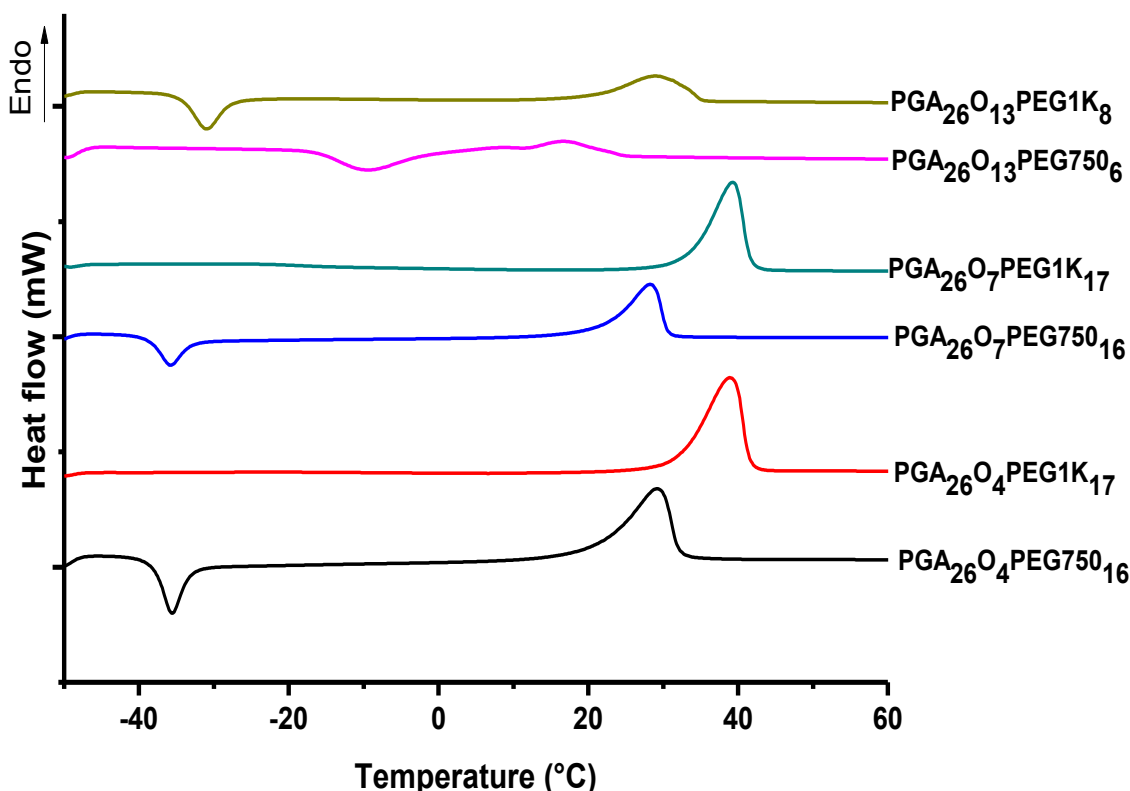


Figure 4.5: Differential scanning calorimetry traces of graft copolymers ($\text{PGA}_x\text{O}_y\text{PEG}_z$) recorded at a heating rate of $10^\circ\text{C}\cdot\text{min}^{-1}$.

It is worth mentioning here, that the crystallinity in graft copolymers is induced by PEG chains as the PGA and oleate grafted PGA are amorphous materials. SAXS and WAXS scans of the bulk polymer are shown in Figure 4.6. A typical pattern of a lamellar crystal phase in the SAXS region and the characteristic pattern of PEG in the WAXS region respectively confirm that the crystallinity is induced by PEG chains.

Figure 4.6(a) shows the SAXS pattern of the bulk polymer $\text{PGA}_{26}\text{O}_4\text{PEG1K17}$. It depicts the presence of the lamellar arrangement, as periodic lamellar peaks are present. The first order lamellar peak appears at $q=0.0513 \text{ \AA}^{-1}$ with the corresponding d -spacing of 47.9 \AA at 25°C . The lamellar thickness value is calculated as 36 \AA by considering the

crystallinity of the polymer (X=67%) obtained from DSC. By increasing the temperature, peaks slightly shift to lower q -values due to the increase of lamellar thickness.²⁸¹

Table 4.2: M_n , PDI, ϕ_{oleate} , ϕ_{mPEG} , T_g , and T_m of all grafted and ungrafted polymers.

Polymer	M_n ($\text{g}\cdot\text{mol}^{-1}$)	PDI	ϕ_{oleate}^d	ϕ_{PEG}^d	T_g^e ($^{\circ}\text{C}$)	T_m^e ($^{\circ}\text{C}$)	Crystallinity ^e (%)
PGA ₂₆	5,300 ^a	1.9 ^a	-	-	-24	-	-
PGA ₂₆ O ₄	6,350 ^b	1.7 ^a	18	-	-33	-	-
PGA ₂₆ O ₇	7,250 ^b	2.0 ^a	0.28	-	-35	-	-
PGA ₂₆ O ₁₃	8,750 ^b	1.9 ^a	0.42	-	-42	-	-
PGA ₂₆ O ₄ PEG750 ₁₆	19,900 ^b	2.7 ^c	0.07	0.64	-	29.2	61
PGA ₂₆ O ₄ PEG1K ₁₇	25,000 ^b	1.8 ^c	0.05	0.73	-	38.9	67
PGA ₂₆ O ₇ PEG750 ₁₆	20,700 ^b	1.8 ^c	0.1	0.62	-	28.4	52
PGA ₂₆ O ₇ PEG1K ₁₇	25,800 ^b	2.4 ^c	0.08	0.71	-	39.2	66
PGA ₂₆ O ₁₃ PEG750 ₆	13,800 ^b	1.9 ^c	0.28	0.33	-	17	32
PGA ₂₆ O ₁₃ PEG1K ₈	17,500 ^b	2.1 ^c	0.22	0.47	-	29	53

^a Obtained from GPC using THF as eluent

^b Calculated on the basis of the degree of grafting obtained from ¹H NMR spectra

^c Obtained from GPC, using DMF (with 0.01M LiBr) as eluent

^d Calculated from material studio software v 4.1

^e Obtained from DSC with a heating rate of 10 $^{\circ}\text{C}\cdot\text{min}^{-1}$

In Figure 4.6(b) the WAXS pattern of the polymer is shown with the presence of characteristics peaks of PEG until melting which corresponds to the typical triclinic crystal structure.²⁸² The peak vanishes by increasing the temperature which confirms that the crystallinity in the polymer was induced by PEG chains.

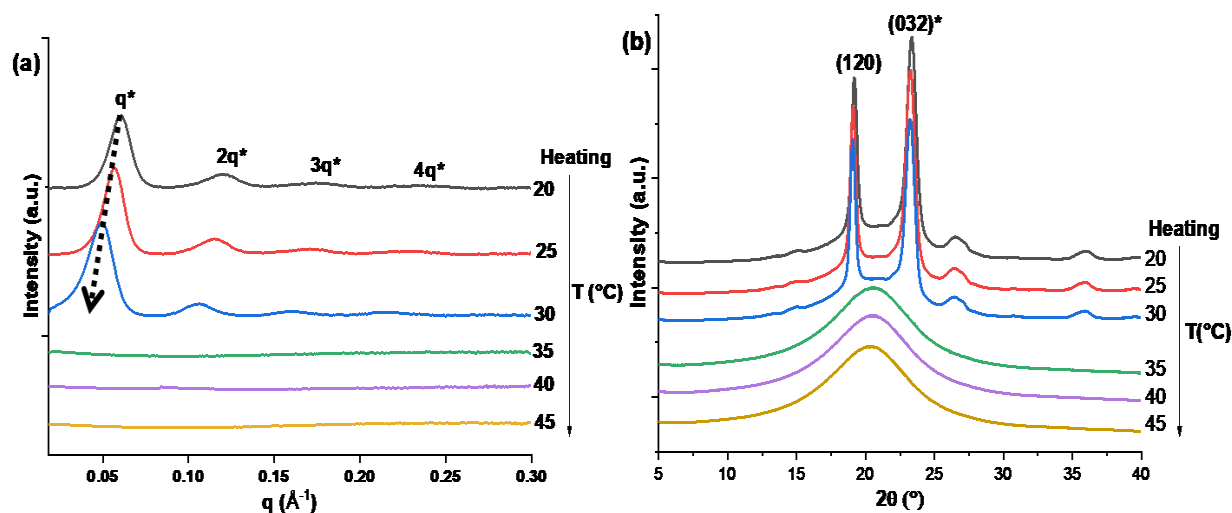


Figure 4.6: (a) SAXS and (b) WAXS patterns of the bulk polymer $\text{PGA}_{26}\text{O}_4\text{PEG1K}_{17}$ measured for different temperatures.

4.3.2 Graft copolymers as steric stabilizers of cubosomes

Out of all synthesized graft copolymers, only two polymers $\text{PGA}_{26}\text{O}_4\text{PEG1K}_{17}$ and $\text{PGA}_{26}\text{O}_{13}\text{PEG1K}_8$ were used further to investigate their properties as steric stabilizers for lyotropic liquid crystalline particles. The reason behind the selection of these polymers is that they have comparable volume fraction of PEG chains but differ in the volume fraction of oleate chains.

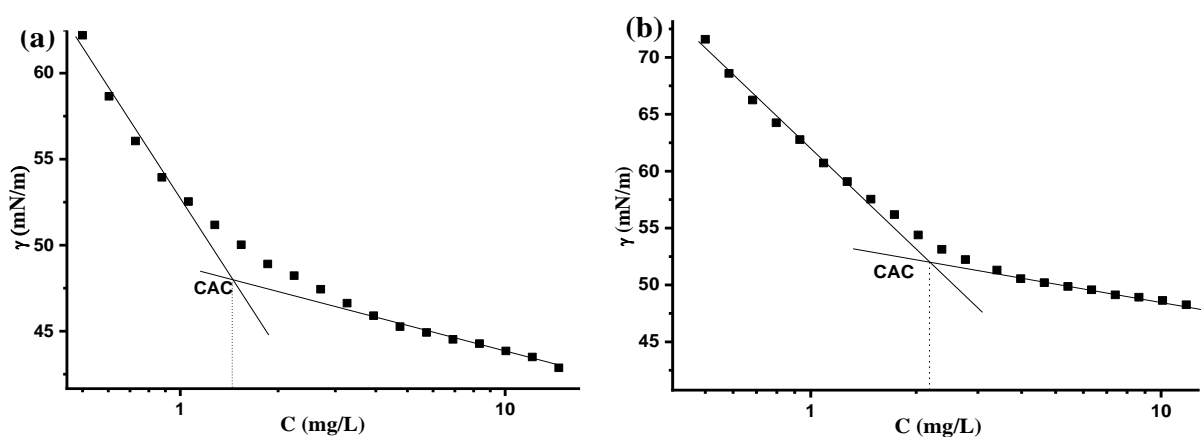


Figure 4.7: Surface tension of (a) $\text{PGA}_{26}\text{O}_4\text{PEG1K}_{17}$ and (b) $\text{PGA}_{26}\text{O}_{13}\text{PEG1K}_8$ in water as a function of polymer concentration at 25 °C.

The basic requirement for a steric stabilizer is that it must be water soluble and has a low critical aggregation concentration. The polymers mentioned fulfill both requirements. The CAC values for these polymers are obtained from tensiometry where

an increase in polymer concentration causes a decrease in surface tension of the aqueous solutions (see Figure 4.7). The CAC values are calculated to 1.45 and 2.2 g·L⁻¹ for the polymers P1 and PGA₂₆O₁₃PEG1K₈, respectively.

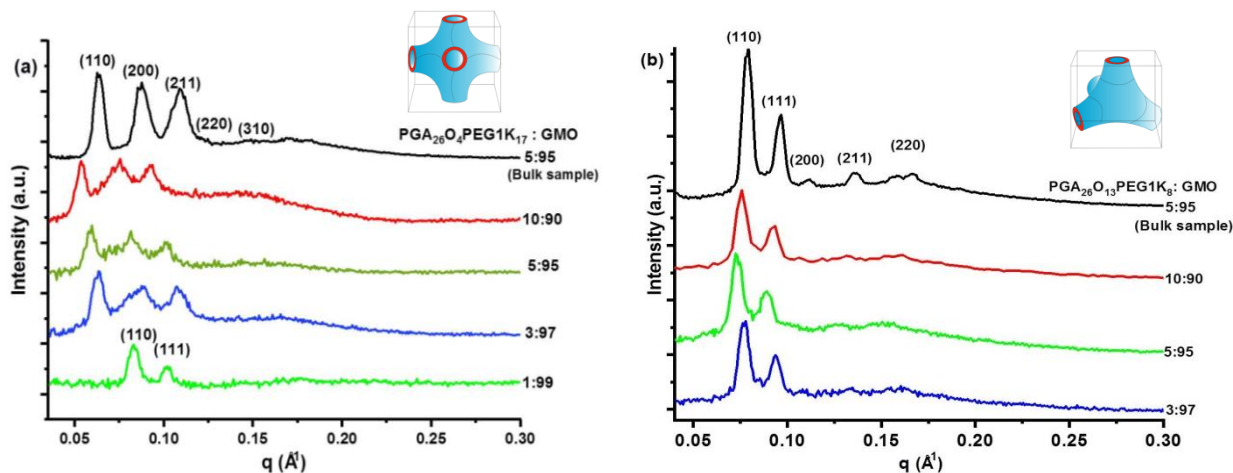


Figure 4.8: SAXS pattern of cubosomes samples stabilized by (a) PGA₂₆O₄PEG1K₁₇ and (b) PGA₂₆O₁₃PEG1K₈ measured at room temperature. Aqueous dispersions of GMO plus stabilizer at 10 wt% concentration were used for measurements. Curves in black correspond to the non-dispersed cubic phase.

For cubosome preparation for SAXS measurement, 1, 3, 5, and 10 wt % of each stabilizer with respect to GMO were used. Aqueous dispersions of GMO plus stabilizer at 10 wt% concentration were used for measurements. As reported before, GMO in excess water shows a *Pn3m* cubic phase. The GMO/water cubic phase could only incorporate as much as 1 wt% of PGA₂₆O₄PEG1K₁₇. Increasing the concentration of PGA₂₆O₄PEG1K₁₇ to more than 1 wt% leads to a change of the cubic symmetry from the cubic *Pn3m* to the cubic *Im3m*. (see Figure 4.8).

The lattice parameter of the *Im3m* cubic phase increases with increasing polymer concentration from 142 Å to 166 Å (with an increase in the diameter of the water channel from 48 to 67.4 Å). It is interesting to note that the lattice parameter of cubosomes is only slightly greater than in the non-dispersed cubic phase for the same ratio of polymer to GMO.

In comparison to PGA₂₆O₄PEG1K₁₇, when PGA₂₆O₁₃PEG1K₈ is used as a steric stabilizer, surprisingly it retains the cubic *Pn3m* symmetry in all tested samples. The lattice parameter of the *Pn3m* cubic phase increases from 115.3 to 121.5 Å (the diameter

of the water channel increase from 48 to 60.6 Å) when the polymer $\text{PGA}_{26}\text{O}_{13}\text{PEG}1\text{K}_8$ concentration increases from 3 wt% to 10 wt%. The lattice parameter of the cubic $Pn3m$ phase is 107 Å for the GMO-water system ($d_w = 48$ Å). It is important to mention here that the sample with 1 wt% of $\text{PGA}_{26}\text{O}_{13}\text{PEG}1\text{K}_8$ also shows a cubic $Pn3m$ phase, but with this amount of stabilizer, only a small amount of GMO is possible to disperse which is not sufficient for SAXS measurement.

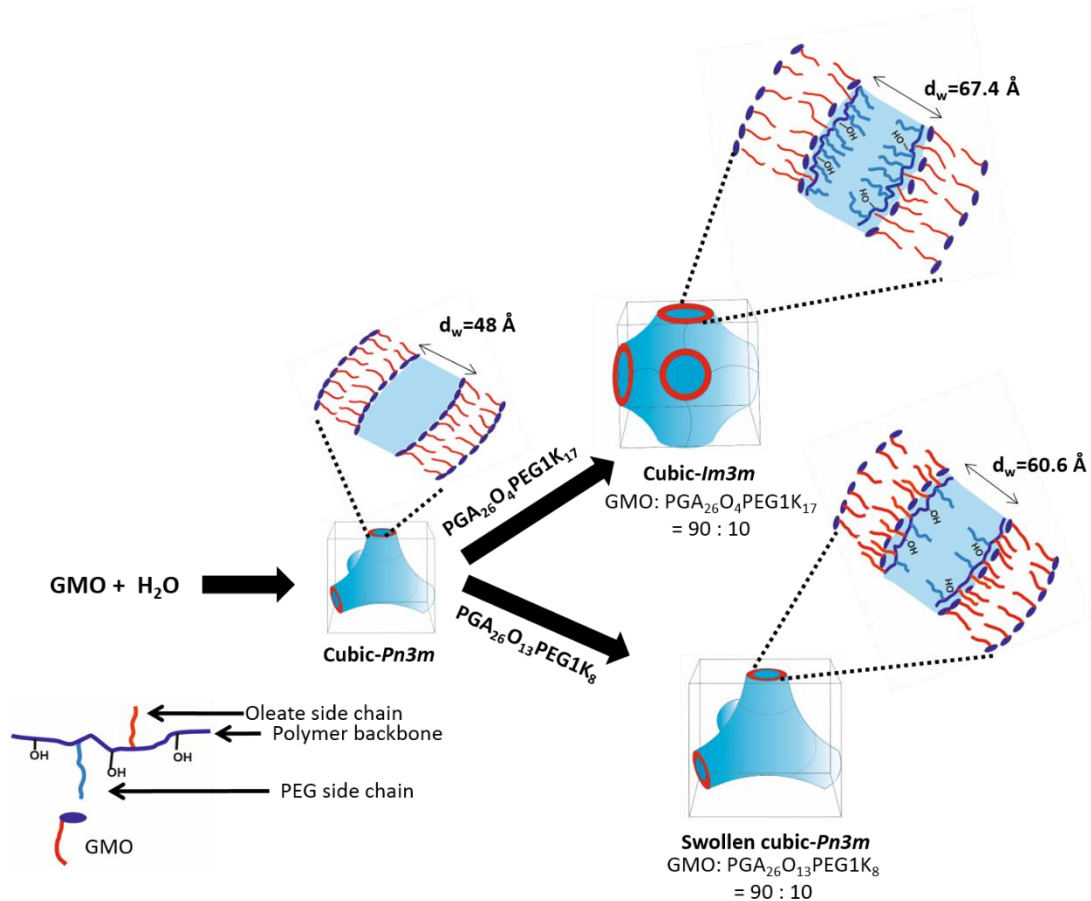


Figure 4.9. Schematic illustration of phase transition and swelling of cubic phases when polymer $\text{PGA}_{26}\text{O}_4\text{PEG}1\text{K}_{17}$, and $\text{PGA}_{26}\text{O}_{13}\text{PEG}1\text{K}_8$ were used as steric stabilizers for cubosome dispersions.

The two polymers behave differently when added to the GMO/water system. As the polymer $\text{PGA}_{26}\text{O}_4\text{PEG}1\text{K}_{17}$ induces a cubic phase transition from $Pn3m$ to $Im3m$, in contrast, the $\text{PGA}_{26}\text{O}_{13}\text{PEG}1\text{K}_8$ polymer retains the cubic $Pn3m$ symmetry. The transition from the $Pn3m$ cubic phase to the $Im3m$ cubic phase indicates that the excess $\text{PGA}_{26}\text{O}_4\text{PEG}1\text{K}_{17}$ molecules, which were saturated at the surface of the cubic phase, are incorporated with GMO and consequently formed the $Im3m$ cubic phase. This could be further explained by taking into account the critical packing parameter. The mesophase

transition could only be observed in the less curved phase (i.e the $Im3m$ cubic phase) when an amphiphile with a larger hydrophilic part compared to hydrophobic part $\gamma < 1$ was added.^{109,122} On the contrary, when the polymer $PGA_{26}O_{13}PEG1K_8$ which is less hydrophilic than $PGA_{26}O_4PEG1K_{17}$ is used as stabilizer, the hydrophobic side chains penetrate into the lipid bilayer, while the hydrophilic part remain at the interface. This results in an increase of the lattice parameter from 107.1 to 121.6 Å (hence an increase in the diameter of the water channel from 48 to 60.6 Å) of the cubic $Pn3m$ phase. A schematic overview of the cubic phase transition and the cubic phase swelling when polymer $PGA_{26}O_4PEG1K_{17}$ and $PGA_{26}O_{13}PEG1K_8$ are used as stabilizers is shown in Figure 4.9.

To find out the particle size of the cubosomes, the samples were diluted to make 2 $g \cdot L^{-1}$ concentrations for DLS measurement. The dilution is necessary in order to minimize undesired multiple scattering effects and, furthermore, to minimize interparticle interactions.²⁸³ The particle size was determined for each sample for 7 different angles (see Figure A5 and A6 in the Appendix). The average hydrodynamic radius of all measured sample varies from 130 nm to 225 nm and the hydrodynamic radius distributions for each sample measured at an angle of 90° is shown in Figure 4.10.

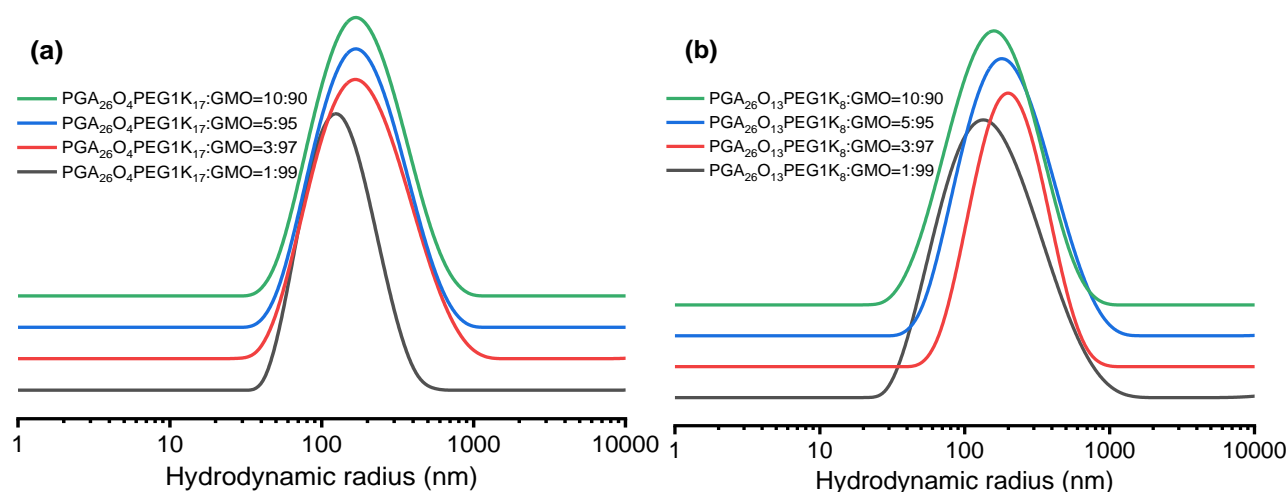


Figure 4.10: The hydrodynamic radius distribution of all cubosome samples stabilized by polymer $PGA_{26}O_4PEG1K_{17}$ and $PGA_{26}O_{13}PEG1K_8$ in different ratios with respect to GMO measured at a scattering angle of 90° . The concentration of the samples was 2 $g \cdot L^{-1}$.

The cubosome dispersions stabilized with polymers $\text{PGA}_{26}\text{O}_4\text{PEG1K}_{17}$ and $\text{PGA}_{26}\text{O}_{13}\text{PEG1K}_8$ are stable for more than 2 weeks. The stability of dispersions was identified by visual inspection, as no large aggregates were observed.

4.4 Conclusion

PEG grafted poly(glycerol adipate)-g-oleate $\text{PGA}_x\text{O}_y\text{PEG}_z$ is synthesized by esterification reactions of oleate and PEG chains to the PGA backbone. DSC measurements showed that the graft copolymers are semicrystalline. The crystallinity was induced by the PEG chains. In some copolymers where the volume fraction of PEG is relatively small ($\phi_{\text{PEG}} \leq 0.64$) the phenomenon of cold crystallization was observed. All the $\text{PGA}_x\text{O}_y\text{PEG}_z$ samples were water soluble. Two of the selected polymers, $\text{PGA}_{26}\text{O}_4\text{PEG1K}_{17}$ and $\text{PGA}_{26}\text{O}_{13}\text{PEG1K}_8$ having CAC values of 1.45 and 2.2 $\text{g}\cdot\text{L}^{-1}$, respectively, were used to investigate their ability as steric stabilizers of cubosomes. It was found that the incorporation of $\text{PGA}_{26}\text{O}_4\text{PEG1K}_{17}$ to GMO-water system causes a mesophase transition of the cubic phase from $Pn3m$ to $Im3m$. On the contrary, when $\text{PGA}_{26}\text{O}_{13}\text{PEG1K}_8$ was introduced into the GMO-water system, $Pn3m$ cubic symmetry retained. It is assumed that the polymer $\text{PGA}_{26}\text{O}_4\text{PEG1K}_{17}$ has a higher volume fraction of the hydrophilic part ($\phi_{\text{PEG}} = 0.73$) in comparison to the polymer $\text{PGA}_{26}\text{O}_4\text{PEG1K}_{17}$ ($\phi_{\text{PEG}} = 0.47$). Hence, when it interacted with the lipid bilayer, it increased the volume of head group leading to cubic phase transition from $Pn3m$ to $Im3m$. The polymer $\text{PGA}_{26}\text{O}_4\text{PEG1K}_{17}$ retained the cubic symmetry of $Pn3m$ and caused only an increase of the lattice parameter and thus of the radius of the water channels. The cubosome dispersions were stable for more than two weeks at room temperature. From these findings, it was concluded that these multi-graft biocompatible copolymers could be effectively used to stabilize several lyotropic liquid crystal systems by controlling the hydrophobic to hydrophilic volume fractions.

CHAPTER 5

5 SUMMARY

The enzymatic synthesis of functional polyesters is the most effective way to obtain them without product contamination with heavy metals. It is especially useful when biobased monomers are used for polymerization as reduced sugars e.g. xylitol and D-sorbitol. The direct esterification of such monomers can result in hyperbranched or crosslinked products. In the first part of this work, linear sugar-based polyesters such as poly(xylitol adipate) and poly(D-sorbitol adipate) of molar masses 5,000 and 3,500 g·mol⁻¹, respectively, were successfully synthesized. These are amorphous polymers and they are highly viscous liquids at room temperature. These polymers are biodegradable with great potential for the application in drug delivery system. The free pendant OH groups of the polymer backbone provide the possibility for further modification to achieve desired properties.

By esterification of hydroxyl groups on the polymer backbone with a saturated fatty acid such as stearic acid, a range of amphiphilic polyesters with different degree of hydrophilic-lipophilic balance are obtained. The study on the bulk properties of these comb-like amphiphilic polymers reveals that all the grafted polymers are semi-crystalline. The crystallinity arises from the immiscibility of the grafted chains with the polymer backbone. Small angle X-ray scattering data show a typical lamellar ordering while the wide-angle X-ray scattering pattern shows a short range order which is a typical hexagonal rotator phase. Furthermore, the self-assembly behavior of these amphiphilic polyesters was studied by negative staining TEM and dynamic light scattering. Stearoyl grafted poly(xylitol adipate) shows spherical self-assemblies whereas stearoyl grafted poly(D-sorbitol adipate) forms nanoparticles with a unique structure. It would be interesting, in the future, to explore the morphology and the hydrolytic stability of the nanoparticles formed from these polymers. This is important for the application of these polymers in drug delivery system. Due to the biodegradability of these nanoparticles, they might be an alternative to many Pluronic[®] based systems.

Previously, intensive work has been done on poly(glycerol adipate) grafted with saturated fatty acids of variable lengths such as lauric acid, stearic acid behenic acid.

However, not much is known about the graft copolymers, when an unsaturated fatty acid is grafted to the polyester backbone. The second part of this work deals with the synthesis and grafting of poly(glycerol adipate) with oleate side chains. Differential scanning calorimetry of all grafted and ungrafted polyesters demonstrates that all the polymers are amorphous having glass transition temperatures which decrease from $-24\text{ }^{\circ}\text{C}$ (for ungrafted) to $-67\text{ }^{\circ}\text{C}$ (for highest grafted polymers). Although, all the oleate grafted PGAs are amorphous, but X-ray diffraction analysis reveals a broad peak in the small angle regime with d -spacing values decreasing with increasing degree of grafting. It is assumed that the broad peak is the result of nanophases separation of oleate side chain from the polymer backbone. Furthermore, one of the selected polymers PGA-*g*-O22 was chosen to study the effect of this polymer on the mesophase behavior of the glycerol monooleate/water system. A ternary phase diagram based on PGA-*g*-O22/GMO/water was established. From the ternary phase diagram, it is clear that the polymer stabilizes the $Pn3m$ cubic phase over a wide range of concentrations. There is a significant increase of the lattice parameter with an increase in polymer concentration. This increase of the lattice parameter is attributed to the widening of lipid bilayer and the water channels of the cubic phase. Later, this oleate grafted polymer was used to stabilize cubosomes. But the polymer is too hydrophobic to be effectively used as a steric stabilizer of cubosomes. So there is a need to modify this polymer to introduce a more hydrophilic character.

The last part of this work deals with the modification of oleate grafted poly(glycerol adipate) with a hydrophilic polymer such as poly(ethylene glycol) and studying the bulk properties of these polymers as well as their ability to stabilize cubosome dispersions. For this study three oleate grafted poly(glycerol adipate)s were further grafted with mPEG750 and mPEG1K chains. All the PEG-grafted polyesters are semi-crystalline. SAXS measurements depict a lamellar morphology in the small angle scattering regime, while WAXS measurements show a typical scattering pattern of the triclinic unit cell of PEG. All the $\text{PGA}_x\text{O}_y\text{PEG}_z$ samples are water soluble. Two polymers $\text{PGA}_{26}\text{O}_4\text{PEG1K}_{17}$ and $\text{PGA}_{26}\text{O}_{13}\text{PEG1K}_8$ having CAC values of 0.028 and $0.151\text{ g}\cdot\text{L}^{-1}$, respectively, were used to investigate their ability as steric stabilizers of cubosomes. It was found that adding the former ($\phi_{\text{PEG}}=0.71$) to the GMO/water system induces a mesophase transition of the cubic phase from $Pn3m$ phase to the less curved $Im3m$ cubic symmetry whereas the later ($\phi_{\text{PEG}}=0.47$) retains the cubic symmetry to the $Pn3m$ with increased lattice parameter. The increase of the lattice parameter of the cubic phase is attributed to the penetration of

hydrophobic chains into the lipid bilayer. The cubosome aqueous dispersions are stable for more than two weeks at room temperature. So, these multi-graft biodegradable copolymers could be effectively used to stabilize several lyotropic liquid crystal systems by controlling the hydrophobic to hydrophilic volume fractions.

Overall it has been shown that functional polyesters offer an interesting toolbox for the preparation of various biodegradable materials. In order to tailor their properties, not only different fatty acids with different grafting densities can be used but also other hydrophilic side chain can be employed to control the hydrophilic to lipophilic balance. The polymer backbones can be used for direct coupling of drugs, proteins and peptides.

Some of the chapters of this thesis are based on the following publications:

Chapter 2 based on

Bilal, M. H.; Prehm, M.; Njau, A.; Samiullah, M.; Meister, A.; Kressler, J. Enzymatic Synthesis and Characterization of Hydrophilic Sugar Based Polyesters and Their Modification with Stearic Acid. *Polymers* 2016, 8, 80.

Chapter 3 based on

Bilal, M. H.; Hussain, H.; Prehm, M.; Baumeister, U.; Meister, A.; Hause, G.; Busse, K.; Mäder, K.; Kressler, J. Synthesis of Poly(Glycerol Adipate)-*g*-Oleate and Its Ternary Phase Diagram with Glycerol Monooleate and Water. *Eur. Polym. J.* 2017, 91, 162–175.

6 REFERENCES

- (1) Nair, L. S.; Laurencin, C. T. Biodegradable Polymers as Biomaterials. *Prog. Polym. Sci.* **2007**, *32*, 762–798.
- (2) El Habnoui, S.; Nottelet, B.; Darcos, V.; Porsio, B.; Lemaire, L.; Franconi, F.; Garric, X.; Coudane, J. MRI-Visible Poly(ϵ -Caprolactone) with Controlled Contrast Agent Ratios for Enhanced Visualization in Temporary Imaging Applications. *Biomacromolecules* **2013**, *14*, 3626–3634.
- (3) Jiang, Y.; Loos, K. Enzymatic Synthesis of Biobased Polyesters and Polyamides. *Polymers* **2016**, *8*, 243.
- (4) Olsson, A.; Lindstro, M.; Iversen, T. Lipase-Catalyzed Synthesis of an Epoxy-Functionalized Polyester from the Suberin Monomer Cis-9,10-Epoxy-18-Hydroxyoctadecanoic Acid. *Biomacromolecules* **2007**, *8*, 757–760.
- (5) Gross, R. A.; Ganesh, M.; Lu, W. Enzyme-Catalysis Breathes New Life into Polyester Condensation Polymerizations. *Trends Biotechnol.* **2010**, *28*, 435–443.
- (6) Stjerndahl, A.; Wistrand, A. F.; Albertsson, A.-C. Industrial Utilization of Tin-Initiated Resorbable Polymers: Synthesis on a Large Scale with a Low Amount of Initiator Residue. *Biomacromolecules* **2007**, *8*, 937–940.
- (7) Borgne, A. Le; Pluta, C.; Spassky, N. Highly Reactive Yttrium Alkoxide as New Initiator for the Polymerization of B-butyrolactone. *Macromol. Rapid Commun.* **1994**, *15*, 955–960.
- (8) Ravi, P.; Gröb, T.; Dehnicke, K.; Greiner, A. Novel [Sm₂I(NPPh₃)₅(DME)] Initiator for the Living Ring-Opening Polymerization of ϵ -Caprolactone and δ -Valerolactone. *Macromolecules* **2001**, *34*, 8649–8653.
- (9) Martin, E.; Dubois, P.; Jérôme, R. Controlled Ring-Opening Polymerization of ϵ -Caprolactone Promoted by “in Situ” Formed Yttrium Alkoxides. *Macromolecules* **2000**, *33*, 1530–1535.
- (10) Yu, Y.; Wu, D.; Liu, C.; Zhao, Z.; Yang, Y.; Li, Q. Lipase/Esterase-Catalyzed Synthesis of Aliphatic Polyesters via Polycondensation: A Review. *Process Biochem.* **2012**, *47*, 1027–1036.
- (11) Kazenwadel, C.; Eiben, S.; Maurer, S.; Beuttler, H.; Wetzl, D.; Hauer, B.; Koschorreck, K. Thiol-Functionalization of Acrylic Ester Monomers Catalyzed by Immobilized Humicola Insolens Cutinase. *Enzyme Microb. Technol.* **2012**, *51*, 9–15.
- (12) Kobayashi, S.; Makino, A. Enzymatic Polymer Synthesis: An Opportunity for Green Polymer Chemistry. *Chem. Rev.* **2001**, *109*, 5288–5353.
- (13) Gross, R. A.; Kumar, A.; Kalra, B. Polymer Synthesis by In Vitro Enzyme Catalysis. *Chem. Rev.* **2001**, *101*, 2097–2124.
- (14) Kadokawa, J.; Kobayashi, S. Polymer Synthesis by Enzymatic Catalysis. *Curr. Opin. Chem. Biol.* **2010**, *14*, 145–153.
- (15) Kobayashi, S.; Uyama, H.; Namekawa, S. In Vitro Biosynthesis of Polyesters with Isolated Enzymes in Aqueous Systems and Organic Solvents. *Polym. Degrad. Stab.* **1998**, *59*, 195–201.
- (16) Shoda, S.; Uyama, H.; Kadokawa, J.; Kimura, S.; Kobayashi, S. Enzymes as Green Catalysts for Precision Macromolecular Synthesis. *Chem. Rev.* **2016**, *116*, 2307–2413.
- (17) Stauch, B.; Fisher, S. J.; Cianci, M. Open and Closed States of Candida Antarctica Lipase B: Protonation and the Mechanism of Interfacial Activation. *J. Lipid Res.* **2015**, *56*, 2348–2358.
- (18) Douka, A.; Vouyiouka, S.; Papaspyridi, L.-M.; Papaspyrides, C. D. A Review on Enzymatic Polymerization to Produce Polycondensation Polymers: The Case of Aliphatic Polyesters, Polyamides and Polyesteramides. *Prog. Polym. Sci.* **2018**, *79*, 1–25.
- (19) Bezborodov, A. M.; Zagustina, N. A. Lipases in Catalytic Reactions of Organic Chemistry. *Appl. Biochem. Microbiol.* **2014**, *50*, 313–337.
- (20) Laszlo, J. A.; Jackson, M.; Blanco, R. M. Active-Site Titration Analysis of Surface Influences on Immobilized Candida Antarctica Lipase B Activity. *J. Mol. Catal. B Enzym.* **2011**, *69*, 60–65.

- (21) Hanefeld, U.; Gardossi, L.; Magner, E. Understanding Enzyme Immobilisation. *Chem. Soc. Rev.* **2009**, *38*, 453–468.
- (22) Franssen, M. C. R.; Steunenberg, P.; Scott, E. L.; Zuilhof, H.; Sanders, J. P. M. Immobilised Enzymes in Biorenewables Production. *Chem. Soc. Rev.* **2013**, *42*, 6491–6533.
- (23) Cyclor, M.; Schrag, J. D. Structure as Basis for Understanding Interfacial Properties of Lipases. *Methods Enzymol.* **1997**, *284*, 3–27.
- (24) Chen, B.; Hu, J.; Miller, E. M.; Xie, W.; Cai, M.; Gross, R. A. Candida Antarctica Lipase B Chemically Immobilized on Epoxy-Activated Micro- and Nanobeads: Catalysts for Polyester Synthesis. *Biomacromolecules* **2008**, *9*, 463–471.
- (25) Uyama, H.; Kobayashi, S. Enzyme-Catalyzed Polymerization to Functional Polymers. *J. Mol. Catal. B Enzym.* **2002**, 117–127.
- (26) Tanaka, A.; Kohri, M.; Takiguchi, T.; Kato, M.; Matsumura, S. Enzymatic Synthesis of Reversibly Crosslinkable Polyesters with Pendant Mercapto Groups. *Polym. Degrad. Stab.* **2012**, *97*, 1415–1422.
- (27) Weiss, V. M.; Naolou, T.; Hause, G.; Kuntsche, J.; Kressler, J.; Mäder, K. Poly(Glycerol Adipate)-Fatty Acid Esters as Versatile Nanocarriers: From Nanocubes over Ellipsoids to Nanospheres. *J. Control. Release* **2012**, *158*, 156–164.
- (28) Naolou, T.; Busse, K.; Kressler, J. Synthesis of Well-Defined Graft Copolymers by Combination of Enzymatic Polycondensation and “Click” Chemistry. *Biomacromolecules* **2010**, *11*, 3660–3667.
- (29) Jbeily, M.; Naolou, T.; Bilal, M.; Amado, E.; Kressler, J. Enzymatically Synthesized Polyesters with Pendant OH Groups as Macroinitiators for the Preparation of Well-Defined Graft Copolymers by Atom Transfer Radical Polymerization. *Polym. Int.* **2014**, *63*, 894–901.
- (30) Jérôme, C.; Lecomte, P. Recent Advances in the Synthesis of Aliphatic Polyesters by Ring-Opening Polymerization. *Adv. Drug Deliv. Rev.* **2008**, *60*, 1056–1076.
- (31) Wu, R.; Al-Azemi, T. F.; Bisht, K. S. Functionalized Polycarbonate Derived from Tartaric Acid: Enzymatic Ring-Opening Polymerization of a Seven-Membered Cyclic Carbonate. *Biomacromolecules* **2008**, *9*, 2921–2928.
- (32) Azim, H.; Dekhterman, A.; Jiang, Z.; Gross, R. A. Candida Antarctica Lipase B-Catalyzed Synthesis of Poly(Butylene Succinate): Shorter Chain Building Blocks Also Work. *Biomacromolecules* **2006**, *7*, 3093–3097.
- (33) Korupp, C.; Weberskirch, R.; Müller, J. J.; Liese, A.; Hilterhaus, L. Scaleup of Lipase-Catalyzed Polyester Synthesis. *Org. Process Res. Dev.* **2010**, *14*, 1118–1124.
- (34) Uyama, H.; Kuwabara, M.; Tsujimoto, T.; Kobayashi, S. Enzymatic Synthesis and Curing of Biodegradable Epoxide-Containing Polyesters from Renewable Resources. *Biomacromolecules* **2003**, *4*, 211–215.
- (35) Tsujimoto, T.; Uyama, H.; Kobayashi, S. Enzymatic Synthesis and Curing of Biodegradable Crosslinkable Polyesters. *Macromol. Biosci.* **2002**, *2*, 329–335.
- (36) Olson, D. A.; Sheares, V. V. Preparation of Unsaturated Linear Aliphatic Polyesters Using Condensation Polymerization. *Macromolecules* **2006**, *39*, 2808–2814.
- (37) Trollsås, M.; Lee, V. Y.; Mecerreyes, D.; Löwenhielm, P.; Möller, M.; Miller, R. D.; Hedrick, J. L. Hydrophilic Aliphatic Polyesters: Design, Synthesis, and Ring-Opening Polymerization of Functional Cyclic Esters. *Macromolecules* **2000**, *33*, 4619–4627.
- (38) Tian, D.; Dubois, P.; Grandfils, C.; Jérôme, R. Ring-Opening Polymerization of 1,4,8-Trioxaspiro[4.6]-9-Undecanone: A New Route to Aliphatic Polyesters Bearing Functional Pendant Groups. *Macromolecules* **1997**, *30*, 406–409.
- (39) Zhang, T.; Howell, B. A.; Dumitrascu, A.; Martin, S. J.; Smith, P. B. Synthesis and Characterization of Glycerol-Adipic Acid Hyperbranched Polyesters. *Polymer* **2014**, *55*, 5065–5072.
- (40) Ning, Z. Y.; Zhang, Q. S.; Wu, Q. P.; Li, Y. Z.; Ma, D. X.; Chen, J. Z. Efficient Synthesis of Hydroxyl Functioned Polyesters from Natural Polyols and Sebacic Acid. *Chinese Chem. Lett.* **2011**, *22*, 635–638.
- (41) Barrett, D. G.; Luo, W.; Yousaf, M. N. Aliphatic Polyester Elastomers Derived from Erythritol and α,ω -Diacids. *Polym. Chem.* **2010**, *1*, 296–302.

- (42) Halpern, J. M.; Urbanski, R.; Weinstock, A. K.; Iwig, D. F.; Mathers, R. T.; Von Recum, H. a. A Biodegradable Thermoset Polymer Made by Esterification of Citric Acid and Glycerol. *J. Biomed. Mater. Res. - Part A* **2014**, *102*, 1467–1477.
- (43) Ottosson, J.; Hult, K. Influence of Acyl Chain Length on the Enantioselectivity of Candida Antarctica Lipase B and Its Thermodynamic Components in Kinetic Resolution of Sec-Alcohols. *J. Mol. Catal. B Enzym.* **2001**, *11*, 1025–1028.
- (44) Padovani, M.; Hilker, I.; Duxbury, C. J.; Heise, A. Functionalization of Polymers with High Precision by Dual Regio- and Stereoselective Enzymatic Reactions. *Macromolecules* **2008**, *41*, 2439–2444.
- (45) Wang, Y. F.; Lalonde, J. J.; Momongan, M.; Bergbreiter, D. E.; Wong, C. H. Lipase-Catalyzed Irreversible Transesterifications Using Enol Esters as Acylating Reagents: Preparative Enantio- and Regioselective Syntheses of Alcohols, Glycerol Derivatives, Sugars and Organometallics. *J. Am. Chem. Soc.* **1988**, *110*, 7200–7205.
- (46) Jiang, Y.; Woortman, A. J. J.; Alberda van Ekenstein, G. O. R.; Loos, K. Enzyme-Catalyzed Synthesis of Unsaturated Aliphatic Polyesters Based on Green Monomers from Renewable Resources. *Biomolecules* **2013**, *3*, 461–480.
- (47) Kim, M. S.; Seo, K. S.; Khang, G.; Cho, S. H.; Lee, H. B. Preparation of Poly(Ethylene Glycol)-Block-Poly(Caprolactone) Copolymers and Their Applications as Thermo-Sensitive Materials. *J. Biomed. Mater. Res.* **2004**, *70A*, 154–158.
- (48) Meier, M. A. R.; Metzger, J. O.; Schubert, U. S. Plant Oil Renewable Resources as Green Alternatives in Polymer Science. *Chem. Soc. Rev.* **2007**, *36*, 1788–1802.
- (49) Montero de Espinosa, L.; Meier, M. A. R. Plant Oils: The Perfect Renewable Resource for Polymer Science?! *Eur. Polym. J.* **2011**, *47*, 837–852.
- (50) Seniha Güner, F.; Yağcı, Y.; Tuncer Erciyes, A. Polymers from Triglyceride Oils. *Prog. Polym. Sci.* **2006**, *31*, 633–670.
- (51) Warwel, S.; Brüse, F.; Demes, C.; Kunz, M.; Klaas, M. R. gen. Polymers and Surfactants on the Basis of Renewable Resources. *Chemosphere* **2001**, *43*, 39–48.
- (52) Sifontes Herrera, V. A.; Oladele, O.; Kordás, K.; Eränen, K.; Mikkola, J.-P.; Murzin, D. Y.; Salmi, T. Sugar Hydrogenation over a Ru/C Catalyst. *J. Chem. Technol. Biotechnol.* **2011**, *86*, 658–668.
- (53) Yang, Y.; Lu, W.; Zhang, X.; Xie, W.; Cai, M.; Gross, R. A. Two-Step Biocatalytic Route to Biobased Functional Polyesters from ω -Carboxy Fatty Acids and Diols. *Biomacromolecules* **2010**, *11*, 259–268.
- (54) Kline, B. J.; Beckman, E. J.; Russell, A. J. One-Step Biocatalytic Synthesis of Linear Polyesters with Pendant Hydroxyl Groups. *J. Am. Chem. Soc.* **1998**, *120*, 9475–9480.
- (55) Kumar, A.; Kulshrestha, A. S.; Gao, W.; Gross, R. A. Versatile Route to Polyol Polyesters by Lipase Catalysis. *Macromolecules* **2003**, *36*, 8219–8221.
- (56) Fu, H.; Kulshrestha, A. S.; Gao, W.; Gross, R. A.; Baiardo, M.; Scandola, M. Physical Characterization of Sorbitol or Glycerol Containing Aliphatic Copolyesters Synthesized by Lipase-Catalyzed Polymerization. *Macromolecules* **2003**, *36*, 9804–9808.
- (57) Kulshrestha, A. S.; Gao, W.; Gross, R. A. Glycerol Copolyesters: Control of Branching and Molecular Weight Using a Lipase Catalyst. *Macromolecules* **2005**, *38*, 3193–3204.
- (58) Tsujimoto, T.; Uyama, H.; Kobayashi, S. Enzymatic Synthesis of Cross-Linkable Polyesters from Renewable Resources. *Biomacromolecules* **2000**, *2*, 29–31.
- (59) Rai, R.; Tallawi, M.; Grigore, A.; Boccaccini, A. R. Synthesis, Properties and Biomedical Applications of Poly(Glycerol Sebacate) (PGS): A Review. *Prog. Polym. Sci.* **2012**, *37*, 1051–1078.
- (60) Li, G.; Yao, D.; Zong, M. Lipase-Catalyzed Synthesis of Biodegradable Copolymer Containing Malic Acid Units in Solvent-Free System. *Eur. Polym. J.* **2008**, *44*, 1123–1129.
- (61) Kim, D.-Y.; Dordick, J. S. Combinatorial Array-Based Enzymatic Polyester Synthesis. *Biotechnol. Bioeng.* **2001**, *76*, 200–206.
- (62) Park, O.-J.; Kim, D.-Y.; Dordick, J. S. Enzyme-Catalyzed Synthesis of Sugar-Containing Monomers and Linear Polymers. *Biotechnol. Bioeng.* **2000**, *70*, 208–216.
- (63) Therisod, M.; Klivanov, A. M. Facile Enzymatic Preparation of Monoacylated Sugars in

- Pyridine. *J. Am. Chem. Soc.* **1986**, *108*, 5638–5640.
- (64) Martin, B. D.; Ampofo, S. A.; Linhardt, R. J.; Dordick, J. S. Biocatalytic Synthesis of Sugar-Containing Polyacrylate-Based Hydrogels. *Macromolecules* **1992**, *25*, 7081–7085.
- (65) Hu, J.; Gao, W.; Kulshrestha, A.; Gross, R. A. “Sweet Polyesters”: Lipase-Catalyzed Condensation–Polymerizations of Alditols. *Macromolecules* **2006**, *39*, 6789–6792.
- (66) Uyama, H.; Klegraf, E.; Wada, S.; Kobayashi, S. Regioselective Polymerization of Sorbitol and Divinyl Sebacate Using Lipase Catalyst. *Chem. Lett.* **2000**, *29*, 800–801.
- (67) Hollmann, F.; Grzebyk, P.; Heinrichs, V.; Doderer, K.; Thum, O. On the Inactivity of *Candida Antartica* Lipase B towards Strong Acids. *J. Mol. Catal. B Enzym.* **2009**, *57*, 257–261.
- (68) MacManus, D. A.; Vulfson, E. N. Reversal of Regioselectivity in the Enzymatic Acylation of Secondary Hydroxyl Groups Mediated by Organic Solvents. *Enzyme Microb. Technol.* **1997**, *20*, 225–228.
- (69) Therisod, M.; Klibanov, A. M. Regioselective Acylation of Secondary Hydroxyl Groups in Sugars Catalyzed by Lipases in Organic Solvents. *J. Am. Chem. Soc.* **1987**, *109*, 3977–3981.
- (70) Chen, X.; Martin, B. D.; Neubauer, T. K.; Linhardt, R. J.; Dordick, J. S.; Rethwisch, D. G. Enzymatic and Chemoenzymatic Approaches to Synthesis of Sugar-Based Polymer and Hydrogels. *Carbohydr. Polym.* **1995**, *28*, 15–21.
- (71) Chaudhary, A. K.; Lopez, J.; Beckman, E. J.; Russell, A. J. Biocatalytic Solvent-Free Polymerization To Produce High Molecular Weight Polyesters. *Biotechnol. Prog.* **1997**, *13*, 318–325.
- (72) Elgharbawy, A. A.; Riyadi, F. A.; Alam, M. Z.; Moniruzzaman, M. Ionic Liquids as a Potential Solvent for Lipase-Catalysed Reactions: A Review. *J. Mol. Liq.* **2018**, *251*, 150–166.
- (73) Loeker, F. C.; Duxbury, C. J.; Kumar, R.; Gao, W.; Gross, R. A.; Howdle, S. M. Enzyme-Catalyzed Ring-Opening Polymerization of ϵ -Caprolactone in Supercritical Carbon Dioxide. *Macromolecules* **2004**, *37*, 2450–2453.
- (74) Takamoto, T.; Uyama, H.; Kobayashi, S. Lipase-Catalyzed Degradation of Polyester in Supercritical Carbon Dioxide. *Macromol. Biosci.* **2001**, *1*, 215–218.
- (75) Matsumura, S.; Ebata, H.; Kondo, R.; Toshima, K. Organic Solvent-Free Enzymatic Transformation of Poly(ϵ -Caprolactone) into Repolymerizable Oligomers in Supercritical Carbon Dioxide. *Macromol. Rapid Commun.* **2001**, *22*, 1325–1329.
- (76) Villarroya, S.; Zhou, J.; Thurecht, K. J.; Howdle, S. M. Synthesis of Graft Copolymers by the Combination of ATRP and Enzymatic ROP in ScCO_2 . *Macromolecules* **2006**, *39*, 9080–9086.
- (77) Corma, A.; Iborra, S.; Velty, A. Chemical Routes for the Transformation of Biomass into Chemicals. *Chem. Rev.* **2007**, *107*, 2411–2502.
- (78) Guo, K.; Chu, C.-C. Biodegradation of Unsaturated Poly(Ester-Amide)s and Their Hydrogels. *Biomaterials* **2007**, *28*, 3284–3294.
- (79) Matsumura, S. Enzyme-Catalyzed Synthesis and Chemical Recycling of Polyesters. *Macromol. Biosci.* **2002**, *2*, 105–126.
- (80) Nagata, M.; Kiyotsukuri, T.; Ibuki, H.; Tsutsumi, N.; Sakai, W. Synthesis and Enzymatic Degradation of Regular Network Aliphatic Polyesters. *React. Funct. Polym.* **1996**, *30*, 165–171.
- (81) Williams, C. K. Synthesis of Functionalized Biodegradable Polyesters. *Chem. Soc. Rev.* **2007**, *36*, 1573–1580.
- (82) Feng, C.; Li, Y.; Yang, D.; Hu, J.; Zhang, X.; Huang, X. Well-Defined Graft Copolymers: From Controlled Synthesis to Multipurpose Applications. *Chem. Soc. Rev.* **2011**, *40*, 1282–1295.
- (83) Kallinteri, P.; Higgins, S.; Hutcheon, G. A.; St. Pourçain, C. B.; Garnett, M. C. Novel Functionalized Biodegradable Polymers for Nanoparticle Drug Delivery Systems. *Biomacromolecules* **2005**, *6*, 1885–1894.
- (84) Orafai, H.; Kallinteri, P.; Garnett, M.; Huggins, S.; Hutcheon, G.; Pourcain, C. Novel Poly(Glycerol Adipate) Polymers Used for Nanoparticle Making: A Study of Surface Free Energy. *Iran. J. Pharm. Res.* **2010**, *7*, 11–19.
- (85) Zhang, Y.-R.; Spinella, S.; Xie, W.; Cai, J.; Yang, Y.; Wang, Y.-Z.; Gross, R. A. Polymeric Triglyceride Analogs Prepared by Enzyme-Catalyzed Condensation Polymerization. *Eur. Polym. J.* **2013**, *49*, 793–803.

- (86) Tsujimoto, T.; Uyama, H.; Kobayashi, S. Enzymatic Synthesis and Curing of Biodegradable Crosslinkable Polyesters. *Macromol. Biosci.* **2002**, *2*, 329–335.
- (87) Weiss, V. M.; Naolou, T.; Hause, G.; Kuntsche, J.; Kressler, J.; Mäder, K. Poly(Glycerol Adipate)-Fatty Acid Esters as Versatile Nanocarriers: From Nanocubes over Ellipsoids to Nanospheres. *J. Control. Release* **2012**, *158*, 156–164.
- (88) Weiss, V. M.; Naolou, T.; Amado, E.; Busse, K.; Mäder, K.; Kressler, J. Formation of Structured Polygonal Nanoparticles by Phase-Separated Comb-like Polymers. *Macromol. Rapid Commun.* **2012**, *33*, 35–40.
- (89) Naolou, T.; Hussain, H.; Baleed, S.; Busse, K.; Lechner, B. D.; Kressler, J. The Behavior of Fatty Acid Modified Poly(Glycerol Adipate) at the Air/Water Interface. *Colloids Surfaces A Physicochem. Eng. Asp.* **2015**, *468*, 22–30.
- (90) Bilal, M.; Prehm, M.; Njau, A.; Samiullah, M.; Meister, A.; Kressler, J. Enzymatic Synthesis and Characterization of Hydrophilic Sugar Based Polyesters and Their Modification with Stearic Acid. *Polymers* **2016**, *8*, 80.
- (91) Pfefferkorn, D.; Pulst, M.; Naolou, T.; Busse, K.; Balko, J.; Kressler, J. Crystallization and Melting of Poly(Glycerol Adipate)-Based Graft Copolymers with Single and Double Crystallizable Side Chains. *J. Polym. Sci. Part B Polym. Phys.* **2013**, *51*, 1581–1591.
- (92) Naolou, T.; Busse, K.; Lechner, B. D.; Kressler, J. The Behavior of Poly(ϵ -Caprolactone) and Poly(Ethylene Oxide)-*b*-Poly(ϵ -Caprolactone) Grafted to a Poly(Glycerol Adipate) Backbone at the Air/Water Interface. *Colloid Polym. Sci.* **2014**, *292*, 1199–1208.
- (93) Wu, W.-X.; Wang, N.; Liu, B.-Y.; Deng, Q.-F.; Yu, X.-Q. Lipase-Catalyzed Synthesis of Azido-Functionalized Aliphatic Polyesters towards Acid-Degradable Amphiphilic Graft Copolymers. *Soft Matter* **2014**, *10*, 1199–1213.
- (94) Parrish, B.; Breitenkamp, R. B.; Emrick, T. PEG- and Peptide-Grafted Aliphatic Polyesters by Click Chemistry. *J. Am. Chem. Soc.* **2005**, *127*, 7404–7410.
- (95) Riva, R.; Schmeits, S.; Jerome, C.; Jerome, R.; Lecomte, P. Combination of Ring-Opening Polymerization and “Click Chemistry”: Toward Functionalization and Grafting of Poly(ϵ -Caprolactone). *Macromolecules* **2007**, *40*, 796–803.
- (96) Riva, R.; Schmeits, S.; Stoffelbach, F.; Jérôme, C.; Jérôme, R.; Lecomte, P. Combination of Ring-Opening Polymerization and “Click” Chemistry towards Functionalization of Aliphatic Polyesters. *Chem. Commun.* **2005**, *42*, 5334–5336.
- (97) Jbeily, M.; Naolou, T.; Bilal, M.; Amado, E.; Kressler, J. Enzymatically Synthesized Polyesters with Pendent OH Groups as Macroinitiators for the Preparation of Well-Defined Graft Copolymers by Atom Transfer Radical Polymerization. *Polym. Int.* **2014**, *63*, 894–901.
- (98) Naolou, T.; Jbeily, M.; Scholtysek, P.; Kressler, J. Synthesis and Characterization of Stearoyl Modified Poly(Glycerol Adipate) Containing ATRP Initiator on Its Backbone. *Adv. Mater. Res.* **2013**, *812*, 1–11.
- (99) Brosnan, S. M.; Brown, A. H.; Ashby, V. S. It Is the Outside That Counts: Chemical and Physical Control of Dynamic Surfaces. *J. Am. Chem. Soc.* **2013**, *135*, 3067–3072.
- (100) Mecerreyes, D.; Humes, J.; Miller, R. D.; Hedrick, J. L.; Detrembleur, C.; Lecomte, P.; Jérôme, R.; San Roman, J. First Example of an Unsymmetrical Difunctional Monomer Polymerizable by Two Living/Controlled Methods. *Macromol. Rapid Commun.* **2000**, *21*, 779–784.
- (101) Wersig, T.; Hacker, M. C.; Kressler, J.; Mäder, K. Poly(Glycerol Adipate) – Indomethacin Drug Conjugates – Synthesis and in Vitro Characterization. *Int. J. Pharm.* **2017**, *531*, 225–234.
- (102) Suksiriworapong, J.; Taresco, V.; Ivanov, D. P.; Styliari, I. D.; Sakchaisri, K.; Junyaprasert, V. B.; Garnett, M. C. Synthesis and Properties of a Biodegradable Polymer-Drug Conjugate: Methotrexate-Poly(Glycerol Adipate). *Colloids Surfaces B Biointerfaces* **2018**, *167*, 115–125.
- (103) Griffin, W. Classification of Surface-Active Agents by “HLB”. *J. Soc. Cosmet. Chem.* **1946**, *1*, 311–326.
- (104) Kulkarni, C. V.; Wachter, W.; Iglesias-Salto, G.; Engelskirchen, S.; Ahualli, S. Monoolein: A Magic Lipid? *Phys. Chem. Chem. Phys.* **2011**, *13*, 3004–3021.
- (105) Misquitta, Y.; Caffrey, M. Rational Design of Lipid Molecular Structure: A Case Study Involving the C19:1c10 Monoacylglycerol. *Biophys. J.* **2001**, *81*, 1047–1058.

- (106) Qiu, H.; Ca, M. The Phase Diagram of the Monoolein / Water System : Metastability and Equilibrium Aspects. *Biomaterials* **2000**, *21*, 223–234.
- (107) Kulkarni, C. V.; Yagmur, A.; Steinhart, M.; Kriechbaum, M.; Rappolt, M. Effects of High Pressure on Internally Self-Assembled Lipid Nanoparticles: A Synchrotron Small-Angle X-Ray Scattering (SAXS) Study. *Langmuir* **2016**, *32*, 11907–11917.
- (108) Katsaras, J.; Donaberger, R. L.; Swainson, I. P.; Tennant, D. C.; Tun, Z.; Vold, R. R.; Prosser, R. S. Rarely Observed Phase Transitions in a Novel Lyotropic Liquid Crystal System. *Phys. Rev. Lett.* **1997**, *78*, 899–902.
- (109) van 't Hag, L.; Gras, S. L.; Conn, C. E.; Drummond, C. J. Lyotropic Liquid Crystal Engineering Moving beyond Binary Compositional Space – Ordered Nanostructured Amphiphile Self-Assembly Materials by Design. *Chem. Soc. Rev.* **2017**, *46*, 2705–2731.
- (110) Kumar, M.; Kumaraswamy, G. Soft Matter Phase Behaviour of Phase Behaviour of the Ternary System: Monoolein–water–branched Polyethylenimine. *Soft Matter* **2015**, *11*, 5705–5711.
- (111) Chong, J. Y. T.; Mulet, X.; Postma, A.; Keddie, D. J.; Waddington, L. J.; Boyd, B. J.; Drummond, C. J. Novel RAFT Amphiphilic Brush Copolymer Steric Stabilisers for Cubosomes: Poly(Octadecyl Acrylate)-Block-Poly(Polyethylene Glycol Methyl Ether Acrylate). *Soft Matter* **2014**, *10*, 6666–6676.
- (112) Conn, C. E.; Darmanin, C.; Mulet, X.; Hawley, A.; Drummond, C. J. Effect of Lipid Architecture on Cubic Phase Susceptibility to Crystallisation Screens. *Soft Matter* **2012**, *8*, 6884–6896.
- (113) Kumar, M.; Patil, N. G.; Choudhury, C. K.; Roy, S.; Ambade, A. V.; Kumaraswamy, G. Compact Polar Moieties Induce Lipid–water Systems to Form Discontinuous Reverse Micellar Phase. *Soft Matter* **2015**, *11*, 5417–5424.
- (114) Chong, J. Y. T.; Mulet, X.; Keddie, D. J.; Waddington, L.; Mudie, S. T.; Boyd, B. J.; Drummond, C. J. Novel Steric Stabilizers for Lyotropic Liquid Crystalline Nanoparticles: PEGylated-Phytanyl Copolymers. *Langmuir* **2015**, *31*, 2615–2629.
- (115) Chen, Y.; Angelova, A.; Angelov, B.; Drechsler, M.; Garamus, V. M.; Zou, R. W.-R. and A. Sterically Stabilized Spongosomes for Multidrug Delivery of Anticancer Nanomedicines. *J. Mater. Chem. B* **2015**, *3*, 7734–7744.
- (116) Gruner, S. Lipid Polymorphism: The Molecular Basis of Nonbilayer Phases. *Annu. Rev. Biophys. Biomol. Struct.* **1985**, *14*, 211–238.
- (117) Fennell Evans, D. Self-Organization of Amphiphiles. *Langmuir* **1988**, *4*, 3–12.
- (118) Tanford, C. The Hydrophobic Effect and the Organization of Living Matter. *Science* **1978**, *200*, 1012–1018.
- (119) Rosen, M. J., Ed. Micelle Formation by Surfactants. In *Surfactants and Interfacial Phenomena*; John Wiley & Sons, Inc.: Hoboken, NJ, 2004; pp 105–177.
- (120) Israelachvili, J. N. Soft and Biological Structures. In *Intermolecular and Surface Forces*; Israelachvili, J. N., Ed.; Academic Press: San Diego, 2011; pp 535–576.
- (121) Qiu, H.; Caffrey, M. The Phase Diagram of the Monoolein/Water System: Metastability and Equilibrium Aspects. *Biomaterials* **2000**, *21*, 223–234.
- (122) Fong, C.; Le, T.; Drummond, C. J. Lyotropic Liquid Crystal Engineering–ordered Nanostructured Small Molecule Amphiphileself-Assembly Materials by Design. *Chem. Soc. Rev.* **2012**, *41*, 1297–1322.
- (123) Kulkarni, C. V. Lipid Crystallization: From Self-Assembly to Hierarchical and Biological Ordering. *Nanoscale* **2012**, *4*, 5779–5791.
- (124) Leite, D. M.; Barbu, E.; Pilkington, G. J.; Lalatsa, A. Peptide Self-Assemblies for Drug Delivery. *Curr. Top. Med. Chem.* **2015**, *15*, 2277–2289.
- (125) Blume, A. Lipids. In *Bioelectrochemistry of Membranes*; Walz, D., Teissié, J., Milazzo, G., Eds.; Birkhäuser Basel: Basel, 2004; pp 61–152.
- (126) Tiddy, G. Surfactant-Water Liquid Crystal Phases. *Phys. Rep.* **1980**, *57*, 1–46.
- (127) Seddon, J. M.; Templer, R. H. Polymorphism of Lipid-Water Systems. In *Handbook of Biological Physics*; R. Lipowsky and E. Sackmann, Ed.; 1995; Vol. 1, pp 97–160.
- (128) Seddon, J. M. Structure of the Inverted Hexagonal H_{II} Phase, and Non-Lamellar Phase Transitions of Lipids. *Biochim. Biophys. Acta* **1990**, *1031*, 1–69.

- (129) Seddon, J. M.; Bartle, E. A.; Mingins, J. Inverse Cubic Liquid-Crystalline Phases of Phospholipids and Related Lyotropic Systems. *J. Phys. Condens. Matter* **1990**, *2*, 285–290.
- (130) Seddon, J. M. Lyotropic Phase Behaviour of Biological Amphiphiles. *Berichte der Bunsengesellschaft für Phys. Chemie* **1996**, *100*, 380–393.
- (131) Nakano, M.; Teshigawara, T.; Sugita, A.; Leesajakul, W.; Taniguchi, A.; Kamo, T.; Matsuoka, H.; Handa, T. Dispersions of Liquid Crystalline Phases of the Monoolein /Oleic Acid / Pluronic® F127 System. *Langmuir* **2002**, *18*, 9283–9288.
- (132) Hyde, S. T. Swelling and Structure . Analysis of the Topology and Geometry of Lamellar and Sponge Lyotropic Mesophases. *Langmuir* **1997**, *7463*, 842–851.
- (133) Ridell, A.; Ekelund, K.; Evertsson, H.; Engström, S. On the Water Content of the Solvent / Monoolein / Water Sponge L_3 Phase. *Colloids Surfaces A Physicochem. Eng. Asp.* **2003**, *228*, 17–24.
- (134) Kaasgaard, T.; Drummond, C. J. Ordered 2-D and 3-D Nanostructured Amphiphile Self-Assembly Materials Stable in Excess Solvent. *Phys. Chem. Chem. Phys.* **2006**, *8*, 4957–4975.
- (135) Alfons, K.; Engstrom, S. Drug Compatibility with the Sponge Phases Formed in Monoolein, Water, and Propylene Glycol or Poly(Ethylene Glycol). *J. Pharm. Sci.* **1998**, *87*, 1527–1530.
- (136) Cherezov, V.; Clogston, J.; Papiz, M. Z.; Caffrey, M. Room to Move: Crystallizing Membrane Proteins in Swollen Lipidic Mesophases. *J. Mol. Biol.* **2006**, *357*, 1605–1618.
- (137) Engstroem, S.; Wadsten-hindrichsen, P.; Hernius, B. Cubic , Sponge , and Lamellar Phases in the Glyceryl Monooleyl Ether - Propylene Glycol - Water System. *Langmuir* **2007**, *23*, 10020–10025.
- (138) Alcaraz, N.; Liu, Q.; Hanssen, E.; Johnston, A.; Boyd, B. J. Clickable Cubosomes for Antibody-Free Drug Targeting and Imaging Applications. *Bioconjug. Chem.* **2018**, *29*, 149–157.
- (139) Astolfi, P.; Giorgini, E.; Gambini, V.; Rossi, B.; Vaccari, L.; Vita, F.; Francescangeli, O.; Marchini, C.; Pisani, M. Lyotropic Liquid-Crystalline Nanosystems as Drug Delivery Agents for 5-Fluorouracil: Structure and Cytotoxicity. *Langmuir* **2017**, *33*, 12369–12378.
- (140) Kulkarni, C. V; Vishwapathi, V. K.; Quarshie, A.; Moinuddin, Z.; Page, J.; Kendrekar, P.; Mashele, S. S. Self-Assembled Lipid Cubic Phase and Cubosomes for the Delivery of Aspirin as a Model Drug. *Langmuir* **2017**, *33*, 9907–9915.
- (141) Caffrey, M. A Comprehensive Review of the Lipid Cubic Phase or in Meso Method for Crystallizing Membrane and Soluble Proteins and Complexes. *Acta Crystallogr. Sect. F* **2015**, *71*, 3–18.
- (142) Andersson, S.; Hyde, S. T.; Larsson, K.; Lidin, S. Minimal Surfaces and Structures: From Inorganic and Metal Crystals to Cell Membranes and Biopolymers. *Chem. Rev.* **1988**, *88*, 221–242.
- (143) Gruner, S. M. Stability of Lyotropic Phases Wlth Curved Interfaces. *J. Phys. Chem.* **1989**, *93*, 7562–7570.
- (144) Schwarz, H. A. *Gesammelte Mathematische Abhandlungen*, First.; Schwarz, H. A., Ed.; Springer Berlin Heidelberg: Berlin, Heidelberg, 1890; pp 1-345.
- (145) Schoen, A. H. *Infinite Periodic Minimal Surfaces without Self-Intersection*; NASA Technical Note D-5441 (Washington D.C, 1970).
- (146) Koynova, R.; Tenchov, B.; MacDonald, R. C. Nonlamellar Phases in Cationic Phospholipids, Relevance to Drug and Gene Delivery. *ACS Biomater. Sci. Eng.* **2015**, *1*, 130–138.
- (147) Anderson, D.; Gruner, S. M.; Leibler, S. Geometrical Aspects of the Frustration in the Cubic Phases of Lyotropic Liquid Crystals. *Proc. Natl. Acad. Sci. U. S. A.* **1988**, *85*, 5364–5368.
- (148) Chung, H.; Caffrey, M. The Neutral Area Surface of the Cubic Mesophase: Location and Properties. *Biophys. J.* **1994**, *66*, 377–381.
- (149) Lutton, E. S. Phase Behavior of Aqueous Systems of Monoglycerides. *J. Am. Oil Chem. Soc.* **1965**, *42*, 1068–1070.
- (150) Luzzati, V.; Tardieu, A.; Gulikkrz.T; Rivas, E.; Reissus.F. Structure of Cubic Phases of Lipid-Water Systems. *Nature* **1968**, *220*, 485–488.
- (151) Chung, H.; Caffrey, M. The Curvature Elastic-Energy Function of the Lipid-Water Cubic Mesophase. *Nature* **1994**, *368*, 224–226.
- (152) Larsson, K. Two Cubic Phases in Monoolein–water System. *Nature* **1983**, *304*, 664.

- (153) Lindblom, G.; Larsson, K.; Johansson, L.; Fontell, K. The Cubic Phase of Monoglyceride-Water Systems . Arguments for a Structure Based upon Lamellar Bilayer Units. *J. Am. Chem. Soc.* **1979**, *101*, 5465–5470.
- (154) Hyde, S. T.; Andersson, S.; Ericsson, B.; Larsson, K. A Cubic Structure Consisting of a Lipid Bilayer Forming an Infinite Periodic Minimum Surface of the Gyroid Type in the Glycerolmonooleat-Water System. *zeitschrift für Krist.* **1984**, *168*, 213–219.
- (155) Clogston, J.; Rathman, J.; Tomasko, D.; Walker, H.; Caffrey, M. Phase Behavior of a Monoacylglycerol (Myverol 18-99K) / Water System. *Chem. Phys. Lipids* **2000**, *107*, 191–220.
- (156) Briggs, J.; Chung, H.; Caffrey, M.; Phase, T. T. The Temperature-Composition Phase Diagram and Mesophase Structure Characterization of the Monoolein / Water System. *J. Phys. II Fr.* **1996**, *6*, 723–751.
- (157) Kulkarni, C. V.; Glatter, O. Water-in-Oil Nanostructured Emulsions : Towards the Structural Hierarchy of Liquid Crystalline Materials. *Soft Matter* **2010**, *27*, 5615–5624.
- (158) Misquitta, Y.; Caffrey, M. Detergents Destabilize the Cubic Phase of Monoolein: Implications for Membrane Protein Crystallization. *Biophys. J.* **2003**, *85*, 3084–3096.
- (159) Vargas, R.; Mateu, L.; Romero, A. The Effect of Increasing Concentrations of Precipitating Salts Used to Crystallize Proteins on the Structure of the Lipidic Q224 Cubic Phase. *Chem. Phys. Lipids* **2004**, *127*, 103–111.
- (160) Takahashi, H.; Matsuo, A.; Hatta, I. Effects of Chaotropic and Kosmotropic Solutes on the Structure of Lipid Cubic Phase: Monoolein-Water Systems. *Mol. Cryst. Liq. Cryst* **2000**, *347*, 231–238.
- (161) Abe, S.; Takahashi, H. Simultaneous Small-Angle/Wide-Angle X-Ray Scattering and Differential Scanning Calorimetry Study of the Effects of Glycerol on Hydrated Monoolein. *J. Appl. Cryst.* **2003**, *36*, 515–519.
- (162) Ericsson, B.; Larsson, K.; Fontell, K. A Cubic Protein-Monoolein-Water Phase. *Biochim. Biophys. Acta - Rev. Biomembr.* **1983**, *729*, 23–27.
- (163) Larsson, K. Cubic Lipid-Water Phases : Structures and Biomembrane Aspects. *J. Phys. Chem.* **1989**, *93*, 7304–7314.
- (164) Tanaka, S. Structural Transitions of the Mono-Olein Bicontinuous Cubic Phase Induced by Inclusion of Protein Lysozyme Solutions. *Phys. Rev. E* **2006**, *73*, 1–7.
- (165) Razumas, V.; Larsson, K.; Mieziš, Y.; Nylander, T. A Cubic Monoolein - Cytochrome c - Water Phase : X-Ray Diffraction , FT-IR , Differential Scanning Calorimetric , and Electrochemical Studies. *J. Phys. Chem.* **1996**, *18*, 11766–11774.
- (166) Mulet, X.; Kennedy, D. F.; Conn, C. E.; Hawley, A.; Drummond, C. J. High Throughput Preparation and Characterisation of Amphiphilic Nanostructured Nanoparticulate Drug Delivery Vehicles. *Int. J. Pharm.* **2010**, *395*, 290–297.
- (167) Van’T Hag, L.; Darmanin, C.; Le, T. C.; Mudie, S.; Conn, C. E.; Drummond, C. J. In Meso Crystallization: Compatibility of Different Lipid Bicontinuous Cubic Mesophases with the Cubic Crystallization Screen in Aqueous Solution. *Cryst. Growth Des.* **2014**, *14*, 1771–1781.
- (168) Szlezak, M.; Nieciecka, D.; Joniec, A.; Pękała, M.; Gorecka, E.; Emo, M.; Stébé, M. J.; Krysiński, P.; Bilewicz, R. Monoolein Cubic Phase Gels and Cubosomes Doped with Magnetic Nanoparticles–Hybrid Materials for Controlled Drug Release. *ACS Appl. Mater. Interfaces* **2017**, *9*, 2796–2805.
- (169) Aleandri, S.; Bandera, D.; Mezzenga, R.; Landau, E. M. Biotinylated Cubosomes: A Versatile Tool for Active Targeting and Codelivery of Paclitaxel and a Fluorescein-Based Lipid Dye. *Langmuir* **2015**, *31*, 12770–12776.
- (170) Patrick T. Spicer. *Cubosomes: Bicontinuous Liquid Crystalline Nanoparticles*; James A. Schwarz, Cristian I. Contescu, K. P., Ed.; Marcel Dekker Inc: New York, NY, 2004; Vol. 1, pp 841-892.
- (171) Chong, J. Y. T.; Mulet, X.; Boyd, B. J.; Drummond, C. J. Steric Stabilizers for Cubic Phase Lyotropic Liquid Crystal Nanodispersions (Cubosomes). In *Advances in Planar Lipid Bilayers and Liposomes*; Aleš Iglíč, Michael Rappolt, A. J. G.-S., Ed.; Elsevier Inc.: San Diego, CA, 2015; pp 131–187.

- (172) Dong, Y. Da; Larson, I.; Barnes, T. J.; Prestidge, C. A.; Boyd, B. J. Adsorption of Nonlamellar Nanostructured Liquid-Crystalline Particles to Biorelevant Surfaces for Improved Delivery of Bioactive Compounds. *ACS Appl. Mater. Interfaces* **2011**, *3*, 1771–1780.
- (173) Matsen, M. W.; Schickf, M. Self-Assembly of Block Copolymers. *Curr. Opin. Colloid Interface Sci.* **1996**, *1*, 329–336.
- (174) Gustafsson, J.; Ljusberg-Wahren, H.; Almgren, M.; Larsson, K. Submicron Particles of Reversed Lipid Phases in Water Stabilized by a Nonionic Amphiphilic Polymer. *Langmuir* **1997**, *13*, 6964–6971.
- (175) Zhao, X. Y.; Zhang, J.; Zheng, L. Q.; Li, D. H. Studies of Cubosomes as a Sustained Drug Delivery System. *J. Dispers. Sci. Technol.* **2008**, *25*, 795–799.
- (176) Campo, L. De; Yaghamur, A.; Sagalowicz, L.; Leser, M. E.; Watzke, H.; Glatter, O. Reversible Phase Transitions in Emulsified Nanostructured Lipid Systems. *Langmuir* **2004**, *20*, 6964–6971.
- (177) Dong, Y.; Larson, I.; Hanley, T.; Boyd, B. J.; Colledge, V.; V, M. U.; Park, V. Bulk and Dispersed Aqueous Phase Behavior of Phytantriol : Effect of Vitamin E Acetate and F127 Polymer on Liquid Crystal Nanostructure. *Langmuir* **2006**, *22*, 9512–9518.
- (178) Chong, J. Y. T.; Mulet, X.; Waddington, L. J.; Boyd, B. J.; Drummond, C. J. Steric Stabilisation of Self-Assembled Cubic Lyotropic Liquid Crystalline Nanoparticles: High Throughput Evaluation of Triblock Polyethylene Oxide-Polypropylene Oxide-Polyethylene Oxide Copolymers. *Soft Matter* **2011**, *7*, 4768–4777.
- (179) Chong, J. Y. T.; Mulet, X.; Boyd, B. J.; Drummond, C. J. Accelerated Stability Assay (ASA) for Colloidal Systems. *ACS Cominatorial Sci.* **2014**, *16*, 205–210.
- (180) Murgia, S.; Bonacchi, S.; Falchi, A. M.; Lampis, S.; Lippolis, V.; Meli, V.; Monduzzi, M.; Prodi, L.; Schmidt, J.; Talmon, Y.; et al. Drug-Loaded Fluorescent Cubosomes: Versatile Nanoparticles for Potential Theranostic Applications. *Langmuir* **2013**, *29*, 6673–6679.
- (181) Caltagirone, C.; Falchi, A. M.; Lampis, S.; Lippolis, V.; Meli, V.; Monduzzi, M.; Prodi, L.; Schmidt, J.; Sgarzi, M.; Talmon, Y.; et al. Cancer-Cell-Targeted Theranostic Cubosomes. *Langmuir* **2014**, *30*, 6228–6236.
- (182) Boyd, B. J.; Dong, Y.; Rades, T. Nonlamellar Liquid Crystalline Nanostructured Particles : Advances in Materials and Structure Determination. *J. Liposome Res.* **2009**, *19*, 12–28.
- (183) Johnsson, M.; Barauskas, J.; Tiberg, F.; Ab, C. Cubic Phases and Cubic Phase Dispersions in a Phospholipid-Based System. *J. Am. Chem. Soc.* **2005**, *127*, 1076–1077.
- (184) Angelov, B.; Angelova, A.; Papahadjopoulos-sternberg, B.; Ho, S. V.; Lesieur, S. Protein-Containing PEGylated Cubosomic Particles: Freeze-Fracture Electron Microscopy and Synchrotron Radiation Circular Dichroism Study. *J. Phys. Chem. B* **2012**, *116*, 7676–7678.
- (185) Koynova, R.; Tenchov, B.; Rapp, G. Effect of PEG-Lipid Conjugates on the Phase Behavior of Phosphatidylethanolamine Dispersions. *Colloids Surfaces A Physicochem. Eng. Asp.* **1999**, *149*, 571–575.
- (186) Johnsson, M.; Edwards, K. Phase Behavior and Aggregate Structure in Mixtures of Dioleoylphosphatidylethanolamine and Poly(Ethylene Glycol)-Lipids. *Biophys. J.* **2001**, *80*, 313–323.
- (187) Koynova, R.; Tenchov, B.; Rapp, G. Low Amounts of PEG-Lipid Induce Cubic Phase in Phosphatidylethanolamide Dispersions. *Biochim. Biophys. Acta - Biomembr.* **1997**, *1326*, 167–170.
- (188) Barauskasa, J.; Cervinb, C.; Jankuneca, M.; Spandyreva, M.; Ribokaite, K.; Tibergb, F.; Johnssonb, M. Interactions of Lipid-Based Liquid Crystalline Nanoparticles with Model and Cell Membranes. *Int. J. Pharm.* **2010**, *391*, 284–291.
- (189) Bode, J. C.; Kuntsche, J.; Funari, S. S.; Bunjes, H. Interaction of Dispersed Cubic Phases with Blood Components. *Int. J. Pharm.* **2013**, *448*, 87–95.
- (190) Chong, J. Y. T.; Mulet, X.; Keddie, D. J.; Waddington, L.; Mudie, S. T.; Boyd, B. J.; Drummond, C. J. Novel Steric Stabilizers for Lyotropic Liquid Crystalline Nanoparticles: PEGylated-Phytanyl Copolymers. *Langmuir* **2014**, *31*, 2615–2629.
- (191) Liu, S.; Maheshwari, R.; Kiick, K. L. Polymer-Based Therapeutics. *Macromolecules* **2009**, *42*, 3–13.

- (192) Chawla, J. S.; Amiji, M. M. Biodegradable Poly(ϵ -Caprolactone) Nanoparticles for Tumor-Targeted Delivery of Tamoxifen. *Int. J. Pharm.* **2002**, *249*, 127–138.
- (193) Mateo, C.; Palomo, J. M.; Fernandez-Lorente, G.; Guisan, J. M.; Fernandez-Lafuente, R. Improvement of Enzyme Activity, Stability and Selectivity via Immobilization Techniques. *Enzyme Microb. Technol.* **2007**, *40*, 1451–1463.
- (194) Kulshrestha, A. S.; Sahoo, B.; Gao, W.; Fu, H.; Gross, R. A. Lipase Catalysis. A Direct Route to Linear Aliphatic Copolyesters of Bis(Hydroxymethyl)Butyric Acid with Pendant Carboxylic Acid Groups. *Macromolecules* **2005**, *38*, 3205–3213.
- (195) Korupp, C.; Weberskirch, R.; Müller, J. J.; Liese, A.; Hilterhaus, L. Scaleup of Lipase-Catalyzed Polyester Synthesis. *Org. Process Res. Dev.* **2010**, *14*, 1118–1124.
- (196) Shafioul, A. S. M.; Pyo, J. I.; Kim, K. S.; Cheong, C. S. Synthesis of Poly (Glycerol-*Co*-Dioate-*Co*-Butanedioate-*Co*-Xanthorrhizol) Ester and a Study of Chain Length Effect on Pendant Group Loading. *J. Mol. Catal. B Enzym.* **2012**, *84*, 198–204.
- (197) T. Naolou D. Conrad, K. Busse, K. Mäder and J. Kressler, V. M. W. Fatty Acid Modified Poly(Glycerol Adipate)-Polymeric Analogues of Glycerides. In *Tailored Polymer Architectures for Pharmaceutical and Biomedical Applications*; Scholz, C., Kressler, J., Eds.; American Chemical Society, 2013; Vol. 1135, pp 39–52.
- (198) Naolou, T.; Meister, A.; Schöps, R.; Pietzsch, M.; Kressler, J. Synthesis and Characterization of Graft Copolymers Able to Form Polymersomes and Worm-like Aggregates. *Soft Matter* **2013**, *9*, 10364–10372.
- (199) Foster, D. P.; Jasnow, D.; Balazs, A. C. Macrophase and Microphase Separation in Random Comb Copolymers. *Macromolecules* **1995**, *28*, 3450–3462.
- (200) Beiner, M.; Huth, H. Nanophase Separation and Hindered Glass Transition in Side-Chain Polymers. *Nat. Mater.* **2003**, *2*, 595–599.
- (201) Ungar, G. Structure of Rotator Phases in N-Alkanes. *J. Phys. Chem.* **1983**, *87*, 689–695.
- (202) Blanco, E.; Shen, H.; Ferrari, M. Principles of Nanoparticle Design for Overcoming Biological Barriers to Drug Delivery. *Nat. Biotechnol.* **2015**, *33*, 941–951.
- (203) Decuzzi, P.; Pasqualini, R.; Arap, W.; Ferrari, M. Intravascular Delivery of Particulate Systems: Does Geometry Really Matter? *Pharm. Res.* **2009**, *26*, 235–243.
- (204) Zhang, H.; Cui, W.; Bei, J.; Wang, S. Preparation of Poly(Lactide-*Co*-Glycolide-*Co*-Caprolactone) Nanoparticles and Their Degradation Behaviour in Aqueous Solution. *Polym. Degrad. Stab.* **2006**, *91*, 1929–1936.
- (205) Fessi, H.; Puisieux, F.; Devissaguet, J. P.; Ammoury, N.; Benita, S. Nanocapsule Formation by Interfacial Polymer Deposition Following Solvent Displacement. *Int. J. Pharm.* **1989**, *55*, 1–4.
- (206) Jiang, Y.; Woortman, A. J. J.; Alberda van Ekenstein, G. O. R.; Loos, K. A Biocatalytic Approach towards Sustainable Furanic-aliphatic Polyesters. *Polym. Chem.* **2015**, *6*, 5198–5211.
- (207) Jiang, Y.; Woortman, A. J. J.; Alberda van Ekenstein, G. O. R.; Loos, K. Environmentally Benign Synthesis of Saturated and Unsaturated Aliphatic Polyesters via Enzymatic Polymerization of Biobased Monomers Derived from Renewable Resources. *Polym. Chem.* **2015**, *6*, 5451–5463.
- (208) Kobayashi, S. Lipase-Catalyzed Polyester Synthesis - A Green Polymer Chemistry. *Proc. Japan Acad. Ser. B* **2010**, *86*, 338–365.
- (209) Uyama, H.; Kobayashi, S. *Enzyme-Catalyzed Synthesis of Polymers*; Kobayashi, S., Ritter, H., Kaplan, D., Eds.; Advances in Polymer Science; Springer Berlin Heidelberg: Berlin, Heidelberg, 2006; Vol. 194, pp 133–158.
- (210) Kennedy, J. F.; Kumar, H.; Panesar, P. S.; Marwaha, S. S.; Goyal, R.; Parmar, A.; Kaur, S. Enzyme-Catalyzed Regioselective Synthesis of Sugar Esters and Related Compounds. *J. Chem. Technol. Biotechnol.* **2006**, *81*, 866–876.
- (211) Li, G.; Yao, D.; Zong, M. Lipase-Catalyzed Synthesis of Biodegradable Copolymer Containing Malic Acid Units in Solvent-Free System. *Eur. Polym. J.* **2008**, *44*, 1123–1129.
- (212) Gustini, L.; Noordover, B. A. J.; Gehrels, C.; Dietz, C.; Koning, C. E. Enzymatic Synthesis and Preliminary Evaluation as Coating of Sorbitol-Based, Hydroxy-Functional Polyesters with Controlled Molecular Weights. *Eur. Polym. J.* **2014**, *67*, 459–475.

- (213) Taresco, V.; Creasey, R. G.; Kennon, J.; Mantovani, G.; Alexander, C.; Burley, J. C.; Garnett, M. C. Variation in Structure and Properties of Poly(Glycerol Adipate) *via* Control of Chain Branching during Enzymatic Synthesis. *Polymer* **2016**, *89*, 41–49.
- (214) Asmus, L. R.; Kaufmann, B.; Melander, L.; Weiss, T.; Schwach, G.; Gurny, R.; Möller, M. Single Processing Step toward Injectable Sustained-Release Formulations of Triptorelin Based on a Novel Degradable Semi-Solid Polymer. *Eur. J. Pharm. Biopharm.* **2012**, *81*, 591–599.
- (215) Jores, K.; Mehnert, W.; Drechsler, M.; Bunjes, H.; Johann, C.; Mäder, K. Investigations on the Structure of Solid Lipid Nanoparticles (SLN) and Oil-Loaded Solid Lipid Nanoparticles by Photon Correlation Spectroscopy, Field-Flow Fractionation and Transmission Electron Microscopy. *J. Control. Release* **2004**, *95*, 217–227.
- (216) Pitzalis, P.; Monduzzi, M.; Krog, N.; Larsson, H.; Ljusberg-wahren, H.; Nylander, T. Characterization of the Liquid - Crystalline Phases in the Glycerol Monooleate / Diglycerol Monooleate / Water System. *Langmuir* **2000**, *16*, 6358–6365.
- (217) Borné, J.; Nylander, T.; Khan, A. Effect of Lipase on Monoolein-Based Cubic Phase Dispersion (Cubosomes) and Vesicles. *J. Phys. Chem. B* **2002**, *106*, 10492–10500.
- (218) Borné, J.; Nylander, T.; Khan, A. Phase Behavior and Aggregate Formation for the Aqueous Monoolein System Mixed with Sodium Oleate and Oleic Acid. *Langmuir* **2001**, *17*, 7742–7751.
- (219) Landh, T. Phase Behavior in the System Pine Oil Monoglycerides-Poloxamer 407-Water at 20 °C. *J. Phys. Chem.* **1994**, *98*, 8453–8467.
- (220) Caboi, F.; Amico, G. S.; Pitzalis, P.; Monduzzi, M.; Nylander, T.; Larsson, K. Addition of Hydrophilic and Lipophilic Compounds of Biological Relevance to the Monoolein/Water System. I. Phase Behavior. *Chem. Phys. Lipids* **2001**, *109*, 47–62.
- (221) Salim, M.; Wan Iskandar, W. F. N.; Patrick, M.; Zahid, N. I.; Hashim, R. Swelling of Bicontinuous Cubic Phases in Guerbet Glycolipid: Effects of Additives. *Langmuir* **2016**, *32*, 5552–5561.
- (222) Tyler, A. I. I.; Barriga, H. M. G.; Parsons, E. S.; McCarthy, N. L. C.; Ces, O.; Law, R. V.; Seddon, J. M.; Brooks, N. J. Electrostatic Swelling of Bicontinuous Cubic Lipid Phases. *Soft Matter* **2015**, *11*, 3279–3286.
- (223) Sun, W.; Vallooran, J. J.; Zabara, A.; Mezzenga, R. Controlling Enzymatic Activity and Kinetics in Swollen Mesophases by Physical Nano-Confinement. *Nanoscale* **2014**, *6*, 6853–6859.
- (224) Leal, C.; Bouxsein, N. F.; Ewert, K. K.; Safinya, C. R. Gene Silencing Activity of SiRNA Embedded in a Bicontinuous Lipid Matrix. *J. Am. Chem. Soc.* **2010**, *132*, 16841–16847.
- (225) Guillot, S.; Salentinig, S.; Chemelli, A.; Sagalowicz, L.; Leser, M. E.; Glatter, O. Influence of the Stabilizer Concentration on the Internal Liquid Crystalline Order and the Size of Oil-Loaded Monolinolein-Based Dispersions. *Langmuir* **2010**, *26*, 6222–6229.
- (226) Hartnett, T. E.; Ladewig, K.; Oconnor, A. J.; Hartley, P. G.; McLean, K. M. Size and Phase Control of Cubic Lyotropic Liquid Crystal Nanoparticles. *J. Phys. Chem. B* **2014**, *118*, 7430–7439.
- (227) Yaghmur, A.; De Campo, L.; Sagalowicz, L.; Leser, M. E.; Glatter, O. Control of the Internal Structure of MLO-Based Isosomes by the Addition of Diglycerol Monooleate and Soybean Phosphatidylcholine. *Langmuir* **2006**, *22*, 9919–9927.
- (228) Fraser, S. J.; Mulet, X.; Hawley, A.; Separovic, F.; Polyzos, A. Controlling Nanostructure and Lattice Parameter of the Inverse Bicontinuous Cubic Phases in Functionalised Phytantriol Dispersions. *J. Colloid Interface Sci.* **2013**, *408*, 117–124.
- (229) Liu, Q.; Dong, Y.-D.; Boyd, B. J. Selective Sequence for the Peptide-Triggered Phase Transition of Lyotropic Liquid-Crystalline Structures. *Langmuir* **2016**, *32*, 5155–5161.
- (230) Zhai, J.; Hinton, T. M.; Waddington, L. J.; Fong, C.; Tran, N.; Mulet, X.; Drummond, C. J.; Muir, B. W. Lipid-PEG Conjugates Sterically Stabilize and Reduce the Toxicity of Phytantriol-Based Lyotropic Liquid Crystalline Nanoparticles. *Langmuir* **2015**, *31*, 10871–10880.
- (231) Chong, J. Y. T.; Mulet, X.; Waddington, L. J.; Boyd, B. J.; Drummond, C. J. High-Throughput Discovery of Novel Steric Stabilizers for Cubic Lyotropic Liquid Crystal Nanoparticle Dispersions. *Langmuir* **2012**, *28*, 9223–9232.
- (232) Almgren, M.; Borne, J.; Feitosa, E.; Khan, A.; Lindman, B. Dispersed Lipid Liquid Crystalline

- Phases Stabilized by a Hydrophobically Modified Cellulose. *Langmuir* **2007**, *23*, 2768–2777.
- (233) Garnett, M. C.; Kallinteri, P. Nanomedicines and Nanotoxicology: Some Physiological Principles. *Occup. Med.* **2006**, *56*, 307–311.
- (234) Uyama, H.; Inada, K.; Kobayashi, S. Regioselectivity Control in Lipase-Catalyzed Polymerization of Divinyl Sebacate and Triols. *Macromol. Biosci.* **2001**, *1*, 40–44.
- (235) Cwynar, V. A.; Hart, D. J.; Lee, J.; Lyons, J. Preparation of 1-Monoacylglycerols via the Suzuki-Miyaura. *Org. Synth.* **2012**, *89*, 183–201.
- (236) Yu Fu; Weng, Y.; Hong, W.-X.; Zhang, Q. Efficient Synthesis of Unsaturated 1-Monoacyl Glycerols for in Meso Crystallization of Membrane Proteins. *Synlett* **2011**, *48*, 809–812.
- (237) Glatter, O. A New Iterative Method for Collimation Correction in Small-Angle Scattering. *J. Appl. Crystallogr.* **1974**, *7*, 147–153.
- (238) Xiao, Q.; Wang, Z.; Williams, D.; Leowanawat, P.; Peterca, M.; Sherman, S. E.; Zhang, S.; Hammer, D. A.; Heiney, P. A.; King, S. R.; et al. Why Do Membranes of Some Unhealthy Cells Adopt a Cubic Architecture? *ACS Cent. Sci.* **2016**, *2*, 943–953.
- (239) Chaudhary, A. K.; Beckman, E. J.; Russell, A. J. Biocatalytic Polyester Synthesis: Analysis of the Evolution of Molecular Weight and End Group Functionality. *Biotechnol. Bioeng.* **1997**, *55*, 227–239.
- (240) Hawker, C. J.; Lee, R.; Frechet, J. M. J. One-Step Synthesis of Hyperbranched Dendritic Polyesters. *J. Am. Chem. Soc.* **1991**, *113*, 4583–4588.
- (241) Hölter, D.; Burgath, A.; Frey, H. Degree of Branching in Hyperbranched Polymers. *Acta Polym.* **1997**, *48*, 30–35.
- (242) Idris, A.; Bukhari, A. Immobilized Candida Antarctica Lipase B: Hydration, Stripping off and Application in Ring Opening Polyester Synthesis. *Biotechnol. Adv.* **2012**, *30*, 550–563.
- (243) Clark, D. S. Characteristics of Nearly Dry Enzymes in Organic Solvents: Implications for Biocatalysis in the Absence of Water. *Philos. Trans. R. Soc. Lond. B. Biol. Sci.* **2004**, *359*, 1299–1307.
- (244) Varma, I. K.; Albertsson, A.-C.; Rajkhowa, R.; Srivastava, R. K. Enzyme Catalyzed Synthesis of Polyesters. *Prog. Polym. Sci.* **2005**, *30*, 949–981.
- (245) Uyama, H.; Inada, K.; Kobayashi, S. Regioselectivity Control in Lipase-Catalyzed Polymerization of Divinyl Sebacate and Triols. *Macromol. Biosci.* **2001**, *1*, 40–44.
- (246) Naba K. Dutta, N. R. C. Self-Assembly and Supramolecular Assembly in Nanophase Separated Polymers and Thin Films. In *Functional Nanostructures Processing, Characterization, and Applications*; Seal, S., Ed.; Nanostructure Science and Technology; Springer: New York, NY, 2008; pp 220–304.
- (247) Faber, M.; Hofman, A. H.; Harinck, N.; Ten Cate, M.; Loos, K.; Ten Brinke, G. Self-Assembly of Hydrogen-Bonded Comb Copolymer Complexes of Poly(*p*-Hydroxystyrene) and 4-Alkylpyridine Amphiphiles. *Polymer* **2016**, *92*, 273–282.
- (248) Hofman, A. H.; ten Brinke, G.; Loos, K. Hierarchical Structure Formation in Supramolecular Comb-Shaped Block Copolymers. *Polymer* **2016**, *107*, 343–356.
- (249) Spicer, P. T.; Hayden, K. L.; Lynch, M. L.; Ofori-Boateng, A.; Burns, J. L. Novel Process for Producing Cubic Liquid Crystalline Nanoparticles (Cubosomes). *Langmuir* **2001**, *17*, 5748–5756.
- (250) Qiu, H.; Caffrey, M. Lyotropic and Thermotropic Phase Behavior of Hydrated Monoacylglycerols: Structure Characterization of Monovaccenin. *J. Phys. Chem. B* **1998**, *102*, 4819–4829.
- (251) Bei, D.; Zhang, T.; Murowchick, J. B.; Youan, B.-B. C. Formulation of Dacarbazine-Loaded Cubosomes. Part III. Physicochemical Characterization. *AAPS PharmSciTech* **2010**, *11*, 1243–1249.
- (252) Mäder, K.; Mehnert, W. Solid Lipid Nanoparticles: Production, Characterization and Applications. *Adv. Drug Deliv. Rev.* **2001**, *47*, 165–196.
- (253) Freitas, C.; Müller, R. H. Correlation between Long-Term Stability of Solid Lipid Nanoparticles (SLNTM) and Crystallinity of the Lipid Phase. *Eur. J. Pharm. Biopharm.* **1999**, *47*, 125–132.

- (254) La, Y.; Park, C.; Shin, T. J.; Joo, S. H.; Kang, S.; Kim, K. T. Colloidal Inverse Bicontinuous Cubic Membranes of Block Copolymers with Tunable Surface Functional Groups. *Nat. Chem.* **2014**, *6*, 534–541.
- (255) He, H.; Rahimi, K.; Zhong, M.; Mourran, A.; Luebke, D. R.; Nulwala, H. B.; Möller, M.; Matyjaszewski, K. Cubosomes from Hierarchical Self-Assembly of Poly(Ionic Liquid) Block Copolymers. *Nat. Commun.* **2017**, *8*, 14057.
- (256) Zhai, J.; Hinton, T. M.; Waddington, L. J.; Fong, C.; Tran, N.; Mulet, X.; Drummond, C. J.; Muir, B. W. Lipid-PEG Conjugates Sterically Stabilize and Reduce the Toxicity of Phytantriol-Based Lyotropic Liquid Crystalline Nanoparticles. *Langmuir* **2015**, *31*, 10871–10880.
- (257) Nilsson, C.; Stergaard, J.; Larsen, S. W.; Larsen, C.; Urtti, A.; Yagmur, A. PEGylation of Phytantriol-Based Lyotropic Liquid Crystalline Particles-the Effect of Lipid Composition, PEG Chain Length, and Temperature on the Internal Nanostructure. *Langmuir* **2014**, *30*, 6398–6407.
- (258) Larsson, K. Aqueous Dispersions of Cubic Lipid-Water Phases. *Curr. Opin. Colloid Interface Sci.* **2000**, *5*, 64–69.
- (259) Driever, C. D.; Mulet, X.; Waddington, L. J.; Postma, A.; Thissen, H.; Caruso, F.; Drummond, C. J. Layer-by-Layer Polymer Coating on Discrete Particles of Cubic Lyotropic Liquid Crystalline Dispersions (Cubosomes). *Langmuir* **2013**, *29*, 12891–12900.
- (260) Guo, C.; Wang, J.; Cao, F.; Lee, R. J.; Zhai, G. Lyotropic Liquid Crystal Systems in Drug Delivery. *Drug Discov. Today* **2010**, *15*, 1032–1040.
- (261) Fleet, B.; Sankar Das Gupta. Equilibrium Bicontinuous Structure. *Nature* **1976**, *263*, 123–125.
- (262) Angelov, B.; Angelova, A.; Garamus, V. M.; Drechsler, M.; Willumeit, R.; Mutafchieva, R.; Štěpánek, P.; Lesieur, S. Earliest Stage of the Tetrahedral Nanochannel Formation in Cubosome Particles from Unilamellar Nanovesicles. *Langmuir* **2012**, *28*, 16647–16655.
- (263) Zeng, N.; Hu, Q.; Liu, Z.; Gao, X.; Hu, R.; Song, Q.; Gu, G.; Xia, H.; Yao, L.; Pang, Z.; et al. Preparation and Characterization of Paclitaxel-Loaded DSPE-PEG-Liquid Crystalline Nanoparticles (LCNPs) for Improved Bioavailability. *Int. J. Pharm.* **2012**, *424*, 58–66.
- (264) Barauskas, J.; Johnsson, M.; Tiberg, F. Self-Assembled Lipid Superstructures: Beyond Vesicles and Liposomes. *Nano Lett.* **2005**, *5*, 1615–1619.
- (265) Gustafsson, J.; Nylander, T.; Almgren, M.; Ljusberg-Wahren, H. Phase Behavior and Aggregate Structure in Aqueous Mixtures of Sodium Cholate and Glycerol Monooleate. *J. Colloid Interface Sci.* **1999**, *211*, 326–335.
- (266) W. Buchheim; Larsson, K. Cubic Lipid-Protein-Water Phases. *J. Colloid Interface Sci.* **1987**, *117*, 582–583.
- (267) Sagalowicz, L.; Guillot, S.; Acquistapace, S.; Schmitt, B.; Maurer, M.; Yagmur, A.; de Campo, L.; Rouvet, M.; Leser, M.; Glatter, O. Influence of Vitamin E Acetate and Other Lipids on the Phase Behavior of Mesophases Based on Unsaturated Monoglycerides. *Langmuir* **2013**, *29*, 8222–8232.
- (268) Vandoolaeghe, P.; Tiberg, F.; Nylander, T. Interfacial Behavior of Cubic Liquid Crystalline Nanoparticles at Hydrophilic and Hydrophobic Surfaces. *Langmuir* **2006**, *22*, 9169–9174.
- (269) Murgia, S.; Falchi, A. M.; Mano, M.; Lampis, S.; Angius, R.; Carnerup, A. M.; Schmidt, J.; Diaz, G.; Giacca, M.; Talmon, Y.; et al. Nanoparticles from Lipid-Based Liquid Crystals: Emulsifier Influence on Morphology and Cytotoxicity. *J. Phys. Chem. B* **2010**, *114*, 3518–3525.
- (270) Sagalowicz, L.; Guillot, S.; Acquistapace, S.; Schmitt, B.; Maurer, M.; Yagmur, A.; De Campo, L.; Rouvet, M.; Leser, M.; Glatter, O. Influence of Vitamin e Acetate and Other Lipids on the Phase Behavior of Mesophases Based on Unsaturated Monoglycerides. *Langmuir* **2013**, *29*, 8222–8232.
- (271) Bilal, M. H.; Hussain, H.; Prehm, M.; Baumeister, U.; Meister, A.; Hause, G.; Busse, K.; Mäder, K.; Kressler, J. Synthesis of Poly(Glycerol Adipate)-*g*-Oleate and Its Ternary Phase Diagram with Glycerol Monooleate and Water. *Eur. Polym. J.* **2017**, *91*, 162–175.
- (272) Wattendorf, U.; Merkle, H. P. PEGylation as a Tool for the Biomedical Engineering of Surface Modified Microparticles. *J. Pharm. Sci.* **2008**, *97*, 4655–4669.
- (273) Ostuni, E.; Chapman, R. G.; Holmlin, R. E.; Takayama, S.; Whitesides, G. M. A Survey of

- Structure-Property Relationships of Surfaces That Resist the Adsorption of Protein. *Langmuir* **2001**, *17*, 5605–5620.
- (274) Lu, C.; Zhong, W. Synthesis of Propargyl-Terminated Heterobifunctional Poly(Ethylene Glycol). *Polymers* **2010**, *2*, 407–417.
- (275) Spicer, P. T.; Small, W. B.; Lynch, M. L.; Burns, J. L. Dry Powder Precursors of Cubic Liquid Crystalline Nanoparticles (Cubosomes). *J. Nanoparticle Res.* **2002**, *4*, 297–311.
- (276) Rangelov, S.; Almgren, M. Particulate and Bulk Bicontinuous Cubic Phases Obtained from Mixtures of Glyceryl Monooleate and Copolymers Bearing Blocks of Lipid-Mimetic Anchors in Water. *J. Phys. Chem. B* **2005**, *109*, 3921–3929.
- (277) Caffrey, M. Crystallizing Membrane Proteins for Structure Determination: Use of Lipidic Mesophases. *Annu. Rev. Biophys.* **2009**, *38*, 29–51.
- (278) Wunderlich, B. Theory of Cold Crystallization of High Polymers. *J. Chem. Phys.* **1958**, *29*, 1395–1404.
- (279) Zhao, L.; Pan, L.; Ji, A.; Cao, Z.; Wang, Q. Recrystallization of Freezable Bound Water in Aqueous Solutions of Medium Concentration. *Chinese Phys. B* **2016**, *25*, 075101.
- (280) Buckley, C. P.; Kovacs, A. J. Melting Behaviour of Low Molecular Weight Poly(Ethylene-Oxide) Fractions. *Colloid Polym. Sci.* **1976**, *254*, 695–715.
- (281) Zhang, M.; Guo, B.-H.; Xu, J. A Review on Polymer Crystallization Theories. *Crystals* **2016**, *7*, 4.
- (282) Takahashi, Y.; Sumita, I.; Tadokoro, H. Structural Studies of Polyethers. Planar Zigzag Modification of Poly(Ethylene Oxide). *J. Polym. Sci. Polym. Phys. Ed.* **1973**, *11*, 2113–2122.
- (283) Schärftl, W. Sample Preparation. In *Light Scattering from Polymer Solutions and Nanoparticle Dispersions*; Springer, Berlin, 2007; pp 43–50.

7 APPENDIX

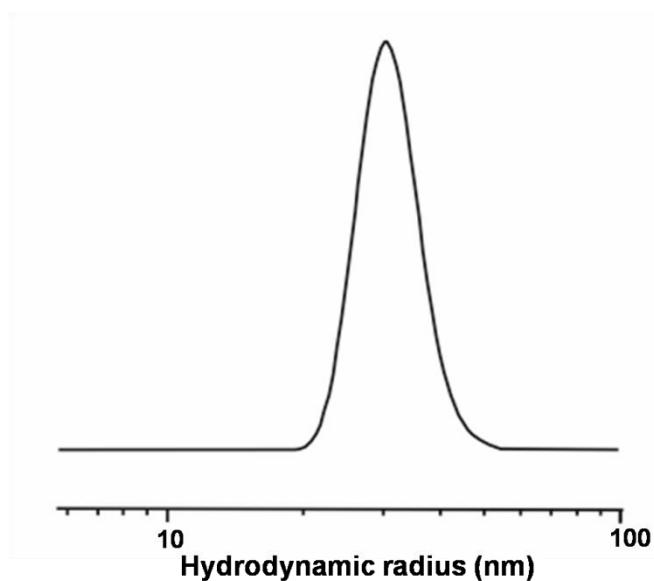


Figure A1. Hydrodynamic radius distribution of PXA at concentration $10 \text{ g}\cdot\text{L}^{-1}$ at temperature $25 \text{ }^\circ\text{C}$.

Table A1. WAXS data of PXA-*g*-S15.

T (°C)	q (Å⁻¹)	d (Å)	
30 °C heating	1.3663	4.599	diffuse
	1.5222	4.128	q _w
70 °C	1.3817	4.547	diffuse
30 °C cooling	1.4138	4.444	diffuse
	1.5204	4.133	q _w

Table A2. SAXS data of PXA-*g*-S15.

T (°C)	q (Å⁻¹)	d (Å)	
30 °C heating	0.1136	55.310	q *
70 °C	0.1284	48.934	Broad Peak
30 °C cooling	0.1230	51.083	q *

q* is the wave vector at the first maximum.

Table A3. WAXS data of PXA-*g*-S36.

T (°C)	q (Å⁻¹)	d (Å)	
30 °C heating	1.5187	4.137	q _w
70 °C	1.3661	4.599	diffuse
30 °C cooling	1.5174	4.141	q _w

Table A4. SAXS data of PXA-*g*-S36.

T (°C)	q (Å⁻¹)	d (Å)	
30 °C heating	0.1648	38.126	q *
	0.3286	19.121	2q *
	0.4903	12.815	3q *
70 °C	0.1676	37.489	Broad Peak
30 °C cooling	0.1649	38.103	q *
	0.3292	19.086	2q *
	0.4896	12.833	3q *

q* is the wave vector at the first maximum.

Table A5. WAXS data of PDSA-*g*-S10.

T (°C)	q (Å⁻¹)	d (Å)	
30 °C heating	1.4299	4.394	diffuse
	1.5199	4.134	q _w
70 °C	1.3788	4.557	diffuse
30 °C cooling	1.3557	4.635	diffuse
	1.5015	4.185	q _w

Table A6. SAXS data of PDSA-*g*-S10.

T (°C)	q (Å⁻¹)	d (Å)	
30 °C heating	0.1100	57.120	q *
	0.1205	52.143	Broad Peak
30 °C cooling	0.1133	55.456	q *

q* is the wave vector at the first maximum

Table A7. WAXS data of PDSA-*g*-S68.

T (°C)	q (Å⁻¹)	d (Å)	
30 °C heating	1.5150	4.147	q _w
	1.3640	4.606	diffuse
30 °C cooling	1.5123	4.155	q _w

Table A8. SAXS data of PDSA-*g*-S68.

T (°C)	q (Å ⁻¹)	d (Å)	
30 °C	0.1734	36.235	q *
heating	0.3464	18.139	2q *
70 °C	0.1856	33.853	Braod Peak
30 °C	0.1768	35.538	q *
cooling	0.3506	17.921	2q *

q* is the wave vector at the first maximum.

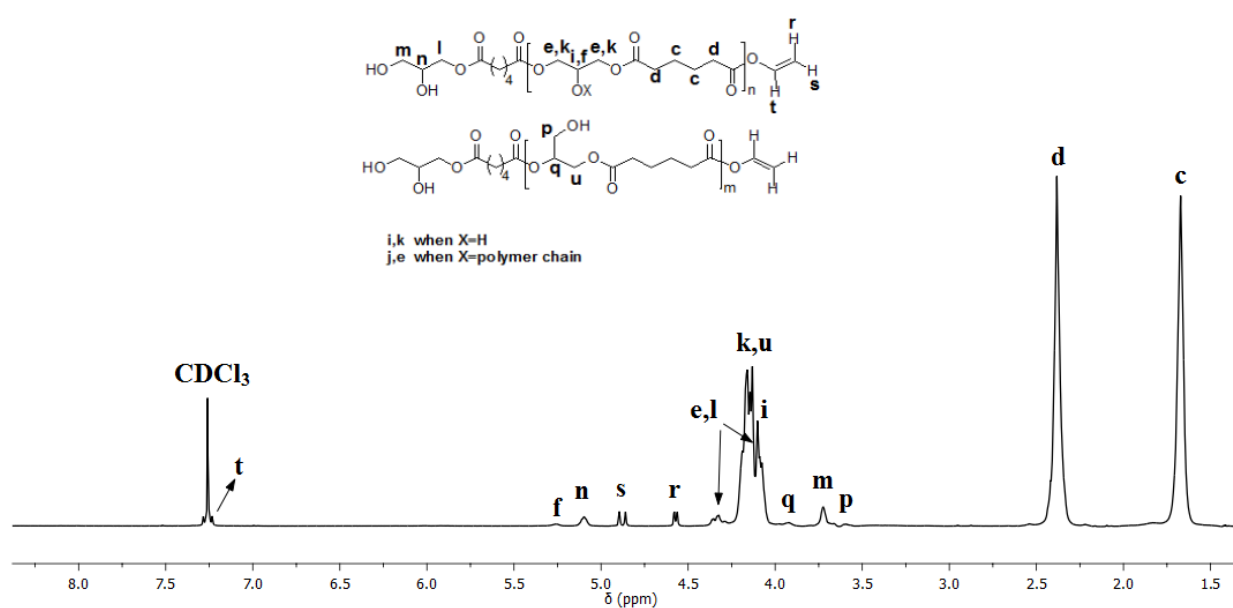


Figure A2. ¹H NMR spectrum of poly(glycerol adipate) recorded at 27°C using CDCl₃ as solvent.

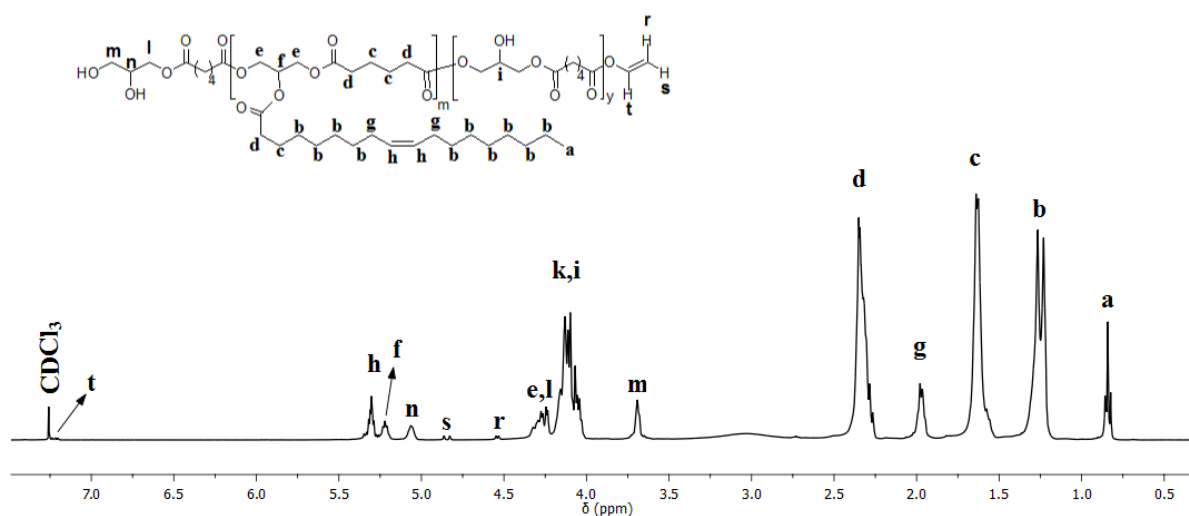


Figure A3. ¹H NMR spectrum of PGA-*g*-O22 recorded at 27 °C using CDCl₃ as solvent.

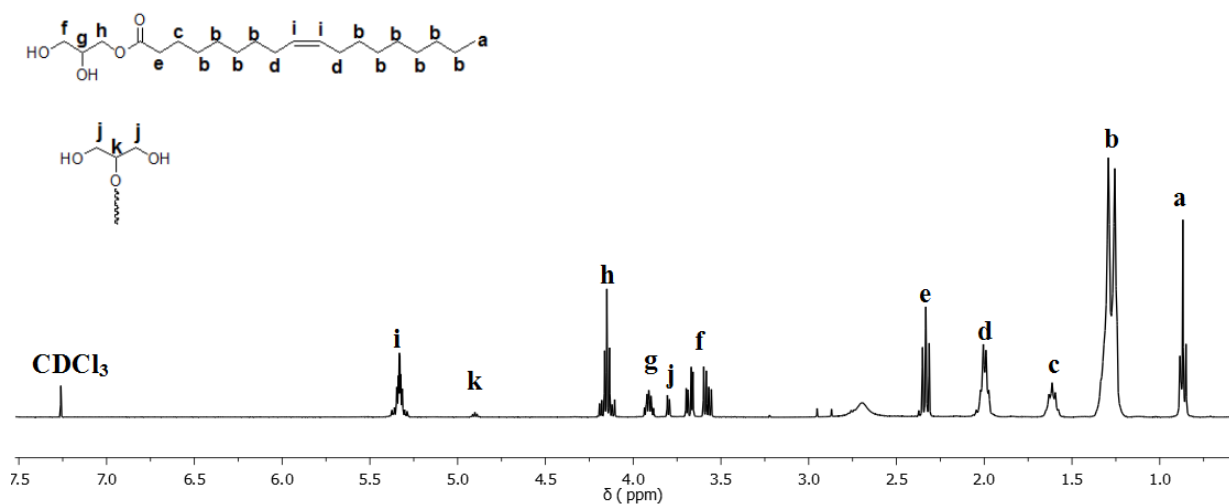


Figure A4. ^1H NMR of spectrum of G1MO and G2MO recorded at 27°C using CDCl_3 as solvent.

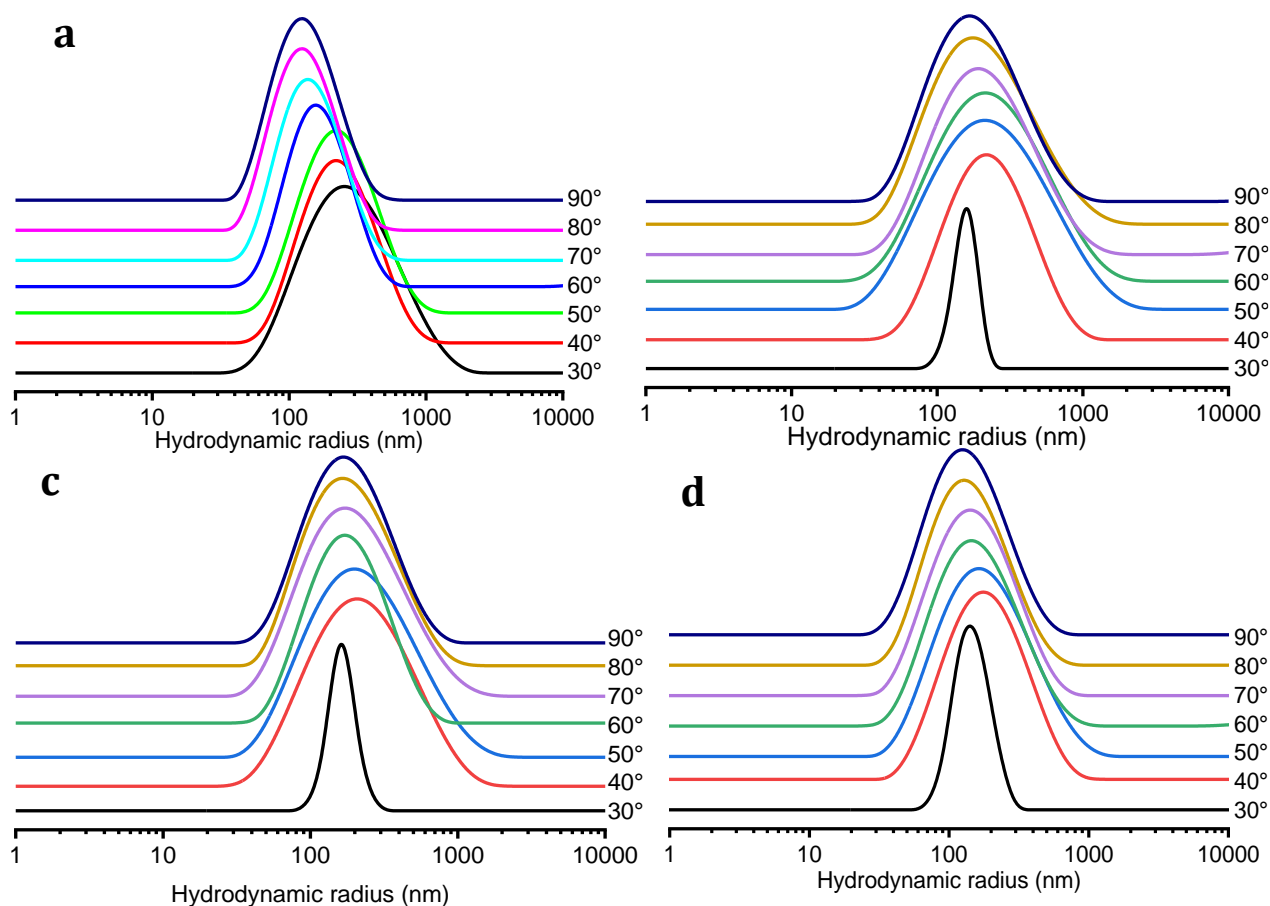


Figure A5. DLS measurements of (a) $\text{PGA}_{26}\text{O}_4\text{PEG1K}_{17}:\text{GMO}=1:99$ (b) $\text{PGA}_{26}\text{O}_4\text{PEG1K}_{17}:\text{GMO}=3:97$ (c) $\text{PGA}_{26}\text{O}_4\text{PEG1K}_{17}:\text{GMO}=5:95$ and (d) $\text{PGA}_{26}\text{O}_4\text{PEG1K}_{17}:\text{GMO}=10:90$ at 7 different angles.

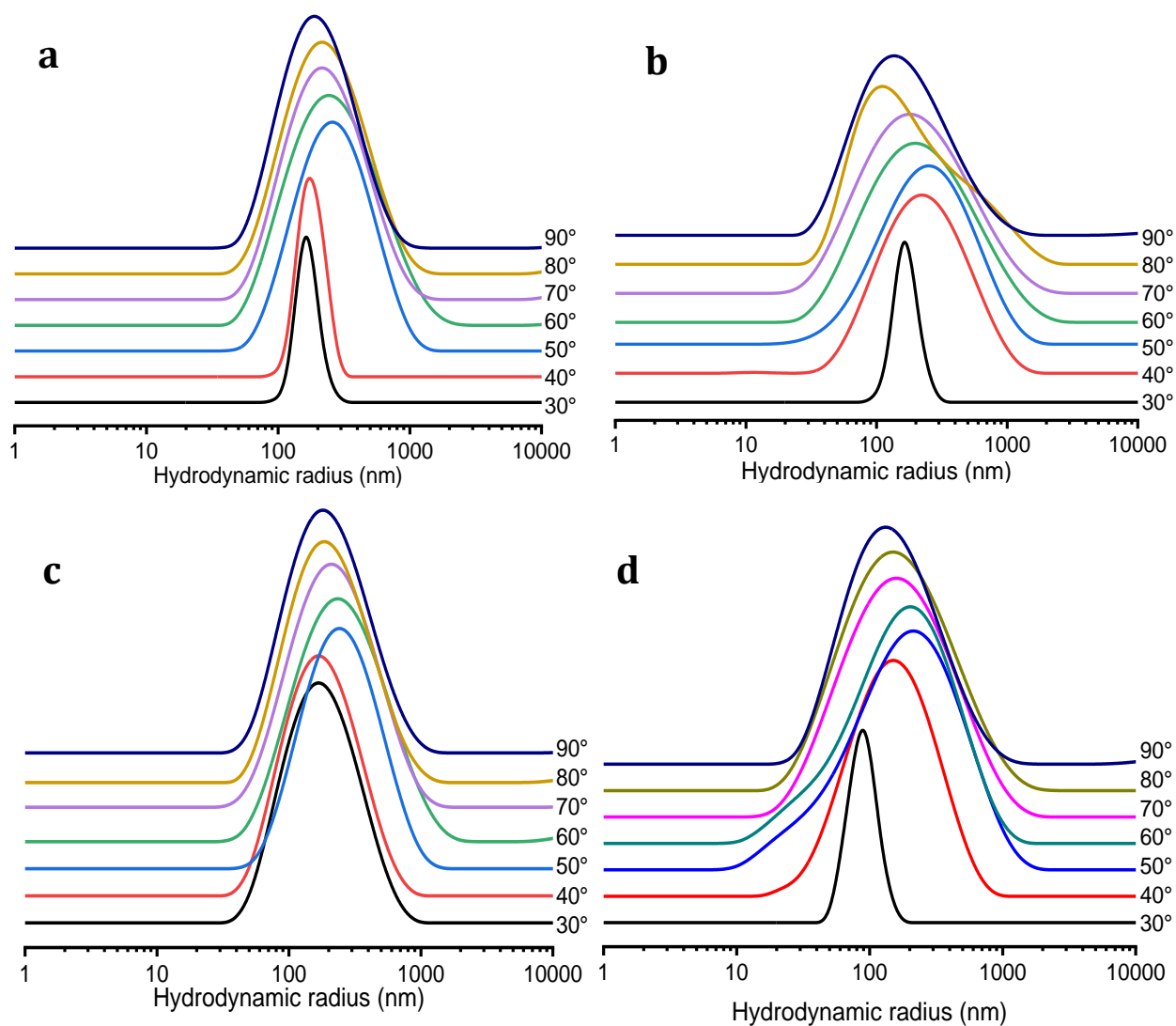


Figure A6. DLS measurements of (a) PGA₂₆O₁₃PEG1K₈ : GMO = 1:99 (b) PGA₂₆O₁₃PEG1K₈ : GMO = 3 : 97 (c) PGA₂₆O₁₃PEG1K₈ : GMO = 5 : 95 and (d) PGA₂₆O₁₃PEG1K₈ : GMO = 10 : 90 at 7 different angles.

8 ACKNOWLEDGMENT

I would like first to express my deepest gratitude and sincere appreciation to my Ph.D. supervisor, Prof. Dr. Jörg Kressler, for his valuable guidance, motivation, suggestions and for giving me the opportunity to work under his mentorship. He always encouraged me to develop myself as an instructor and independent researcher which I strongly believe will help me throughout the rest of my scientific career. It was a privilege for me to work in his laboratory at Martin Luther University. I am indebted to Dr. Karsten Busse for his assistance and guidance in the field of physical chemistry of polymers. I am also grateful to Dr. Toufik Naolou, Dr. Syed Waqar Hussain Shah and Dr. Mark Jbeily who helped me tremendously at the early phase of this work to develop my chemical synthesis skills. I would also like to acknowledge all members of Prof. Jörg Kressler's group including Dr. Henning Kausche, Dr. Elkin Amado, Frau Claudia Hochbach and Frau Elvira Stark. Many thanks go to Frau Susanne Tanner and Julia Weichhold for the GPC measurements, to Dr. Ute Baumeister, Dr. Marko Prehm, and Matthias Fischer for XRD measurements and to Dr. Annette Meister and Dr. Gerd Hause for TEM measurements. I offer my thanks to Prof. Dr. Karsten Mäder from the Pharmacy Institute and his students Dr. Alexander Gomes Rodrigues and Tom Wersig for the interesting scientific cooperation. The collaboration with Prof. Mäder group has strengthen my research work and made it of more value. I am deeply grateful to my parents who devoted their life to reach this point of my study. Finally, I come to address my appreciation to my wife for her love, moral support, and kind indulgence over the years of this thesis.

9 CURRICULUM VITAE

Personal Information

Name: Muhammad Humayun Bilal

Date and place of birth: 18th January 1983, Lahore, Pakistan

Marital status: Married

Nationality: Pakistani

Educational Background

5/2014 – present	Ph.D. student at the Institute of Chemistry Martin Luther Universität Halle-Wittenberg, Halle (Saale), in the groups of Prof. Dr. Jörg Kreßler (Physical Chemistry of Polymers)
10/2011 – 03/2014	M.Sc Polymer Material Science, Martin Luther Universität Halle-Wittenberg, Halle (Saale)
09/2006 – 10/2008	M.Sc. Chemistry, Govt. College University, Lahore, Pakistan
09/2002 – 08/2006	B.Sc. (Physics, Chemistry, Mathematics), University of the Punjab, Lahore, Pakistan

Work Experience

09/2009 – 12/2011	Serve as Subject Specialist (Chemistry) at Garrison Boys High School and Intermediate College, Lahore, Pakistan
03/2009 – 09/2009	Quality Assurance Officer at Schazoo Zaka Pharmaceuticals, Lahore, Pakistan
09/2008 – 03/2009	Quality Control Analyst at Aneeb Pharmaceuticals Lahore, Pakistan

Halle (Saale), 10/09/2018

Muhammad Humayun Bilal

10 LIST OF PUBLICATIONS

1. Mubashar-Ur-Rehman, H.; Arshad, M.; Asiri, A. M.; Ullah Khan, I.; **Bilal, M.** 2-(Naphthalene-2-Sulfonamido)-3-Phenylpropanoic Acid. *Acta Crystallogr. Sect. E. Struct. Rep. Online* **2013**, *69*, o194.
2. Jbeily, M.; Naolou, T.; **Bilal, M.**; Amado, E.; Kressler, J. Enzymatically Synthesized Polyesters with Pendent OH Groups as Macroinitiators for the Preparation of Well-Defined Graft Copolymers by Atom Transfer Radical Polymerization. *Polym. Int.* **2014**, *63*, 894–901.
3. **Bilal, M. H.**; Prehm, M.; Njau, A.; Samiullah, M.; Meister, A.; Kressler, J. Enzymatic Synthesis and Characterization of Hydrophilic Sugar Based Polyesters and Their Modification with Stearic Acid. *Polymers* **2016**, *8*, 80.
4. **Bilal, M. H.**; Hussain, H.; Prehm, M.; Baumeister, U.; Meister, A.; Hause, G.; Busse, K.; Mäder, K.; Kressler, J. Synthesis of Poly(Glycerol Adipate)-*g*-Oleate and Its Ternary Phase Diagram with Glycerol Monooleate and Water. *Eur. Polym. J.* **2017**, *91*, 162–175.

Abstracts and posters

Bilal, M. H.; Samiullah, M. H.; Kressler, J. Preparation and characterization of nanoparticles from fatty acid modified polyesters. 248th ACS National Meeting, San Francisco, CA. August 2014

Bilal, M. H.; Maryam Eivazi; Andrew Njau; Kressler, J. Biodegradable polyesters from renewable resources. 251st ACS National Meeting & Exposition, San Diego, CA. March 2016

11 SELBSTSTÄNDIGKEITSERKLÄRUNG

Hiermit erkläre ich, dass ich die Ergebnisse der vorliegenden Dissertationsarbeit

Enzymatic synthesis and characterization of grafted polyesters and their use as steric stabilizers for cubosomes

am Institut für Chemie der Martin-Luther Universität Halle-Wittenberg unter Anleitung von Herrn Prof. Dr. Jörg Kreßler selbstständig erarbeitet habe.

Hiermit erkläre in an Eides statt, dass ich die vorliegende Arbeit selbständig und ohne fremde Hilfe verfasst habe. Ich habe keine anderen Quellen und Hilfsmittel als die angegebenen verwendet und anderen Werken wörtlich oder inhaltlich entnommene Stellen als solche gekennzeichnet. Diese Arbeit habe ich an keiner anderen Hochschule vorgelegt und mich zu keinem früheren Zeitpunkt um den Doktorgrad beworben.